ROLE OF *FUSARIUM GRAMINEARUM* STE3 RECEPTOR IN MEDIATING FUNGAL HYPHAL CHEMOTROPISM AND PATHOGENESIS

TANYA SHARMA

Thesis submitted to the University of Ottawa

in partial fulfillment of the requirements for the degree of

Doctor of Philosophy

Department of Chemistry and Biomolecular Sciences

Faculty of Science

University of Ottawa

Supervised by: Dr. Michele Loewen

Co-Supervisor: Dr. John Pezacki

ABSTRACT

Fusarium head blight is one of the devastating diseases of cereal crops caused by *Fusarium graminearum*. This fungal pathogen produces mycotoxins like deoxynivalenol (DON), depositing it in wheat kernels and making them unfit for consumption. In addition, it causes decreases in the nutritional content of the wheat. Since wheat contaminated with DON above permissible levels must be discarded, it also leads to huge economic losses to the farmers. Fungi have a complex network of hyphae that lets them sense their surroundings. These are advantageous for nutrition and pathogenesis needs. Fungi have evolved nuanced mechanisms to orient hyphae towards external cues. Through our studies described in Chapter 2, we have elucidated the role of Ste3 GPCR in mediating fungal chemotropism towards peroxidases (previouly shown for Ste2). Both of these receptors were shown to activate the CWI-MAPK pathway in response to peroxidases. In addition, pathology assays on germinating wheat coleoptiles and detached Arabidopsis leaves showed that a Ste3 knockout strain was significantly compromised in its' ability to cause lesion development. In Chapter 3, we investigated the heterodimerization between *Fg*Ste3 and *Fg*Ste2 in response to peroxidase and a potential HRP-derived ligand of fungal origin. BRET and pull-down experiments confirmed the interaction. Chapter 4 consists of ongoing projects that go beyond the scope of the timeline for this dissertation. This includes establishing an *Sf21* insect cell expression platform for the expression and purification of full length *Fg*Ste3 with a goal to elucidate the structure of the protein. Together these studies enhance our understanding of the mechanistic aspects of fungal pathogenesis and represent a step forward toward the development of novel anti-fungal compounds.

Co-Authorship

Chapter 2 is co-authored with Dr. Pooja Sridhar, Christopher Blackman, Simon. J Foote, Dr. John S. Allingham, Dr. Rajagopal Suramaniam and Dr. Michele C. Loewen published as:

Sharma, T. *et al*. *Fusarium graminearum* Ste3 G-Protein Coupled Receptor: A Mediator of Hyphal Chemotropism and Pathogenesis. mSphere 7, (2022). Contributions: T.S. planned and carried out most of the experiments, analyzed and interpreted the data, and wrote the first draft of the paper. P.S. performed the coleoptile assays. C.B. performed the wheat head pathology assays and processed the whole-genome sequencing results. S.F. processed the transcriptomic data. G.S. helped plan the CRISPR experiment and the pathology assays and validated interpretations of the results. J.S.A. contributed to designing some experiments and contributed to interpretation of some of the results. M.C.L. conceived the idea, obtained the funding, oversaw the planning of experiments, interpreted the data, and helped write the final version of the paper. All co-authors edited the manuscript.

Chapter 3 is co-authored with Robert Jomphe, Dongling Zhang, Dr. Ana Megastheles, Dr. Michele C. Loewen. T. S. planned and carried out most of the experiments, analyzed and interpreted the data, and wrote the first draft of the paper. R.J. contributed to designing the BRET experiments and methodology and helped with preliminary experiments. D. Z. and A. M. contributed to confocal microscopy imaging. M.C.L. conceived the idea, obtained the funding, oversaw the planning of experiments, interpreted the data, and helped write the final version of the manuscript.

Chapter 4 – Section 1 is co-authored with Pooja Sridhar, Idin Lantz, John A. Allingham and Michele C. Loewen. T.S planned and carried out most of the experiments, analyzed the data. P.S. carried out initial optimizations for insect cell expression system using *Fg*Ste2. I.L. helped running experiments. J.A.L. contributed to interpreting data and M.C.L. obtained funding and oversaw the implementation of the experiments.

Chapter 4 - Section 2 is co-authored with Leann M. Buhrow, Ziying Liu, Dustin Cram, Tanya Sharma, Nora A. Foroud, Youlian Pan & Michele C. Loewen and published as:

Buhrow, L. M. *et al*. Wheat transcriptome profiling reveals abscisic and gibberellic acid treatments regulate early-stage phytohormone defense signaling, cell wall fortification, and metabolic switches following Fusarium graminearum-challenge. BMC Genomics 22, 1–21 (2021). Contributions: L. M. B. performed all experiments, as well as contributed to the design of experiments, data analysis, interpretation and writing of the manuscript. Z.L. and D.C. contributed to data processing and analysis. T.S. contributed to analysis of the fungal data. N.A.F. contributed to methods development, data analysis and writing of the manuscript. Y.P. contributed to data processing, analysis, interpretation and writing of the paper. M.C.L. conceived of the idea and contributed to experimental design, data analysis and interpretation and writing of the manuscript.

Acknowledgements

I would like to thank my family, my mom, Veena Sharma, for believing in me and supporting me in my endeavors to move abroad for completing my PhD.
My dad, Guru Dutt Sharma, my brother Chetan Sharma, my grandparents, Jaswant Rai Sharma and my grandmother Shobha Sharma.

A special thanks to my mentors through the journey without whom this wouldn't have been possible, my supervisor for funding and guidance, Dr. Michele Loewen. Dr. Gopal Subramaniam for his help and advice along the project as well. In addition, my other TAC members, Dr. Chris Boddy, Dr. Natalie Goto and Dr. John Pezacki.

To my other friends, Surbhi for always being there to chat and listen and offer perspective. Thanks to Amar for always pushing and motivating me. To my friends, Akshaya, Anupam, Stuti, Shresth, Sujay, Vineetha for making Ottawa fun and with all our memorable trips!

Last but not the least, some of my amazing lab members and forever friends. Kelly for always looking out for me and baking amazing cookies! Zee for sharing his wisdom, Pooja for tremendous help with anything that I needed to learn, Fang and Nadia for their help. I was lucky to work with hard working undergrads who helped me along this project. Robert Jomphe, Idin Lantz, Audrey Bahia.

This is Dedicated to my Family

Table of Contents

List of Figures

List of Tables

List of Abbreviations

5 HT	5-hydroxytryptamine receptors
ABA	Abscisic acid
AC	Adenylyl cyclase
AMP	Adenosine monophosphate
ANG	Angiotensin
ASK	Apoptosis signal-regulating kinase
ATF1	Activating transcription factor 1
ATP	Adenosine triphosphate
BCAA	Branched chain amino acid
BEVS	Baculovirus expression vector system
bHLH	Basic helix-loop-helix
BLAST	Basic Local Alignment Search Tool
BRET	Bioluminescence resonance energy transfer
cAMP	Cyclic adenosine monophosphate
CaSR	Calcium-sensing receptor
CCFC	Canadian Collection of Fungal Cultures
CGIAR	Consultative Group for International Agricultural Research
CHS	Chitin synthases
CHS	Cholesteryl Hemisuccinate Tris Salt
CMC	Carboxymethyl cellulose
CRD	Cysteine-rich domain
CWI	Cell wall integrity
CYP	Cytochromes P450
CYPOR	Cytochrome P450 oxidoreductase
DAPG	2,4-diacetylphloroglucinol
DDM	Dodecyl-β-D-maltoside
DEG	Differentially expressed genes
DI	Disease Index
DNA	Deoxyribonucleic acid
DON	Deoxynivalenol
DSC	Differential scanning calorimetry
ECL	Extracellular loops
EDTA	Ethylenediaminetetraacetic acid
ETI	Effector triggered immunity
Fg	Fusarium graminearum
FHB	Fusarium head blight
FOA	Food and Agricultural Organization
FPP	Farnesyl pyrophosphate

GABA	Gamma-aminobutyric acid
GAL	Galactose
GPD	Glyceraldehyde 3-phosphage dehydrogenase
GAP	GTPase-activating protein
GDP	Guanosine diphosphate
GEF	Guanine exchange factor
GIV1-5	GPCR important for virulence 1-5
GPA1	G-protein α protein 1
GPA2	G-protein α protein 2
GPCR	G-protein coupled receptor
GPMK1	Gibberella pathogenicity MAP kinase 1
GTP	Guanosine triphosphate
HEPES	4-(2-hydroxyethyl)-1-piperazineethanesulfonic acid
HOG	High osmolarity glycerol
HRP	Horse radish peroxidase
Hyg	Hygromycin
IAA	Indole-3-acetic acid
ICL	Intracellular loop
IE	Ionylideneethane
IPM	Integrated pest management
IPP	Isopentenyl diphosphate
JA	Jasmonic acid
LCP	Lipidic cubic phase
Leu	Leucine
MALS	Multi-angle light scattering
MAP	Mitogen activated protein
MAPK	Mitogen-activated protein kinase
MAPKK	Mitogen-Activated Protein Kinase Kinase
MAPKK	Mitogen activated protein kinase kinase
MAPKKK	Mitogen-Activated Protein Kinase Kinase Kinase
MAT	Mating type
MFS	Major facilitator superfamily
mGluR	Metabotropic glutamate receptors
MGV1	MAPK for growth and virulence
MKK1	Mitogen activated protein kinase kinase
MOI	Multiplicity of Infection
MVA	Mevalonic acid
Nluc	Nano Luciferase
NOX	NADPH oxidase
NR	No reporter

ORF	Open reading frame
PAGE	Polyacrylamide gel electrophoresis
PAMPs	Pathogen-associated molecular pattern molecules
PBS	Phosphate-buffered saline
PCA	Principal component analysis
PCR	Polymerase chain reaction
PDA	Potato Dextrose Agar
PEG	Polyethylene glycol
PSGWAY	Pre-stabilization of a GPCR by weak association
pHc	Cytosolic pH
PKA	Protein kinase A
PKS	Polyketide synthetase
PLC	Phospholipase C
PMSF	Phenylmethylsulfonyl fluoride
PPI	Protein-protein interaction
PTM	Post translational modifications
RAS1	Homologous to RAS proto-oncogene 1
RGS	Regulator of G protein signaling
Rho	Ras homologous
RLU	Relative luminescence units
RNA	Ribonucleic acid
ROS	Reactive oxygen species
RQ	Relative quantification
RT	Room temperature
SA	Salicyclic acid
SDS	Sodium dodecyl sulfate
SEC	Size exclusion chromatography
SHD	Spa homology domain
SPK	Spitzenkörper
SR	Synthetic raffinose
TEV	Tobacco Etch Virus
TF	Transcriptional factor
TM	Trans membrane
TMD	Transmembrane domain
TOR	Target of Rifampicin
TORC	Target of rapamycin complex
Ura	Uracil
VFTM	Venus flytrap module
WSD	Web of Science database
WT	Wildtype

YFP	Yellow fluorescent protein
YPD	Yeast Extract–Peptone–Dextrose

Chapter 1

Introduction

Fusarium graminearum is a fungal phytopathogen and one of the primary causes of Fusarium head blight (FHB), a destructive disease that affects several crop species such as wheat, barley, oat, and maize. FHB is characterized by bleached or discolored spikelets, shrunken or deformed kernels with the presence of fungal mycelium or spores on them[1]. The infected kernels are unsuitable for consumption due to contamination with toxic compounds produced by the fungus, particularly trichothecene mycotoxins like deoxynivalenol (DON; aka vomitoxin). When wheat contaminated with DON is consumed by humans or livestock, it leads to nausea, mycotoxicosis and in severe cases death. Most of the crops that have DON above the permissible levels (2 mg/kg for adults and 1 mg/kg for adolescents) are discarded leading to annual losses of at least $100 million to farmers in Canada alone[2].

1.1 Taxonomic classification of *Fusarium graminearum*

F. graminearum, also known as the wheat scab fungus or ear rot fungus, belongs to the kingdom Fungi and the phylum Ascomycota. Within the Ascomycota phylum, it falls under the class Sordariomycetes and the order Hypocreales[1]. The family it belongs to is Nectriaceae, and the genus is *Fusarium*. *Fusarium graminearum* is the species name for this particular fungus.

1.1.2 Life cycle of *Fusarium* and symptoms of Fusarium Head Blight (FHB)

F. graminearum (*Gibberella zeae)* are two different names for the same fungus. Fusarium produces ascospores within perithecia, which develop on plant debris or infected cereal spikes

from the previous season. Ascospores are then released in the spring and can infect nearby cereal spikes. *F. graminearum* also produces conidia, which are abundant and dispersed by wind and rain, providing a source of infection for the next crop. The ascospores, which are formed inside the ascus are generally larger and more robust than the conidia and can survive for longer periods[4]. Spores survive best at temperatures between 5°C and 15°C and pH values between 6 and 7.5.

The life cycle of *F. graminearum* is classified as hemibiotrophic. A hemibiotroph organism colonises the host in two phases. First, it establishes and grows hyphae intracellularly on the host with no visible disease symptoms. As the mycelia grows inside the host cells, it transitions into a necrotrophic phase resulting in DON production and shriveled kernels commonly known as "tombstone kernels". The fungus colonizes susceptible tissues such as the adaxial surfaces of the lemma and palea of the florets, exposed anthers, stomata, and the base of the wheat glumes, where the epidermis and arenchyma have thin walls[5].

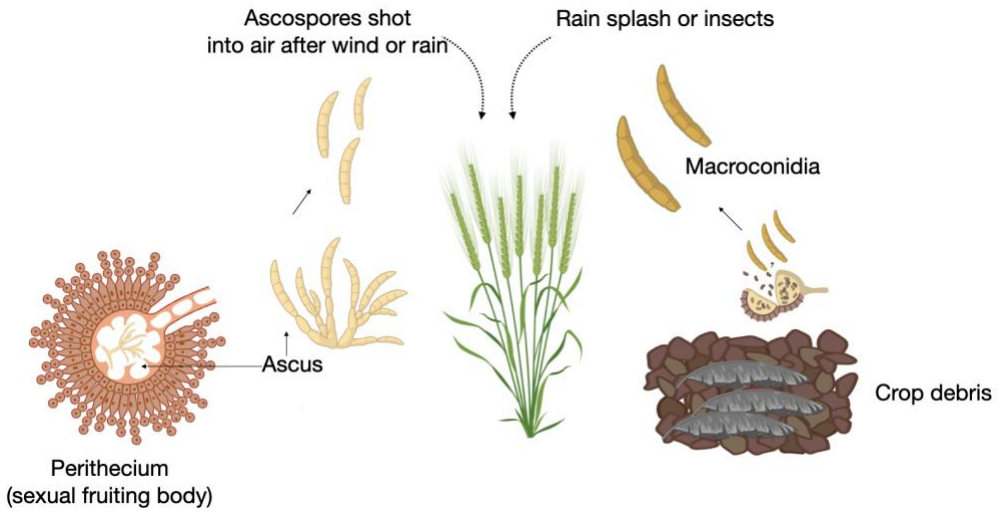

Figure 1-1. Life cycle of *F. graminearum*. *F. graminearum* during its overwintering period, resides on crop residues that are infested such as corn stalks, wheat straw, and other host plants. On these infested residues, the fungus generates spores known as macroconidia or under warm,

humid, and wet conditions, the fungus transitions to its sexual stage, referred to as *Gibberella zeae*, which develops on the infested plant debris.

The MAT locus, or the mating-type locus, is a genetic region in fungi that determines the sexual compatibility and mating behavior of the organism. The MAT1-1 and MAT1-2 loci are involved in the recognition and fusion of sexual spores during mating. Homothallism refers to a mating system in fungi where a single individual possesses both the male and female reproductive structures, allowing self-fertilization. In other words, homothallic fungi can reproduce sexually without the need for a compatible mating partner[3]. In homothallic *F. graminearum*, all MAT1 genes are found within a single nucleus, whereas *Fusarium oxysporum* is asexual in nature where separate cells containing MAT1-1 genes and MAT1-2 genes are found (**Figure 1-2**).

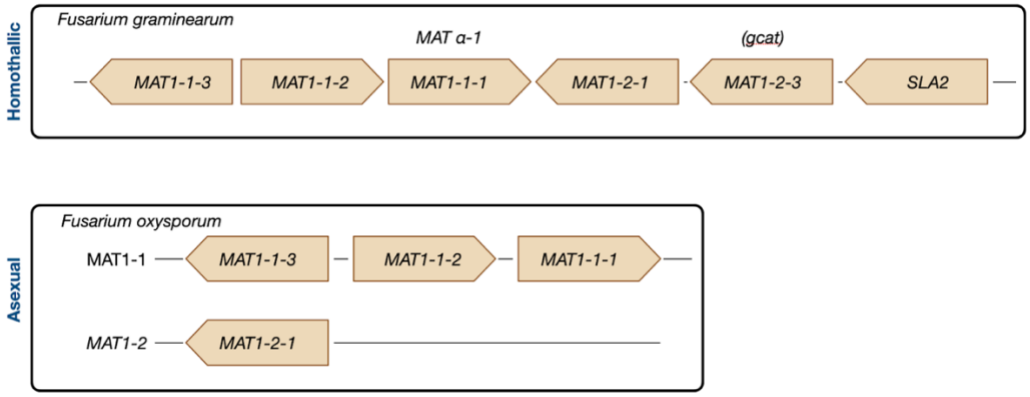

Figure 1-2. Mating type locus (MAT) in Fusarium species. The positioning of idiomorphs MAT1-1 and MAT1-2 at the MAT1 locus is depicted for two of *Fusarium* species: homothallic (*F. graminearum)* and asexual (*Fusarium oxysporum*). The arrows depict the direction of transcription.

1.1.3 Past incidences of FHB outbreaks

FHB has been reported in many regions of the world, including Asia, Europe, North America, South America, and Australia[6]. The prevalence of this disease is a significant concern in many parts of the world, including Canada and its trading partners. Though first detected on the Canadian prairies in Manitoba in 1923, it remained innocuous for many decades. Since then, there have been 3 major FHB epidemics in Canada with humid weather accentuating its severity. A rise in the scientific community focusing on FHB research has been observed highlighting the growing concern (**Figure 1-3A**). The first major outbreak in Manitoba occurred in 1993 with severe yield and quality losses[7]. Since then, estimates suggest that losses in Canada have ranged from $50 million to $300 million annually. Direct and secondary economic losses due to FHB for all crops in the Northern Great Plains and central USA were estimated to be $2.7 billion from 1998 to 2000 alone[7].

A recent survey in Canada spanning from 2001 to 2017 revealed 11 FHB epidemic years where the disease was present in more than 90 % of surveyed spring wheat fields across the country, with an average disease index (DI) of 5.3 % to 27 %, as compared to 0.02 % to 3.7 % in non-disease years (DI = (Disease incidence*Disease severity)/100). The report from the Canadian grain commission shows the spread of disease from central to Western provinces (Alberta and British Columbia) and a subsequent trend of increased DON production in wheat kernels (**Figure 1-3B, 3C**)[2]. Aberrant global climatic conditions will likely increase the chances of this happening more frequently.

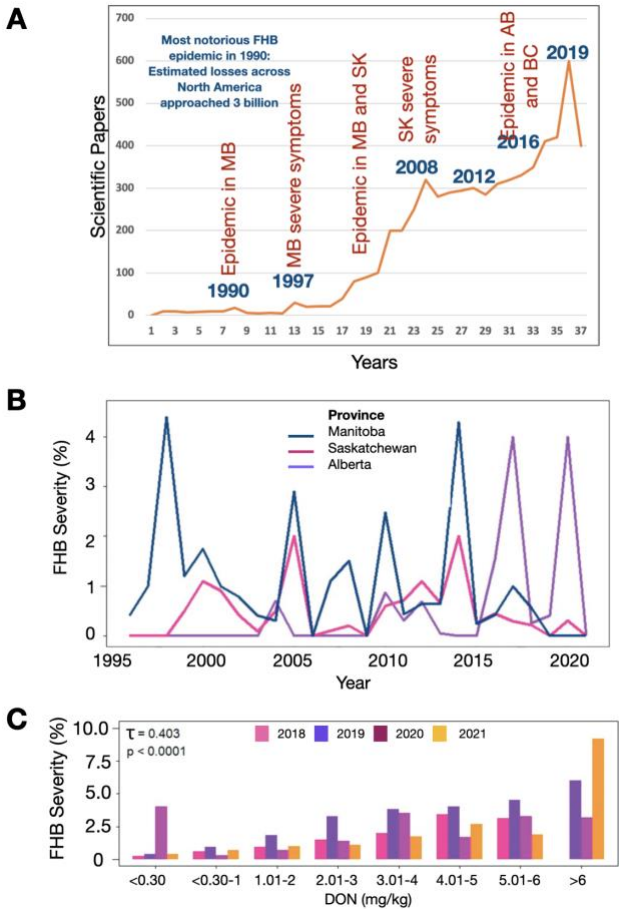

Figure 1-3. Spread of FHB infection in Canada. A) The scientific papers from the Web of Science database (WSD) from 1985 to 2020 reveal the progression and historical development of FHB in Canada. This development can be categorized into three phases: (i) a period of slow growth spanning from 1985 to 1996, (ii) a phase of exponential growth between 1991 and 2007, and (iii) a period of extensive growth from 2008 to 2016. (Adapted from Powell and Vujanovic 2021)[8]. B) The severity of FHB in wheat from 1995 to 2021 was described as % of Fusarium damaged kernels or FDK (per kg of produce) from 1995 to 2021 across western Canadian provinces for Alberta, Saskatchewan, and Manitoba. (Source: Canadian grain commission, 2022.)[2] C) Percent FHB severity associated with DON (mg/kg) in wheat samples from 2018 to 2021 for all classes of wheat. Bars represent the percent of FHB severity. Kendall's tau correlation coefficient (τ) and p-value (p) for the relationship of FHB severity and DON for each wheat classes are shown on the upper left of each plot. (Adapted from Chin *et al.*, Canadian Journal of plant pathology, 2023)[2].

1.1.4 FHB mitigation strategies

Several methods that can be used to control Fusarium head blight (FHB) infection include the following. i) Fungicides: Fungicides are used to protect wheat and barley spikes from FHB infection. Triazole-based fungicides are commonly used. For example, triazole fungicides such as tebuconazole and prothioconazole have been shown to reduce FHB symptoms in wheat and barley in laboratory studies[9]. Strobilurin fungicides, such as azoxystrobin, have also shown some efficacy against FHB in laboratory and field trials[10]. ii) Biological control agents: Several biological control agents have been developed to control FHB, including phages, fungi, and bacteria[11]. These agents can be applied as seed treatments or foliar sprays to control FHB. Several microorganisms have been reported to be effective in controlling FHB. These include *Clonostachys rosea*, *Trichoderma spp*., *Bacillus spp.*, *Pseudomonas spp*., and *Streptomyces spp*[12]. These microorganisms produce antibiotics or compete for nutrients and space with the pathogen, thereby reducing its growth and colonization. iii) RNA interference: RNA interference (RNAi) is a promising biocontrol strategy for controlling FHB. It involves the use of small RNA molecules to silence specific genes in the fungus, thereby reducing its virulence and growth[13]. For example: The silencing of the *Fg*AGO and *Fg*DCL genes has improved resistance in Barley[14]. iv) Genetic resistance: Developing wheat cultivars with genetic resistance to FHB is a long-term solution to control FHB infections. Researchers are working to identify and breed wheat cultivars with improved resistance to FHB. For instance: DT2009, DT2005 cultivars developed at Agriculture and Agri-Food Canada have shown higher natural resistance[15]. v) Crop rotation: Avoid planting cereals in fields with a history of FHB. Rotation with non-host crops can help reduce the inoculum levels in the soil[16]. vi) Integrated pest management (IPM): Using a combination of the above methods, along with monitoring and forecasting tools, can help manage FHB in a sustainably and effectively. It should

be noted that the use of fungicides alone is not sufficient to control FHB, and usually a combination of scientific and cultural management strategies is recommended for effective control of the disease.

1.2 G-protein Coupled Receptors

G-protein coupled receptors (GPCRs) form a diverse family of transmembrane proteins representing the largest family encoded in the human genome. They have been identified in yeast and choanoflagellates. It is believed that they evolved from microbial rhodopsins that function as H+ pumps for cation or anion channels, as Na^+ or Cl^- pumps or as photosensors[17]. In eukaryotes, these GPCRs have a wide range of functions, including vision, taste, olfaction, hormone signaling, and neurotransmission, making them important targets for drug development. About ~ 45 % of approved drugs target these receptors due to their surface location and significance in mediating important cellular functions[18–20].

The structure of GPCRs consists of a single polypeptide chain that spans the cell membrane seven times (thus being called serpentine receptors), creating an extracellular N-terminal domain, seven transmembrane segments forming a bundled transmembrane domain, three intracellular loops, and three extracellular loops. They recognize various ligands such as small molecules, peptides, and lipids. A ligand is a molecule that interacts with the receptor and triggers a cellular response. Upon ligand binding, GPCRs undergo conformational changes that activate downstream signaling pathways, typically involving G proteins[21]. The ligand interacts with specific amino acids, such as serine, threonine, and arginine residues, among others, forming hydrogen bonds, van der Waals interactions, and electrostatic interactions. The binding site of a GPCR is highly

specific to its ligand, allowing for selective recognition and activation. Even subtle structural differences in ligands can result in varying affinities and activation of different GPCRs.

GPCRs have been categorized into 6 major classes based on sequence homology and functional similarity. Class A (Rhodopsin-like): A variety of receptors in this class have high sequence identity and similar activation mechanism to Rhodopsin receptor. Examples include receptors for adrenaline, dopamine, serotonin, and histamine. This is the largest family consisting of about 719 GPCRs[22]. Most family A GPCRs feature a disulfide bridge linking the E2-loop and the upper portion of TMIII, and a palmitoylated cysteine at the C-terminus. A few highly conserved residues, such as the DRY motif, have been identified in this receptor class. Ligands for biogenic amine receptors typically bind between the transmembrane domains of the receptor, whereas the binding site for peptide and glycoprotein hormone receptors is found between the N-terminus, extracellular loops, and upper transmembrane domains. It includes receptors that are activated by a variety of ligands, such as neurotransmitters, hormones, and odorants. Class B (Secretin-like): It includes receptors for peptides such as calcitonin, secretin, and parathyroid hormone. These receptors are distinguished by their long N-terminus, which contains three conserved disulfide bridges. Additionally, a disulfide bridge connects the extracellular loop E2 and the upper portion of transmembrane domain III. Typically, ligands for family B GPCRs bind between the long N-terminus and the extracellular loops. These receptors are involved in regulating processes such as cell adhesion and migration. Class C (Metabotropic glutamate/pheromone receptors): Presently 22 receptors have been recognised. This class includes receptors that are activated by amino acids, such as glutamate and GABA, and also includes receptors for pheromones. These receptors are involved in processes, such as synaptic transmission, learning, and memory. Examples of GPCR belonging to family C include metabotropic glutamate receptors (mGluR), gamma-aminobutyric

acid type B (GABAB), and calcium-sensing receptors (CaR). Class C GPCRs are typically characterized by a long N-terminus and C-terminus, as well as a disulfide bridge connecting the extracellular loop E2 with the upper part of transmembrane domain III. The ligand binding site of family C GPCRs is formed by a venus flytrap module (VFTM), which is connected to the transmembrane domain I by a cysteine-rich domain (CRD)[23]. They are known to form homo and heterodimers. Class D (Fungal mating pheromone receptors): This class includes receptors Ste2 and Ste3 that are found in fungi and are involved in regulating mating behaviors. Agonist binding to the inactive state of Ste2 causes a reorientation of the extracellular end of H5 to facilitate ligand binding, an outward movement of the extracellular end of H6 and a shift of ECL3. Class E (Cyclic AMP receptors): These are exclusively found in *Dictyostelium species*. This class includes receptors that are activated by cyclic AMP, a signaling molecule that is involved in a variety of processes, such as cell growth and differentiation. There are currently no structures resolved for Class E receptors. Class F (Frizzled/smoothened receptors): This class includes receptors that are involved in the Wnt and Hedgehog signaling pathways, which are important for regulating embryonic development and tissue homeostasis[19,24,25].

1.2.1 GPCR Signal transduction

The activation mechanism of GPCRs involves ligand binding to the receptor's extracellular domain, causing conformational changes that propagate through the receptor and trigger intracellular signaling pathways (**Figure 1-4**). The change in conformation allows the receptor to interact with and activate a heterotrimeric G-protein, which is bound to the intracellular portion of the receptor.

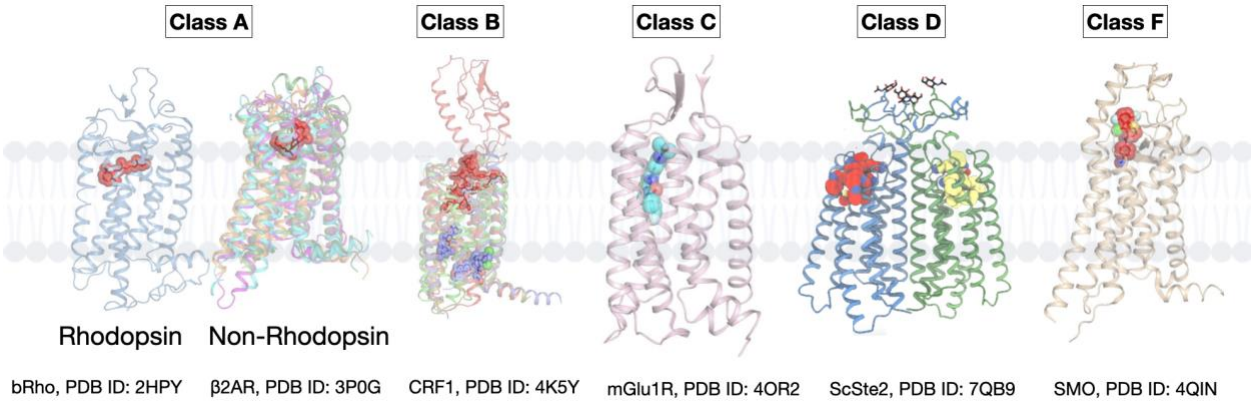

Figure 1-4. Ligand binding sites across different classes of GPCRs. The diverse ligand-binding sites of G-protein-coupled receptors (GPCRs) belonging to classes A, B, C, D and F are illustrated with their examples and PDB ID through crystal structures of representative GPCR-ligand complexes. Within these complexes, agonists are depicted as red and yellow sticks, antagonists as purple sticks, and negative allosteric modulators as a light blue stick model (Adapted from Basith *et al.,* 2019, Frontiers in Pharmacology[26]).

In humans, the heterotrimeric G-protein family consists of three subunits: α, β, and γ. Upon GPCR activation, α dissociates from βγ and activates the signaling cascade. GPCRs can interact with different Gα subunit types (Gαs, Gαi/o, Gαq, and Gα12/13). Gαs stimulates adenylyl cyclase (AC) to produce cAMP, activating protein kinase A (PKA). Gαi/o inhibits AC, reducing cAMP levels. Gαq activates phospholipase C (PLC), generating IP3 and DAG. These pathways regulate cellular physiology. The regulation of GPCRs is also tightly controlled by a variety of factors, including ligand concentration, receptor desensitization (response of the receptor to a ligand is decreased over time, even in the presence of constant ligand concentration), and receptor trafficking (movement of GPCRs between different cellular compartments, such as the plasma

membrane and intracellular vesicles). Ligand concentration can affect the activation of GPCRs by altering the number of ligand-receptor complexes that are formed[27–29].

1.2.2 Functional selectivity for different ligands

Functional selectivity is a phenomenon observed in GPCR signaling, where different ligands can activate the same receptor but trigger different downstream signaling pathways or responses. Functional selectivity is an important concept in GPCR pharmacology, allowing for the development of drugs with greater selectivity and efficacy, and with fewer side effects. This phenomenon has been observed in various GPCRs, such as serotonin receptors like 5-HT2A, 5-HT2C, and 5-HT1A[30,31]. While traditional agonists can activate multiple downstream signaling pathways, biased agonists selectively stabilize specific receptor conformations, promoting certain intracellular signaling circuits and resulting in pathway-specific biological responses. This suggests an ability of biased agonists to preferentially activate specific effector pathways by modulating receptor conformations differently than unbiased ligands.

With the discovery of biased agonists, it has become clear that drugs can be designed to selectively activate certain downstream signaling pathways while avoiding others, leading to more precise and efficient therapies with fewer side effects. For example, the opioid receptor is a GPCR that mediates pain relief, but its activation can also lead to side effects such as respiratory depression, constipation, and addiction[32]. The traditional opioid drug morphine activates both G-protein $G\alpha_i$ and $G\alpha_o$ and β-arrestin pathways, leading to both analgesic effects due to G-protein activation and the side effects due to β-arrestin recruitments which leads to receptor internalization promoting desensitization [33]. However, a biased agonist called TRV130 has been developed, which

selectively activates the G-only protein pathway while minimizing β-arrestin signaling[34]. This results in potent pain relief without the typical side effects associated with opioid use.

1.2.3 Class D Fungal GPCRs

Class D GPCRs, also known as fungal pheromone receptors, are a distinct family of GPCRs found in fungi. Class D GPCRs have a unique structure compared to other GPCRs, with a large extracellular N-terminus and a relatively short intracellular C-terminus[35]. Fungal GPCRs are categorized into ten categories based on sequence alignment and structural similarity. Among these categories, the classical fungal GPCRs consist of Pheromone receptors (classes I and II): Classes I and II include GprA (PreB) and GprB (PreA), which are similar to the yeast pheromone receptors Ste2 and Ste3, and function in self-fertilized sexual development[36,37]. Carbon receptors (Class III): It includes GprC, GprD, and GprE receptors that might be involved in carbon source sensing based on their high similarity to the *Saccharomyces cerevisiae* Gpr1 receptor[38]. Nitrogen receptors (Class IV): These includes GprF and GprG, which are similar to the *Schizosaccharomyces pombe* Stm1 receptor, and the nutrient sensor Stm1-like proteins. The Stm1 receptor senses the cell's nutritional state, thereby driving the cells to enter meiosis when encountering nutritionally deficient conditions. cAMP receptor-like receptors (Class V): Class V includes GprH and GprI, which are similar to the *Dictyostelium discoideum* cAMP receptor cAR1 and thus have been proposed to be involved in cAMP sensing[39]. Microbial opsin receptors (Class IX): It included Nop-1 and Orp-1[40]. The focus of this dissertation is limited to the Pheromone receptors (classes I and II). Due to their crucial role in fungal sexual reproduction and surface localization, Class D GPCRs have been studied as potential targets for antifungal drugs.

1.2.4 GPCR homodimerization/heterodimerization and modulation of receptor function

GPCR homodimerization and heterodimerization refer to the formation of complexes between two GPCRs of the same or different types, respectively. This process can modulate receptor function by altering ligand binding, signaling pathway activation and receptor trafficking. For example: The homodimerization of Ste2 in *Saccharomyces cerevisiae* is important for several aspects of its function like efficient binding of the α factor ligand and the activation of downstream signaling pathways[41]. Its formation relies on the conserved GXXXG motif in the TM segment (**Figure 1-5**)[42]. GXXXG motifs are short conserved sequences of amino acids commonly found in the transmembrane regions of GPCRs[43]. They are characterized by the presence of two glycine (G) residues separated by variable amino acids (X). This motif plays a crucial role in facilitating GPCR dimerization and oligomerization more broadly. GXXXG motifs can be found in different transmembrane I domains of various GPCRs. This motif has also been identified in the Ste3 receptor in TM3 (IVI**KL**QV**GA**NI**GI**SC**A**VTNIIYNL). Adjacent residues surrounding the GXXXG motif contribute additional binding energy. Efficient interaction of GXXXG motifs occurs when they are positioned at a similar "depth" in the membrane, as determined by their location within the linear sequence of the TM domain. Other motifs in TM domains may also be crucial for GPCR oligomerization. Indeed, leucine-rich or serine/threonine-rich motifs are known to drive the assembly of dimers/oligomers in other transmembrane proteins[43].

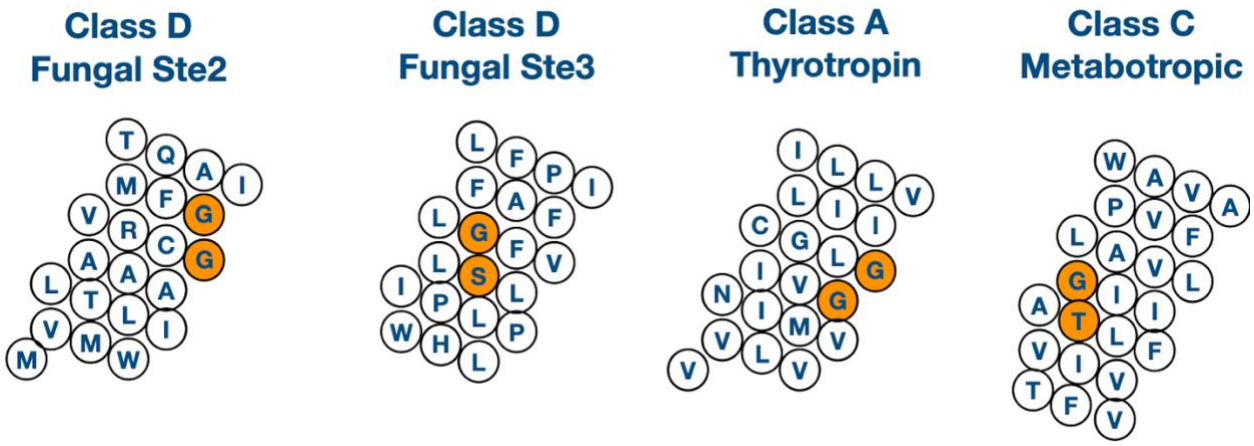

Figure 1-5. The presence of a GXXXG motif or its variations in the first transmembrane domain (TM1) of GPCRs. Helical bundles were constructed for each class of GPCR using information gathered from the GPCR database (www.gpcr.org). The fungal ones represent corresponding receptors from *S. cerevisiae*. In these helical bundles, the consensus sequence for TM1 in each GPCR class was utilized. The top of the helix represents the N terminus, while the bottom represents the C terminus. Within this arrangement, there are GPCR subfamilies in which the TM1 consensus sequence contains a sequence that matches a typical GXXXG motif or variations, as defined by the consensus sequence (AGSTP)XXX(GAS), which is indicated in orange. The single-letter amino acid code is employed in this representation.

Heterodimerization in human GPCRs has been well documented and is known to involve cysteine residues. For example, heterodimerization of glutamate and CaSR occurs via disulphide linkage between cysteine residues of the N-terminal regions. Upon mutations in cysteine 140 (Cys140), significant increases in monomers were observed[44]. As well, the extracellular amino-terminal domain plays a critical role in the dimerization of glutamate receptors and CaSRs, as well as the homodimerization of the bradykinin 2 receptor (B2R).

Functionally, heterodimerization can result in the emergence of novel signaling pathways not activated by either receptor individually. For example, bradykinin B2 and angiotensin AT1 receptors form heterodimers and these receptor pairs exhibit a change in the type of G-proteins they are coupled from Gq to Gi upon heterodimerization, in contrast to their behavior when they form homodimers[45].

To date, no GPCR heterodimers have been identified for fungal Class D receptors. In the case of *Fg*Ste2 and *Fg*Ste3, both activate the CWI-MAPK pathways on exposure to peroxidase and mediate peroxidase linked chemotropism[46,47]. Genetic studies and biochemical analysis in *S. cerevisiae* have demonstrated that Ste2 and Ste3 are coupled to the same heterotrimeric G-protein, composed of Gpa1/Scg1 (Gα) and Ste4-Ste18 (Gβγ), and engage the same downstream components[48].

1.3 Intracellular signaling pathways found in *Fusarium*

The MAP (mitogen-activated protein) kinase-type pathway is one of the major signaling pathways that is involved in a wide range of cellular processes, such as cell growth, differentiation, proliferation, and apoptosis in fungi. MAP kinases are a family of serine/threonine kinases that are activated by various extracellular stimuli, including growth factors, cytokines, and stress signals[49].

The MAP kinase pathway (**Figure 1-6**) is typically initiated by the activation of cell surface receptors, such as receptor tyrosine kinases or GPCRs, which activate intracellular signaling cascades. They are composed of three kinases: MAP kinase kinase kinase (MAPKKK), MAP kinase kinase (MAPKK), and MAP kinase (MAPK). The canonical MAP kinase pathway involves the activation of the Raf-MEK-ERK signaling module, where MAPKKK activates MAPKK, which in turn activates MAPK. Upon activation, MAPK translocates into the nucleus and

phosphorylates various transcription factors, leading to changes in gene expression and cellular responses. The MAP kinase pathway is tightly regulated to ensure appropriate cellular responses and dysregulation of this pathway has been implicated in numerous diseases, including cancer, autoimmune disorders, and neurodegenerative diseases[50,51]. Three kinds of MAPK pathways are described here, in addition to other signaling pathways that also exist in Fungi.

1. cAMP-PKA signaling

Adenylyl cyclases are responsible for catalyzing the conversion of ATP to cyclic adenosine mono phosphate (cAMP) under normal circumstances. In many *Fusarium* species, the defects of adenylyl cyclase deletion mutants can be partially restored by exogenous cAMP. Exogenous cAMP has been shown to modulate branching and DON production in *F. graminearum*[52]. The degradation of intracellular cAMP is mediated by cAMP phosphodiesterases (PDE) in eukaryotic organisms. In *F. graminearum*, two PDEs (PDE1 and PDE2) have been identified and have overlapping functions in growth, conidiation, sexual development, and pathogenicity[53]. However, PDE2 has a significant role in DON production by activating protein kinase A (PKA) activities through PKR. Similarly, the pkr deletion mutant, like the mutant deletion of both PDE genes, exhibits a notable decrease in pathogenicity and increased DON production in *F. graminearum*. Meanwhile, the deletion of CPK1 in *F. graminearum* results in defects in asexual and sexual developments, as well as plant infection[54].

2. Fus3/Kss1 MAPK signaling

The invasive growth (IG) pathway, also known as Fus3/Kss1 MAPK signaling, serves a general function in pathogenicity in *Fusarium* species. Apart from its role in pathogenesis, the Kss1/Fus3 pathway is generally linked to secondary metabolism and the production of cell wall degrading enzymes for host invasion. *Fg*Gpmk1 is an orthologue of Fus3/Kss1 in *Fusarium* plays

a role in regulating the early induction of extracellular endoglucanase, xylanolytic, and proteolytic activities, as well as the overall induction of secreted lipolytic activities in *F. graminearum*. The downstream targets of Gpmk1, include the transcription factors *Fg*Ste12 and *Fg*Mcm1[55,56]. *Fg*Ste12 is necessary for the secretion of cellulase and protease, which play a crucial role in infection. On the other hand, *Fg*Mcm1 is involved in the initial colonization and subsequent spread of *F. graminearum* within wheat heads by regulating the expression of pathogenicity factors[57].

3. Cell Wall Integrity (CWI) MAPK signaling

The CWI MAPK cascade is required for the remodeling of the fungal cell wall and ensures its integrity under cell wall stress. *Fusarium* has 3 MAPK orthologous to *S. cerevisiae*: the p42/22 MAPK fmk1, MAPKK ste7 and the MAPKKK ste11 that sequentially activate each other by phosphorylation. The Slt2 signaling pathway, which consists of the MAPK Slt2, MEKs Mkk1/Mkk2, and MEKK Bck1, is responsible for maintaining the cell wall integrity in yeast[58]. This function is conserved in many pathogenic fungi, including *Fusarium* species. In *F. graminearum*, disruption of the Slt2-type MAPK called Mgv1 results in heightened sensitivity to cell wall-degrading enzymes and increased temperatures. In addition this pathway also plays a role in fungal development, secondary metabolism, and pathogenicity. For instance, in *F. graminearum*, Mgv1 is required during sexual reproduction and plant infection and its disruption affects hyphal growth and increases sensitivity to peroxide stress. In *F. graminearum*, deletion of *Fg*Swi6, downstream transcription factor in the CWI pathway leads to defects in cellulose utilization, lithium tolerance, DON production, and pathogenicity. Deletion of Slt2 homologs of filamentous fungi results in defects in hyphal growth, hypersensitivity to cell wall-damaging agents, and often reduced pathogenicity against plant or animal hosts [59,60]. Apart from its role in the chemotropic response to plant signals, Mpk1 in *F. oxysporum* has also been implicated in the

response to α-pheromone as a cell density-dependent autocrine signal to control germination of conidia[61,62]. *F.graminearum* Ste2 receptor known to mediate hyphal bending towards peroxidase involves activation of the CWI-MAPK pathway.

4. High Osmolarity Glycerol (HOG) MAPK signaling

The HOG pathway in *F. graminearum* responds to high osmotic stress by phosphorylating and translocating Hog1 to the nucleus. The deletion of *Fg*HOG1 in this species results in impaired hyphal growth, perithecium formation, and DON production, as well as a reduced ability to colonize wheat heads after initial infection[63]. The downstream transcription factor Atf1, a bZIP-type protein, interacts with *Fg*Hog1 in the nucleus under osmotic stress. *Fg*Atf1 and *Fg*Hog1 are both necessary for osmoregulation and pathogenicity, and constitutive expression of *Fg*ATF1 can partially restore the defects in the *Fg*hog1 mutant[64].

5. Target of Rapamycin (TOR) signaling

The nutrient signal transduction in eukaryotic cells is significantly influenced by the TOR pathway. While two Tor kinases have been discovered in the budding yeast, most filamentous fungi have only a single Tor ortholog. In *F. graminearum*, the TOR pathway is responsible for nitrogen sensing and contributes to mycelial growth induced by glutamine. Furthermore, the pathway regulates the biogenesis of lipid droplets (LDS) through the *Fg*Pah1-Nem1-Spo7 cascade and modulates DON production via LDS biogenesis[65].

In filamentous fungi, the TOR signaling pathway is involved in the regulation of nutrient sensing, hyphal growth and morphogenesis, cell cycle regulation, and stress response[66]. The GTPases Rag1/2 and Rheb, as well as their respective repressors GATOR1 and TSC1/2, are important regulators of the TOR kinase complex 1 (TORC1) in higher eukaryotes, and they are

conserved in fungi (i.e., GTPases Gtr1/2 and Rhb1, and GAP repressors SEACIT and TSC1/2, respectively)[67].

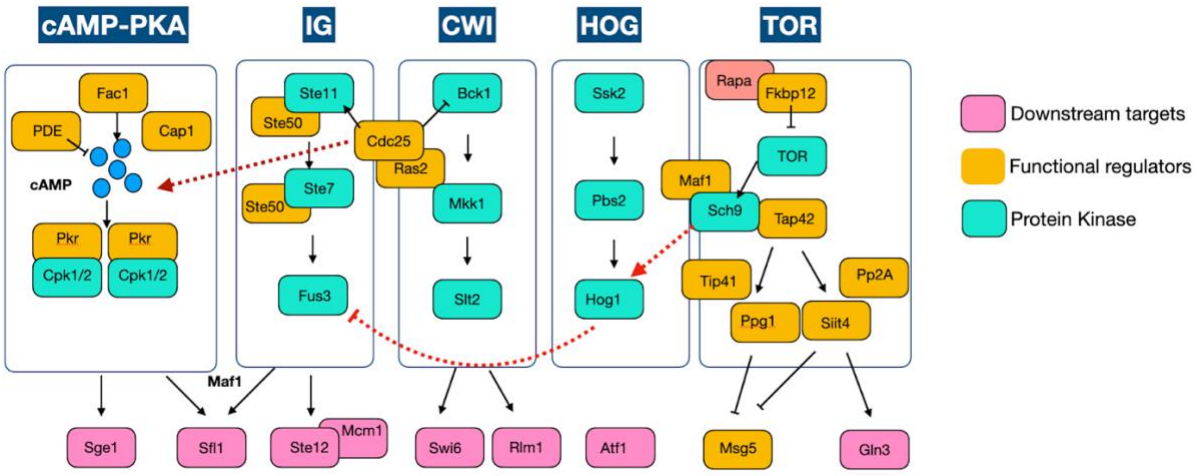

Figure 1-6. Pathways involved in infectious responses in *F. graminearum*. In Fusarium, the MAPK pathways exhibit functional cross-talk, where the activation or modulation of one pathway can influence the activity of another pathway. For instance, the CWI (Cell Wall Integrity) MAPK pathway, regulated by the MAPK Mpk1, interacts with other pathways such as the TOR (Target of Rapamycin) pathway or the cAMP/PKA (Cyclic Adenosine Monophosphate/Protein Kinase A) pathway. This crosstalk enables coordination between cell wall remodeling, nutrient sensing, and cellular metabolism, ensuring proper cell wall maintenance and growth under varying conditions.

1.3.1 *Fusarium* Ste2 and Ste3 receptors signaling

CWI-MAPK signaling pathway has been shown to be involved in *Fg*Ste2 and *Fg*Ste3 activation by peroxidase and has been extensively studied in *F. oxysporum and F. graminearum*[47,68]. The CWI-MAPK pathway is conserved in fungi and is known to be essential for virulence in a wide array of fungal species. Previous studies on *F. oxysporum* and *F. graminearum* have shown that loss of MAPK components mpk1, bck1 and mgv1 impairs hyphal chemotropism. All these components are central to the CWI-MAPK pathway in fungus (**Figure 1-**

7). This was also validated in wild type *F. graminearum* where peroxidase exposure led to an increase in phosphorylation of the Mgv1 protein. All this while Ste2 was only considered a receptor for sensing α- pheromone for mating but its new role in pathogenesis was discovered.

Recently, Vitale *et al.* showed that *F. oxysporum* cells expressing both the receptors, Ste2 and Ste3 at the same time and exhibit competitive pheromone signaling whereby the α-Ste2 interaction leads to repression of conidial germination while the a-Ste3 interaction relieves repression in a single cell in an autocrine fashion (cell produces pheromone that binds to the receptor on the same cell)[62]. Interestingly, this phenomenon also utilizes the core Rho GTPase dependent CWI- MAPK components for signaling.

In Verticillium dahlia, it was found that the homologs of the Rag GTPase Gtr1 and the GTPase-activating protein Tsc2, an activator and a repressor of the TOR kinase respectively, play important roles in hyphal chemotropism towards nutrients, plant-derived signals, and heterologous α-pheromone of *Fusarium oxysporum*[59].

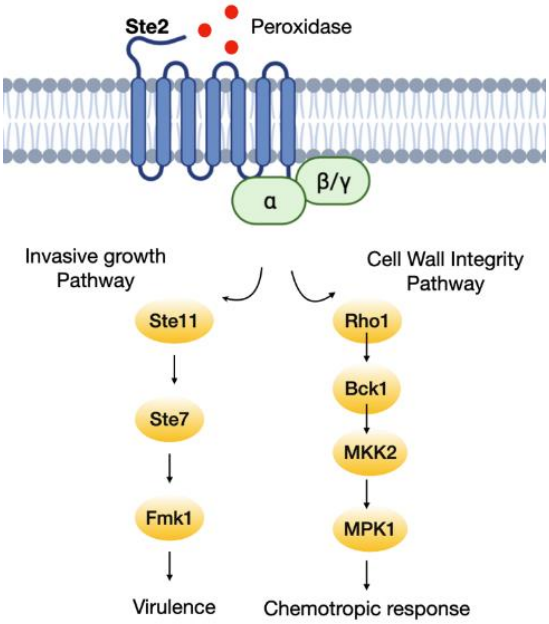

Figure 1-7. Fusarium species invasive growth and CWI-MAPK pathway. In *F. oxysporum* and *F. graminearum*, Ste2 is responsible for perceiving pheromones, nutrients, and signals from the host, thereby impacting fungal development, chemotropism, and virulence. The activation of G-proteins (depicted in orange) by Ste2 influences both the filamentous growth pathway and the cell wall integrity MAPK pathways.

1.3.2 *F. graminearum* GPCRs involved in pathogenic responses

The genome of *F. graminearum*, a plant pathogenic fungus that causes Fusarium head blight (FHB), has been sequenced and annotated. The genome is 35.9 Mb in size (PH-1 isolate)[69]. According to the current genome annotation available at the Fungal Genome Initiative, there are 123 (a few pending verification) GPCRs in the genome of *F. graminearum*[70].

There are several types of GPCRs identified that are known to be involved in infection mediated responses. For example, GIV1–GIV5 are significantly upregulated during plant infection and important for virulence[71]. It was shown that *Fg*Giv1 (a CFEM domain containing GPCR) leads to activation of both cAMP-PKA and Gpmk1 MAPK pathways suggesting potential cross-talk between them. Loss of Giv1 led to a decrease in infection cushion formation by 70% and a subsequent decrease in virulence. GIV2 is involved in cell-to-cell movement and spreading of invasive hyphae. The class X Pth11-like receptor is essential for the detection of hydrophobic surfaces and appressoria development on plant hosts[72]. Ste2 is known to be involved in mediating hyphal polarization towards host released peroxidases. Coleoptiles infected with Δ*Fgste2* strain showed a significant decrease in lesion development[68].

1.4 Fungal chemotropism

Chemotropism is defined as the growth of organisms directed by chemical stimulus gradient from outside of the organism. Chemotropism is different from chemotaxis, as chemotropism is related to directional growth, while chemotaxis is related to directional locomotion[73]. The specific molecular mechanisms underlying fungal chemotropism vary depending on the fungal species and the type of chemical signal being detected. However, generally, all involve a complex interplay between extracellular signaling molecules, membrane receptors, intracellular signaling pathways, and cytoskeletal elements that regulate cell growth and movement.

1.4.1 The history of fungal chemotropism

The term chemotropism is composed of the English word chemical and the Greek term trépomai "I turn around" and therefore designates a movement of organisms due to a chemical stimulus[74]. The first report of fungal chemotropism dates back to a century in 1866 when a German surgeon, Anton de Bary (considered the father of modern pathology) described his findings on the growth of germ tubes of the *Uromyces Appendiculatus* (rust fungus) towards stomata on bean leaves in his famous work "Comparative morphology and biology of fungi, mycetozoa and bacteria"[75]. At the same time, Pfeffer reported hyphal turning of Saprolegnia towards nutrient substances, while Brefeld suggested the presence of a "directional chemical influence'' during pairwise conjugation of adjacent *Ustilaginaceae* sporidia.[4] In breakthrough research, Miyoshi reported preferential movement of hyphae towards sugars or meat extract (positive chemotropism) as compared to other substances which led to a repelling action (negative chemotropism)[76]. He also stated that water did not affect their orientation and growth (thus acting as a solvent control)

and excess of a positive chemoattractant could lead to it acting as a repellent. Masee explored this idea further and probed the nature of these chemoattractants. He observed that obligate plant pathogens were attracted specifically by extracts from their hosts, while facultative parasites like *Botrytis* were attracted by sugars but repelled by certain plant compounds[77]. Researchers still questioned the chemoattraction theory and wondered if it was just an increase in hyphal growth speed towards the chemoattractant or a change in the growth direction. Altogether, in a broader sense, these studies paved the way for further research in this sphere and concluded that it is both hyphal attraction and avoidance that mediates the growth direction of fungi[78]. Although still in its infancy at that time, these studies broadly characterized three classes of fungal chemotropism:

1) Response to compounds released by host organisms 2) Meet nutritional requirements 3) Fungal intercommunication purposes.

1.4.2 Chemotropism in the fungal model system *S. cerevisiae*

Saccharomyces cerevisiae has served as a model organism for studying molecular mechanisms governing yeast mating[79]. Directional growth, a critical process in yeast mating, relies on the establishment of precise chemical gradients composed of peptide-mating pheromones. These gradients play a pivotal role in guiding the mating partners toward each other. To achieve this, specific cell types secrete or export the pheromones, creating concentration differences in the surrounding environment. Upon reaching the receiving cells, the pheromones undergo specific degradation processes.

Yeast populations are comprised of two haploid mating cell types: Matα and MATa. Matα cells produce α-factor pheromone (WHWLQLKPGQPMY) and responds to a-factor. MATa cells produce a-factor pheromone (YIIKGVFWDPAC) that is farnesylated on the C terminus and

respond to α-factor. During mating, pheromone gradients generated by the diffusible peptides lead to G1 cell cycle arrest followed by shmoo formation and fusion of nuclei forming Matα/MATa diploid[21,80].

GPCRs are critical for detecting these pheromones. The MAT a-cell specific Ste2p receptor which binds α-factor, and the MAT α-cell specific Ste3p receptor which binds a-factor to mediate this interaction in a paracrine fashion (reproductive mechanism in organisms where adjacent cells or individuals exchange mating pheromones that act on opposite cell type as local chemical signals to attract mating partners)[81]. The binding of the α-factor to Ste2p leads guanosine triphosphate (GTP) to bind G-Protein α subunit, Gpa1. The βγ (Ste4p and Ste18p) subunits activate the Mitogen Activated protein kinase (MAPK) signaling cascade that activates GTPase Cdc42, protein kinase Ste20 and scaffold protein Ste5 (**Figure 1-8**). Cdc42 is a key regulator of the actin cytoskeleton and plays a central role in the establishment of cell polarity. Fus3 MAP Kinase further phosphorylates the Ste12 transcription factor that leads to cellular transcription of mating genes[82,83]. The conserved transmembrane protein Prm1 and transmembrane proteins Kex2 and Fig1 cooperate to elicit plasma membrane fusion. MAPK Fus3, cell surface glycoprotein leads to cell-cell fusion promoting cell adhesions and merging of plasma membranes. Genetic studies and biochemical analysis have demonstrated that Ste2 and Ste3 are coupled to the same Gα protein[82]. Because of the relative insolubility due to farnesylation on the C terminus, difficulty in purification and the highly hydrophobic nature of the a-factor, the analysis of Ste3 has lagged behind Ste2.

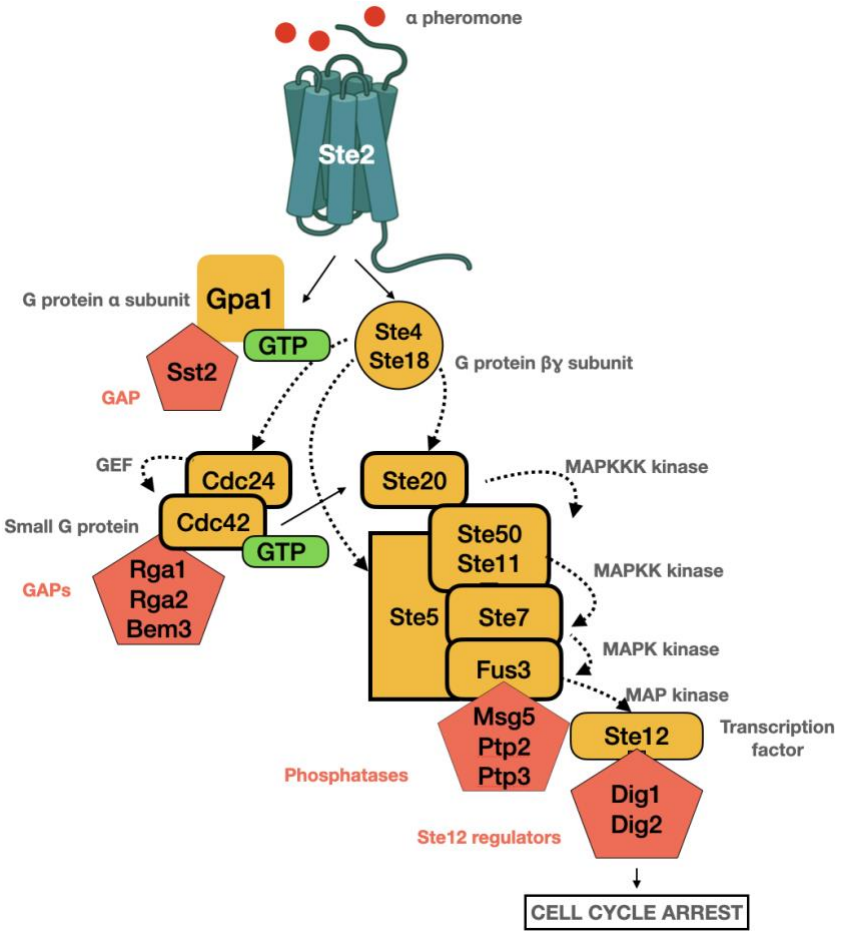

Figure 1-8. The *S.cerevisiae* pheromone response pathway for Ste2. A pheromone binds to the Ste2 receptor, facilitating the binding of GTP to the G-protein α subunit known as Gpa1. This GTP binding event leads to the separation of Gα from the βγ subunit comprising Ste4 and Ste18. Subsequently, a downstream signaling cascade is initiated, activating the guanine nucleotide exchange factor Cdc24, the protein kinase Ste20, and the scaffold protein Ste5. Within this cascade, the MAPK Fus3 phosphorylates and activates the transcription factor Ste12, which ultimately triggers cellular transcription. The inhibitors are shown in red where Dig1 and Dig2 inhibit Ste12, Msg complex inhibits Fus3. In addition to the mentioned components, there are other factors that regulate the signaling process.

1.4.3 Mechanism of chemotropic sensing in fungi

Filamentous fungi grow continuously at their hyphal tips and exhibit remarkable polarization[84]. As described for yeast mating in *S. cerevisiae*, other fungi also sense external stimulus that leads to activation of the surface sensory molecules which can be surface proteins and other GPCRs. For this chemotropic bending to occur, proteins and lipids must be supplied sequentially to the hyphal tip, which is accomplished through vesicle trafficking managed by the actin and microtubule cytoskeleton. Prior to fusing with the plasma membrane, secretory vesicles accumulate at the Spitzenkörper located at the tips of the hyphae. The Spitzenkörper is a unique structure in filamentous fungi that determines the shape and growth direction of the hyphae[85,86]. It contains a variety of membrane and cytoskeletal components, including secretory vesicles, actin filaments, and microtubules. It acts as a hub for the delivery of secretory vesicles to the growing tip, where they fuse with the plasma membrane and deposit new cell wall material. Microtubules in fungi are arranged in a polarized manner, with the plus ends oriented toward the growing tip of the cell. This polarity is important for establishing and maintaining fungal polarity, as it provides a framework for the transport of vesicles and other cargoes to the growing tip. Actin filaments, on the other hand, are thin, flexible filaments that are involved in a wide range of cellular processes, including cell motility, cytokinesis, and organelle movement. In fungi, actin filaments are also arranged in a polarized manner, with the filaments concentrated at the growing tip of the hyphae[87].

Several signaling pathways are involved in regulating the polarity of fungal cells. For example, the Ras/cAMP pathway and the protein kinase A (PKA) pathway plays important role in polarity and establishment of polarisome in fungi. These pathways are activated in response to extracellular signals, and they regulate the activity of downstream effectors that control

cytoskeletal dynamics and vesicle trafficking. The polarisome is a protein complex involved in establishing cell polarity by guiding the focused formation of actin filaments at sites of polarization **(Figure 1-9)**. In budding yeast, the polarisome is made up of Spa2, Pea2, Bni1, and Bud628, which are factors involved in F actin polymerization. Bni-1 is known to be an effector of RHO-1 a. These components are found together at cell growth sites and are essential for maintaining proper cell shape. Another component of the polarisome called Aip5, works together with Bni-1 to promote F-actin polymerization. Spa2 binds to Bni1 and Aip5 using its C-terminal domain, while its conserved Spa homology domain (SHD) interacts with MAP kinase components and Rab GTPase activating (GAP) proteins, suggesting that it has a central role as a scaffold. Pea2 is necessary for the tip-localization of SPA-2. It was predicted that the vesicles present in the Spitzenkörper contains the enzymes involved in cell wall synthesis, as well as enzymes that are secreted into the extracellular space. Chitin synthases (CHS) were observed to localize at the tips of various fungal species. On the other hand, GS-1, a protein essential for glucan synthase activity, and RGF-1, a specific GDP-GTP exchange factor for RHO-1, were both found in the region rich in larger vesicles surrounding the core of CHS[88,89].

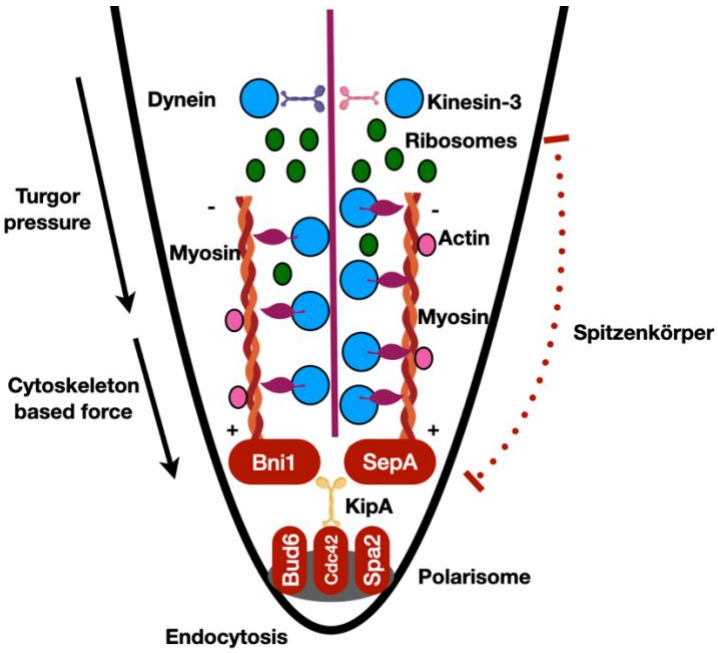

Figure 1-9. Mechanism of hyphal tip growth. Myosin plays a role in the initial steps of endocytosis by promoting actin polymerization. Additionally, the polarisome is formed consisting of Bud6, Spa2 and Cdc42. Spa2 and Bud6 interacting with formins (Bni1 and SepA), which are involved in initiating and orienting the F-actin cytoskeleton. Consequently, this enables the transportation of exocytic vesicles toward the tip. Microtubules (MTs) could be anchored at the tip through kinesin motors, facilitating long-distance transport mediated by dynein and kinesin-3. This transport mechanism delivers vesicles and potentially transports mRNA to the tip, where it undergoes translation at apical ribosomes and subsequent processing in the endoplasmic reticulum and the apical Golgi apparatus.

1.4.4 Chemotropism in *Fusarium* species

The class of pathogenic genus of *Fusarium* includes (but is not limited to) *Fusarium oxysporum* and *Fusarium graminearum.* Usually, to combat pathogenic fungi, plants secrete exudates from their roots, leaves and stem that contain a wide range of chemicals with broad-spectrum antimicrobial activities such as phytoalexins, phenolic compounds, and defense-related

proteins. One such class of these proteins is a family of secreted haem containing class III peroxidases which are conserved in all land plants. These enzymes catalyze the reduction of hydrogen peroxide increasing reactive oxygen species (ROS), the accumulation of which creates a toxic environment for the invading pathogens by causing DNA damage. Turra *et al*. showed how *Fusarium oxysporum* has diversified the mating pheromone receptors for chemosensing functions like detecting tissue damage in host plants [61,90]. They showed that *F. oxysporum* senses Class III peroxidases leading to polarized hyphal growth towards tomato roots. These signals are perceived by *Fo*Ste2. A similar response was seen in *F. graminearum* where loss of *Fg*Ste2 compromised chemotropic response and development of lesions on germinating coleoptiles. Though the exact mechanism that leads to chemotropic response is still enigmatic, a few linking studies have been done. NADPH oxidase genes, specifically Nox A and NoxD in *F. oxysporum* are known to be upregulated during the host sensing response in *Fusarium*. Their activity has been shown to be necessary for the synthesis of ROS and subsequently controlling chemotropism in *F. oxysporum*[91]. In addition, a pH dependent mechanism in hyphal chemotropism has been demonstrated in *F. oxysporum*, acidic pH favours accumulation of dihydrosphingosine whose exogenous addition activates CWI-MAPK Mpk1 phosphorylation leading to chemotropic growth[92].

1.5 Objectives for my research

Extensive research has been conducted to elucidate the molecular mechanisms involved in fungal hyphal chemotropism and pathogenesis. Through our work, the broader aim is to identify potential targets for antifungal therapies to combat the growing issue of antifungal resistance. However, several questions in this field remain unanswered. One such question pertains to the role of GPCRs in mediating fungal chemotropism, including transduction of the signal and the

underlying mechanism governing response to host peroxidases. Through my research, I investigated the involvement of *F. graminearum* GPCR Ste3 in mediating fungal hyphal chemotropism towards peroxidase and any potential role in *F. graminearum* pathogenesis. Towards this, I generated a *Fg*Ste3 gene knockout strain and showed that it is compromised in chemotropism towards peroxidases. In addition, I examined the global transcriptomic gene regulation of wildtype *F. graminearum* and the Ste3 deletion mutant following peroxidase stimulation. Secondly, I tested heterodimerization between Ste2 and Ste3 receptors with the goal of understanding the mechanism of chemotropic sensing, based on the observation that neither of these two receptors could mediate chemotropism in the absence of the other. Lastly, I conducted recombinant expression and purification of *Fg*Ste3 in insect cells with a future goal to determine its structure. By addressing these research questions, my goal is to unravel the molecular mechanisms underlying pathogenic responses of *Fusarium graminearum* and contribute to the development of novel targeted anti-fungals with improved efficacy.

Chapter 2

Fusarium graminearum Ste3 G-protein coupled receptor: A mediator of hyphal chemotropism and pathogenesis

2.0 Abstract

Fungal hyphal chemotropism has been shown to be a major contributor to host-pathogen interactions. Previous studies on *Fusarium* species have highlighted the involvement of the Ste2 G-protein-coupled receptor (GPCR) in mediating polarized hyphal growth toward host-released peroxidase. Here, the role of the opposite mating type GPCR, Ste3, is characterized with respect to *Fusarium graminearum* chemotropism and pathogenicity. *Fgste3Δ* deletion strains were found to be compromised in chemotropic response toward peroxidase, lesion development on germinating wheat and infection of *Arabidopsis thaliana* leaves. In the absence of *Fg*Ste3 or *Fg*Ste2, *F. graminearum* cells exposed to peroxidase showed no phosphorylation of the cell-wall integrity mitogen-activated protein kinase pathway component Mgv1. In addition, transcriptomic gene expression profiling yielded a list of genes involved in cellular reorganization, cell wall remodeling and infection mediated responses that were differentially modulated by peroxidase when *Fg*Ste3 was present. Deletion of *Fg*Ste3 yielded down-regulation of genes associated with mycotoxin biosynthesis and appressorium development, compared to the wild-type strain, both in the presence of peroxidase. Together, these findings contribute to our understanding of the mechanism underlying fungal chemotropism and pathogenesis, while raising the novel hypothesis that *Fg*Ste2 and *Fg*Ste3 are interdependent on each other for mediation of the redirection of hyphal growth in response to host-derived peroxidase.

2.1 Introduction

In nature, fungi conduct spatio-temporal sensing and associated responses through their hyphae. Thus, their ability to extend and control the trajectory of hyphal extension is tightly coordinated. A range of environmental cues control this hyphal behavior by either acting as a positive stimulus, encouraging hyphal growth as seen in the case of nutrients, mating pheromones and host signals, or acting as a negative stimulus, repelling the hyphae away as in the case of toxins[93]. The phenomenon of polarized hyphal growth toward, or away from, external stimuli is referred to as chemotropism, and is quintessential to fungal symbiotic, parasitic and host-pathogen interactions.

A classic example of fungal chemotropism lies in the process of mating between *MATa* and *MATα* cell types in model organisms like *Saccharomyces cerevisiae* and *Neurospora crassa*, highlighting growth toward a pheromone gradient[94–98] Similarly, the chemotropic responses of hyphae to nutrient sources were also demonstrated in several saprophytic and parasitic oömycetes fungi[99–101]. However, evidence of hyphal chemotropism in phytopathogenic fungi is relatively sparse. Some of the earliest reports were in the phytopathogen *Cochliobolus sativus* that exhibited preferential growth towards barley roots[102]. Others demonstrated that when located adjacent to their host root, *Phytophthora cinnamoni* cysts germinated rapidly and grew in the direction of the root[103]. More recently researchers showed that soil-borne *Fusarium oxysporum* displayed positive chemotropic growth towards catalytically active class III peroxidases released by host tomato roots[61].

With respect to the molecular machinery mediating hyphal chemotropism, GPCRs have been shown to play a critical role[104,105]. Characterized by their cell membrane localization and seven transmembrane domain structure, GPCRs classically function as molecular switches where

binding of an external ligand elicits conformational changes in the receptor that lead to dissociation of intracellular heterotrimeric G-proteins with corresponding exchange of GDP to GTP on the G-α subunit[106]. The released G-protein domains activate downstream signaling cascades, leading to activation of various cellular responses. In the model system *S. cerevisiae*, the diffusible α-factor and a-factor pheromones bind their respective *Sc*Ste2p and *Sc*Ste3p receptors to mediate mating in a paracrine fashion[62]. Stimulation of these receptors activates the filamentous growth mitogen-activated protein kinase (MAPK) pathway (Ste11p, Ste7p, Fus3p and Ste12p), yielding physiological changes in each mating cell type, leading to cell cycle arrest and shmoo formation[82,94]. A cooperative role for *Sc*Ste2p and *Sc*Ste3p in subsequent zygote development has also been proposed[94]. In *F. oxysporum* receptors *Fo*Ste2 and *Fo*Ste3 have been shown to be stimulated by pheromones in an autocrine fashion to control conidial germination in a density-dependent manner[62]. High concentrations of α-factor repress germination, but when Bar1 protease is secreted from the cells, it cleaves α-factor, increasing the relative concentration of a-factor and relieving the repression.

Interestingly, Ste2 was recently shown to be responsible for perceiving and transmitting the peroxidase-mediated chemotropic responses in *F. oxysporum, F. graminearum* and *Verticillium dahlia*, underscoring the general relevance of this GPCR in chemotropism[46,59,61]. Deletion of Ste2 also led to a decrease in the virulence of these pathogens on their known hosts including tomato roots, germinating wheat coleoptiles and eggplant seedlings[46,59,61]. The peroxidase-stimulated response in *Fusarium* and *Verticillium* species was shown to be transduced by the highly conserved cell wall integrity (CWI) MAPK pathway. Mutants lacking genes integral to the CWI pathway including *Rho1, Bck1, Mkk2, or Mgv1 (Mpk1; Slt2)* were impaired in peroxidase-mediated chemotropism. This is in contrast to genes belonging to the filamentous growth MAPK pathway

including *Ste11, Ste7, Gpmk1 (Fmk1; Fus3)* or *Ste12*, whose deletion had no impact on peroxidase-mediated chemotropism. In addition to chemo-sensing, the CWI pathway has been implicated in pathogenesis by promoting infection and penetration through appressorium formation, osmotic stress response and deoxynivalenol (DON) biosynthesis[107,108].

The prior observation of synergistic relationships between Ste2 and Its cognate pheromone receptor Ste3, raised the novel hypothesis that Ste3 may also play a role in host sensing. To address this, the chemotropic and virulence potential of *STE3* was explored through a reverse genetic approach using a CRISPR-generated *FgSTE3* deletion mutant. Downstream signalling pathway activation and transcriptomic studies revealed functional relevance and mechanistic aspects underlying the observed chemotropic responses to host peroxidase and associated pathogenesis.

2.2 Results

2.2.1 Deletion of *F. graminearum STE3* compromises chemotropism toward peroxidase

To determine whether *Fg*Ste3 is involved in mediating the chemotropic response to peroxidase, the annotated *F. graminearum STE3* gene sequence (*FGSG_07270* [3,109,110]*)* was deleted from *F. graminearum.* A CRISPR-CAS9-mediated transformation strategy was applied using a homology-directed repair mechanism where the entire *FgSTE3* open reading frame was replaced with a hygromycin-resistance gene cassette (**Appendix A, Figure A1**). Hygromycin-resistant transformants were isolated (*Fgste3Δ-1*, *Fgste3Δ-2*, *Fgste3Δ-3* and *Fgste3Δ-4*) and validated by PCR amplification using primers specific to the *FgSTE3* gene (**Appendix A , Figure A2**). Sanger sequencing was performed on the obtained strains, and whole genome sequencing was performed on strain *Fgste3Δ-3*, validating insertion and confirming that the observed phenotype was exclusively due to loss of *FgSTE3*, with no off-target effects.

The three positive *FgSTE3* deletion knockout strains were subjected to chemotropism plate assays and screened against commercially available peroxidase (horseradish peroxidase; HRP) (**Figure 2-1**). The wild-type strain was assayed as a positive chemotropic control, and the previously characterized *Fgste2Δ-5* was also included for comparison and as a negative control[46]. All three *Fgste3Δ* strains consistently showed random hyphal growth in the presence of HRP, compared to the directed growth observed for the wild-type strain. This indicates that the chemotropic response to HRP was completely abolished with deletion of *FgSTE3*. Chemotropism of the wild-type strain was fully characterized again for hyphal length, angle of hyphal growth and sensitivity of the activity to active peroxidase, with obtained values consistent with its prior characterization from our previous work (**Appendix A, Figures A3A-C**; (Sridhar *et al*., 2020)).

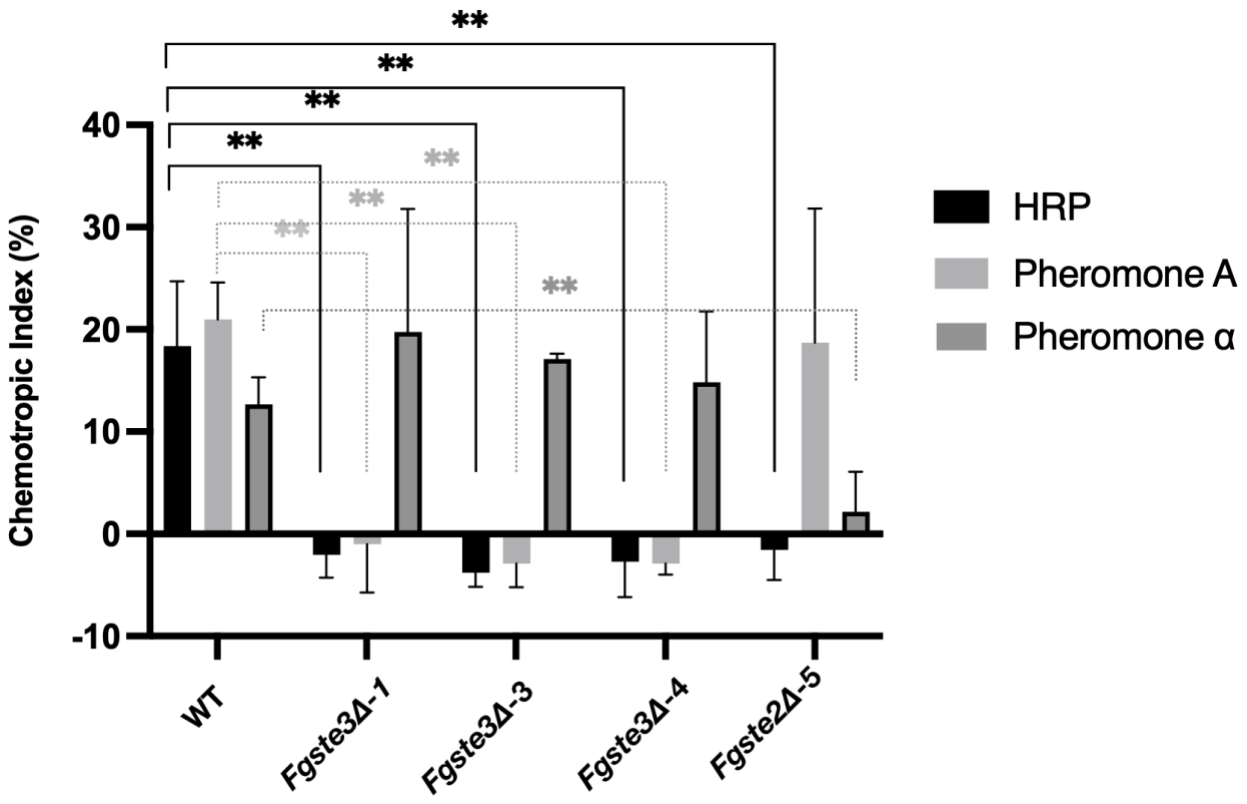

Figure 2-1. *F. graminearum* chemotropic growth towards peroxidase is mediated by both Ste3 and Ste2 receptors. Polarized hyphal growth of wild type, *Fgste3Δ-1*, *Fgste3Δ-3*, *Fgste3Δ-4* and *Fgste2Δ-5* were calculated 12 h after exposure to the indicated chemoattractants. Hyphae growing toward either 4 μM horseradish peroxidase (HRP), pheromones a-factor or α-factor (378 μM) were counted against a competing solvent control gradient (water or 50% *v/v* methanol respectively). Data is representative of average of 3 independent replicates (n = 500 hyphae / interaction / replicate; ** $p < 0.001$). Error bars represent standard deviation and statistics were assessed by the Student's *t* test.

2.2.2 Deletion of *FgSTE2* or *FgSTE3* does not affect pheromone-induced chemotropism arising from the remaining opposite pheromone receptor

The chemotropic preferences of *Fgste2Δ* or *Fgste3Δ* strains toward *F. graminearum* pheromones were also investigated. Hyphae growing toward either *F. graminearum* a-factor or α-factor pheromones were quantified compared to wild type (**Figure 2-1**). While wild type showed a strong response toward both pheromones, the *Fgste3Δ* strains had no response to a-factor, consistent with the absence of *Fg*Ste3. However, chemotropic response to α-factor was retained, consistent with native expression of *FgSTE2* in these deletion strains. Similarly, the *Fgste2Δ-5* strain showed no chemotropic response to the *Fg*Ste2 α-factor pheromone, but retained its response to the *Fg*Ste3 a-factor pheromone. Overall, the responses of these strains to pheromones differs from their response to HRP, where all response to HRP was lost regardless of which receptor was deleted (**Figure 2-1**). This finding suggests different receptor mechanisms underlying perception of the pheromones versus the HRP signal.

2.2.3 *FgSTE3* deletion has no effect on cell wall stress responses or osmotic stress tolerance

Initial observations of colony growth indicated no significant difference in growth pattern, colony color or morphology for the *Fgste3Δ* strains compared to wild type or the *Fgste2Δ-5* strain. They all displayed normal growth with no visible change in the presence of Congo red (cell wall stressor) or NaCl (an osmotic stressor) respectively (**Figure 2-2A**). Microscopic examination showed the *Fgste3Δ-3* conidia to be slightly longer and narrower compared to wild type (**Figure 2-2B**).

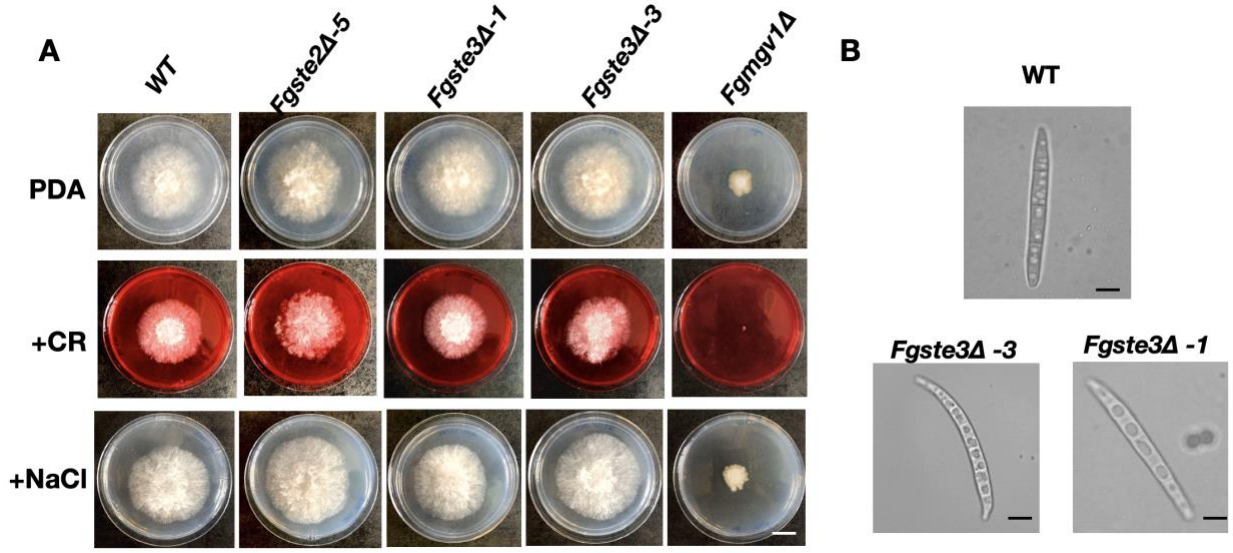

Figure 2-2. ***FgSTE3*** **deletion has no effect on** ***F. graminearum*** **morphology or osmotic stress tolerance. A)** Images of wild-type and mutant strains *Fgste2Δ-5, Fgste3Δ-1, Fgste3Δ-3,* and *Fgmgv1Δ* conidia grown on PDA, Congo red (CR; 150 µg/ml) and NaCl (0.7 M). Similar results were obtained for two independent experiments. Size bar = 1cm **B)** Conidia for wild type and *Fgste3Δ-3* were imaged under 100x using oil immersion. The images were captured using cellSens software version 1.12. Size bar = 10 µM.

2.2.4 *FgSTE3* deletion leads to decreased virulence and pathogenicity

To further investigate whether *Fg*Ste3 is involved in mediating fungal pathogenesis, a coleoptile infection assay was performed on wild type and *Fgste3Δ-3*. This assay has been shown to be an effective, reliable and easily quantifiable method to investigate the pathogenicity and extent of Fusarium head blight infection[111]. The *Fgste3Δ-3* strain showed an average 50 % decrease

in lesion length compared to the wild-type strain (**Figures 2-3A & B**). This trend is consistent with results arising from an *A. thaliana* leaf infection assay where decreased lesions for *Fgste3Δ-3* were observed compared wild-type strain (**Figure 2-4A & 4B**). qPCR analysis for fungal biomass quantification in the *A. thaliana* assay showed a 50% decrease in the absence of *Fg*Ste2, and 99% reduction in the absence of *Fg*Ste3 (**Figure 2-4C).** In the case of *Fg*Ste3 deletion, that such a small amount of pathogen could elicit the observed lesion at all, goes to the point that a lot of the lesion arises from host-mediated responses leading to cell-death.

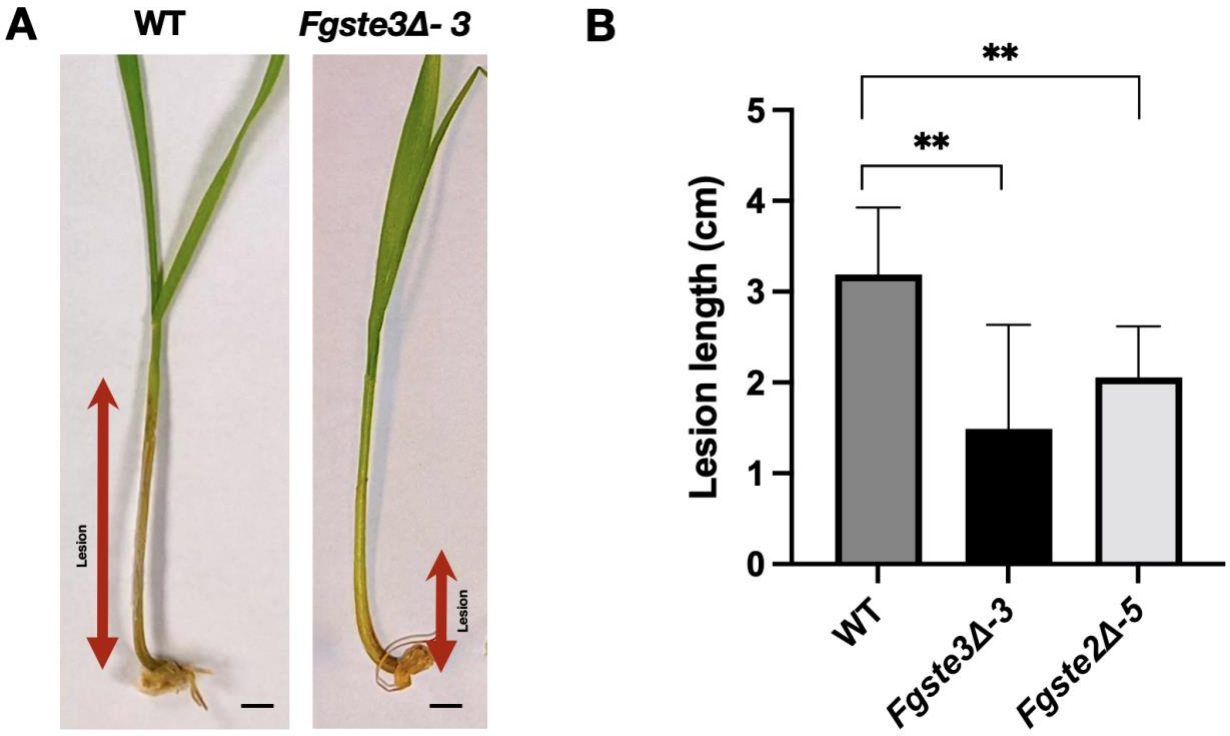

Figure 2-3. Deletion of *FgSTE3* leads to decreased *F. graminearum* pathogenicity against wheat. A) The pathogenicity was quantified by measurement of the length of infected stalk, or lesion, formed on germinating 'Roblin' coleoptiles that were infected with the indicated *F. graminearum* strains. Shown are representations of lesions formed around the wound site 10 days

after infection with *F. graminearum* conidia. **B)** Quantification of average lesion length formed on germinating 'Roblin' coleoptile stalks infected with *F. graminearum* wild-type and mutant strains *Fgste3Δ-3* and *Fgste2Δ-5*. The averages of two representative experiment are shown (compared to wild-type strain; n=18, $**P < 0.005$). Error bars represent standard deviation and statistics were assessed by the Student's *t* test.Size bar = 1 cm.

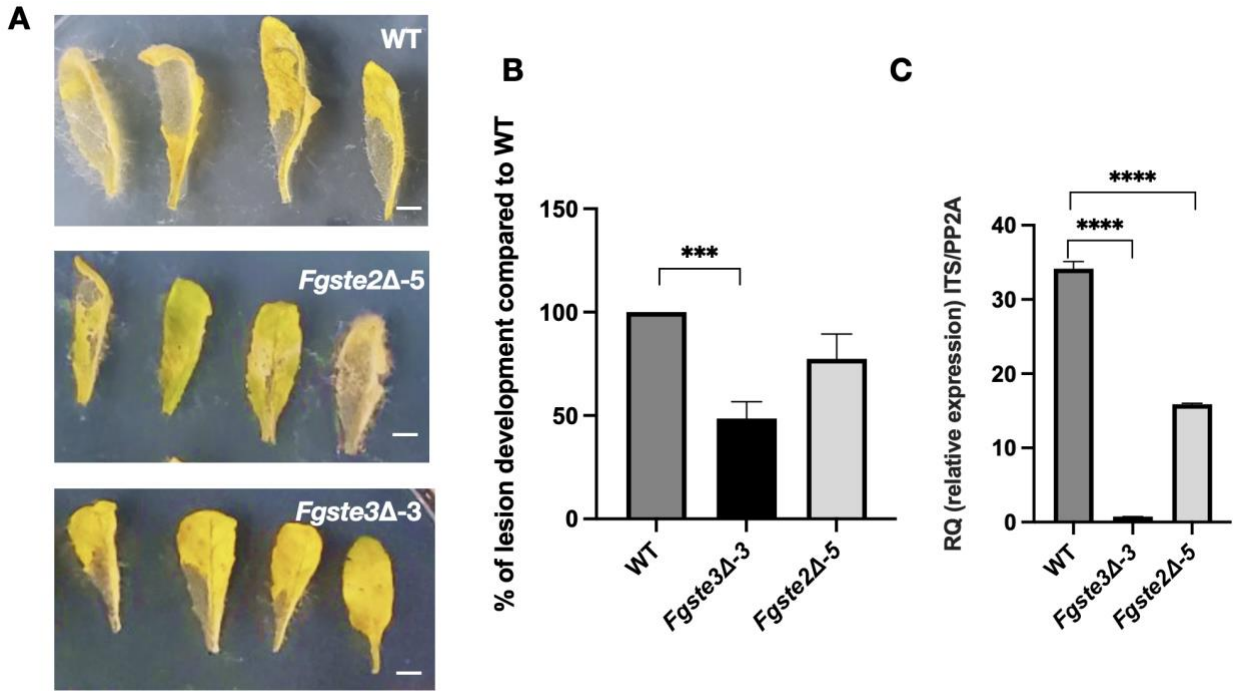

Figure 2-4. Deletion of *FgSTE3* leads to decreased *F. graminearum* pathogenicity against *A. thaliana*. **A)** Representative images of *A. thaliana* leaf infected with *F. graminearum* strains. **B)** Assessment of lesion development on *A. thaliana* leaves. Leaves were infected with wild type and *Fgste3Δ-3* and *Fgste2Δ-5* strains and quantified 3-days post infection using Image J software. **C)** Assessment of *F. graminearum* infection by quantitative PCR. Quantitative PCR was performed with genomic DNA isolated from Arabidopsis leaves infected with the wild-type, *Fgste3Δ-3* or

Fgste2Δ-5 strain. The relative quantification (RQ) was measured with the *Fusarium ITS2* with respect to the Arabidopsis *PP2A.* The experiment was performed three times (three biological replicates with n=12 for each) with similar results. Error bars denote standard deviation. Statistical analysis was performed using Student's *t* test (****$p < 0.0005$). Size bar = 1 cm.

Consistent with this, investigations of pathogenesis on flowering wheat heads yielded decreased % infected spikelets for both the *Fgste3Δ* and *Fgste2Δ* deletion mutants (**Appendix A, Figure A4A**), although these differences were not deemed significant compared to wild type under the conditions tested. The production of the mycotoxin DON, a *Fusarium* virulence factor and critical component in fungal infection on wheat was also assessed for the deletion mutants[112]. Extracts were taken from suspension cultures of wild type, *Fgste3Δ and Fgste2Δ* deletion strains grown on media that induces production of trichothecenes. Consistent with wheat head infection results, both deletion mutants produced lower levels of DON on average (**Appendix A, Figure A4B**), with *Fgste3Δ-3* yielding a reduction of 30% compared to wild type, but with a p value slightly above the cutoff (p-value 0.069).

2.2.5 Activation of the CWI-MAPK pathway by peroxidase is mediated by *Fg*Ste3 and *Fg*Ste2

It has been previously shown that the presence of peroxidase activates the CWI-MAPK pathway in *F. graminearum*[46]. However, the role of *Fg*Ste3 and *Fg*Ste2 in transducing this signal across the membrane to the CWI-MAPK had not been tested. Here, the phosphorylation of CWI-MAPK pathway component Mgv1 was assayed using phospho-p44/42 antibody in the presence and absence of *Fg*Ste3 or *Fg*Ste2. Phosphorylation of Mgv1 (expected MW 47 kDa) showed a 3-

fold decrease in both mutants compared to the wild type (**Figures 2-5A & B; Appendix A, Figure A5**). Gpmk1 (expected MW 41 kDa; MAP kinase in the filamentous signalling pathway that is also detectable by the phospho-p44/42 antibody[46]) was not detected using the phospho-p44/42 antibody. However, neither of the relative total amounts of Mgv1 or Gpmk1 varied from wild-type levels in the knockout strains when probed with the total p44/42 antibody or with the water control. The *Fgmgv1Δ* strain served as a negative control and validated the detected 47 kDa band as Mgv1. These results indicate that deletion of either *FgSTE3* or *FgSTE2* individually decreases the phosphorylation of Mgv1 to some extent compared to wild type.

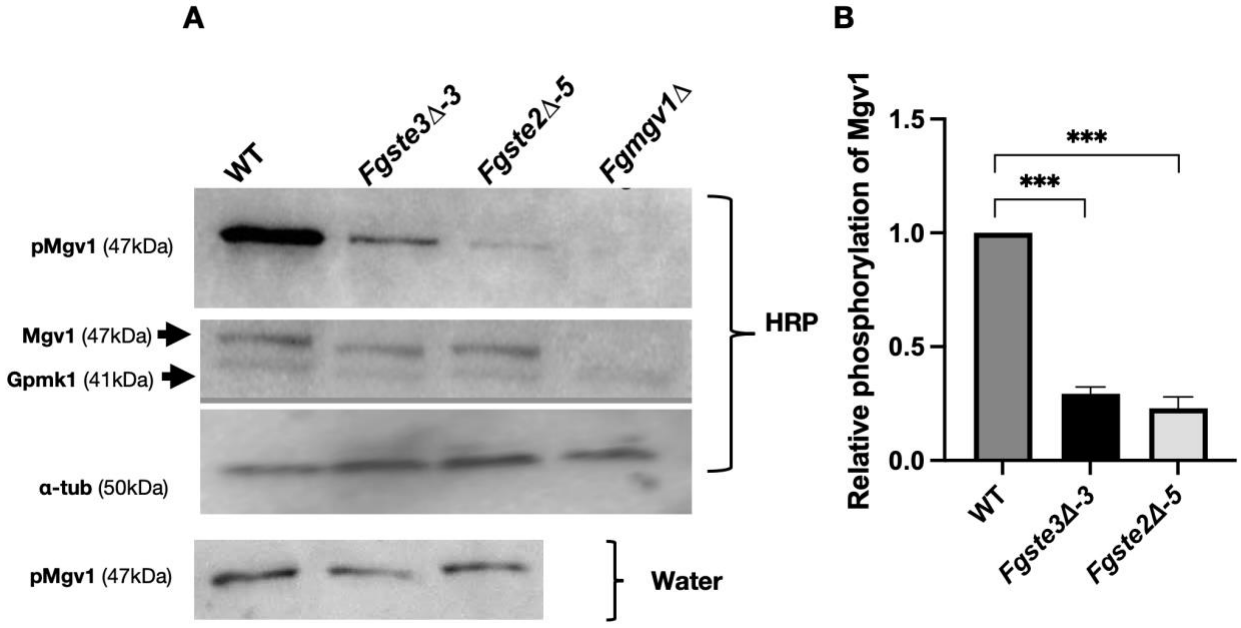

Figure 2-5. **Activation of the CWI-MAPK pathway by peroxidase is mediated by *Fg*Ste3 and *Fg*Ste2. A)** Representative images of a quantitative Western blot to probe CWI pathway activation by tracking phosphorylation of Mgv1 and total MAPK isolated from wild type and mutant strains *Fgste3Δ-3* and *Fgste2Δ-5 and Fgmgv1Δ.* The conidia were grown for 48 h in regular PDB culture

and treated with commercially available HRP or water control for 1 h before total protein extraction. For normalization of quantification, α-tubulin was probed. The molecular weights of detected proteins are indicated on the blot. **B)** The intensity of phospho-Mgv1 was quantified and normalized to tubulin, with relative intensities compared to wild type (***$p < 0.0005$). Quantification analysis was performed using ImageJ software. Data represents the average of three independent experiments. Error bars represent standard deviation and statistical analysis performed with the Student's *t* test.

2.2.6 Comparative transcriptomic analysis of the regulation of *F. graminearum* gene expression by peroxidase and *Fg*Ste3

RNA-seq reads were mapped to the genomic sequence of *F. graminearum* resulting in 99.3 % of the reads being successfully mapped. The different strains and treatments analyzed resulted in limited distinguishable changes to the transcriptome (**Figure 2-6A**). After normalization of the read counts, a total of 382 differentially expressed genes (DEGs) were identified for three pairwise comparisons relevant to this analysis, based on p-adjust ≤ 0.05 (**Table 2-1**). The bulk (96.9 %) of the DEGs arose from the comparison of wild type in the presence and absence of HRP. Consistent with this, the transcriptomic responses were most clearly divided based on the presence or absence of HRP, found to be contributing 75.3 % of the variance in the PCA (**Figure 2-6B**).

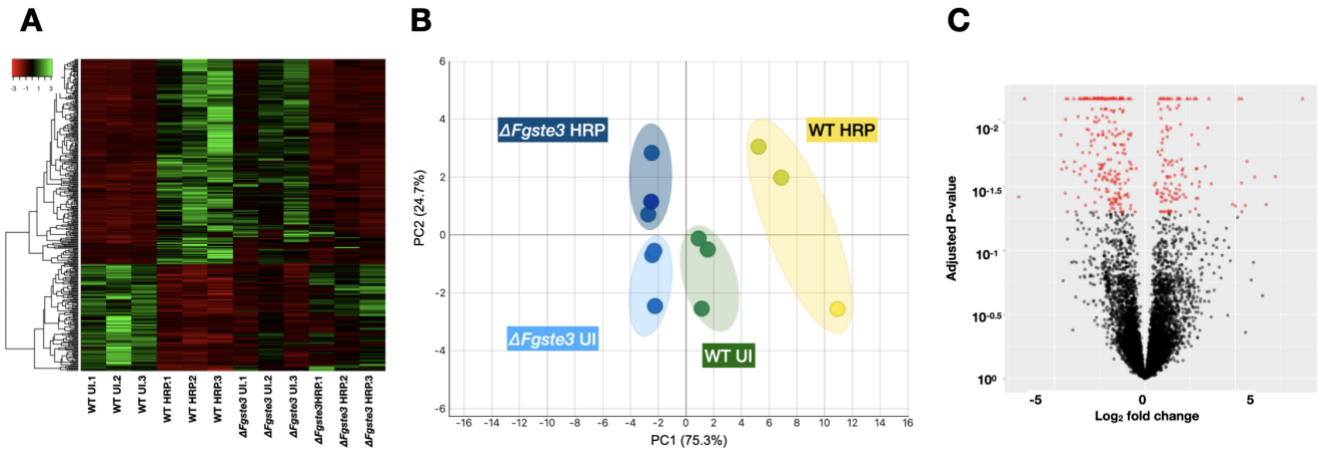

Figure 2-6. Transcriptomic overview of *F. graminearum* responses in the presence and absence of peroxidase and *Fg*Ste3. A) Heat map showing the differential gene expression for different strains and conditions highlighting varying levels of up-regulation and down-regulation. **B)** PCA plot showing the clustering of three biological replicates for each representative condition. **C)** Volcano plot showing upregulated responses in the wild type + HRP vs wild type uninduced pairwise comparison.

Table 2-1: Total numbers of DEGs upregulated or downregulated arising from each pairwise comparison considered in this study.

DEG Regulation	Pairwise Comparison		
	wild type + HRP / wild type un-induced	***Fgste3Δ-3* + HRP / wild type + HRP**	***Fgste3Δ-3* un-induced / wild type un-induced**
Up	127	4	1
Down	243	4	4

Comparison 1: wild-type F. graminearum in the presence versus the absence of HRP The pairwise comparison of the DEGs from the wild-type strain in the presence and absence of HRP was investigated to obtain broader insight into genes potentially contributing to the HRP-induced chemotropic response in *F. graminearum*. While almost twice as many genes were downregulated as were upregulated (**Table 2-1; Figure 2-6A**), a volcano plot analysis of the DEGS emphasizes the stronger nature of the upregulated responses (**Figure 2-6C**). This is consistent with the idea of HRP inducing significantly increased expression of elements required to elicit chemotropism. Thus, the focus of this particular analysis is with the upregulated genes.

A gene ontology analysis of the upregulated genes highlighted significant modulation of integral membrane transport activity (**Table 2-2**). *F. graminearum* is well known to employ transporters to pump out the DON mycotoxin that it produces, depositing it on host cells[113]. Major Facilitator Transporters are also known to act as energy centers to obtain nutrition that the pathogen needs for its survival[114]. The best representative hits here include one of the top 10 most highly upregulated genes, the Major Facilitator Superfamily (MFS) transporter, *FGSG_13980*, although its function is not clearly defined (**Table 2-2**). Also notable is the significant upregulation of MFS family pantothenate transporter Liz1 (*FGSG_04217*), known to contribute to septa formation and cellular development. Mutants of this gene have been shown to be defective in cell elongation and cell division in *S. pombe*[115].

Table 2-2: List of genes upregulated in wild type + HRP *vs* wild type uninduced comparison

Gene Identifier	Description	log_2 Fold Change	p-value
Membrane transporters			
FGSG_13980	The Major Facilitator Superfamily (MFS)	40.473	0.0008059030136
FGSG_07502	Transmembrane amino acid transporter	32.113	0.001594424155
FGSG_05731	Major facilitator superfamily transporter	11.643	2.43e-05
FGSG_00195	Monocarboxylate transporter 2	6.029	0.0008284057597
FGSG_04217	Pantothenate transporter liz1	5.969	0.0001984533517
FGSG_04426	Major facilitator superfamily transporter	2.853	0.0003898785871
FGSG_04095	Na(+)/H(+) antiporter 1	2.609	0.0004091487212
FGSG_00924	The Major Facilitator Superfamily	2.394	0.0006870875037
Cell wall remodeling			
FGSG_03616	6-hydroxy-d-nicotine oxidase	46.812	0.001572254889
FGSG_03925	Alpha/beta hydrolases	40.945	0.001858777969
FGSG_13343	NBD_sugar-kinase_HSP70_actin	7.06	1.70e-05
FGSG_00659	Endoplasmic reticulum mannosyl-oligosaccharide -alpha-mannosidase	2.446	0.001764702055
Pathogenesis			
FGSG_01586	Retinol dehydrogenase 14	4.152	0.0006120705837
FGSG_11438	Ankyrin repeat	3.148	0.0006318247356
FGSG_04314	ATP-dependent Clp protease ATP-binding subunit	2.829	0.0004512020458
FGSG_07493	Sensor gacS	2.328	0.0009534158274
FGSG_05147	Putative SCRAMM family adhesin clumping factor ClfB	2.111	0.001365630372
Peroxisomes			
FGSG_07104	Peroxisome biosynthesis	2.398	8.06e-05
FGSG_00724	Peroxisomal biogenesis factor 2	2.028	0.001092628833
FGSG_05596	Peroxisomal biogenesis factor 6	1.866	0.001059428996
FGSG_01174	Peroxisomal targeting signal receptor	1.677	7.47e-05
Mitochondria			

FGSG_12693	Altered inheritance of mitochondria 32	7.087	0.0005160525821
FGSG_01639	Enoyl- delta isomerase mitochondrial	2.685	0.0001528329539
FGSG_05197	Fmp40 found in mitochondrial proteome	2.611	9.19e-05
FGSG_11231	MOSC mitochondrial	2.073	2.44e-05

With relevance to chemotropism, a wider variety of genes and their homologues involved in cellular development and cell wall organization are highlighted (**Table 2-2**). Up-regulation of hippurate and alpha/beta hydrolases (*FGSG_03925*), known to be involved in cell wall remodeling in fungi, was detected[116]. In addition, alpha-mannosidase (*FGSG_00659*), required for the synthesis of mannose rich-N-glycans and one of the major constituents of cell wall biosynthesis in rapidly dividing cells, was also upregulated[117]. Up-regulation of NBD sugar-kinase HSP70 actin (*FGSG_13343*), which regulates the formation of actin filaments in cells was noted[118]. Finally, and perhaps most clearly related to chemotropism at this time, was the observed up-regulation of 6-hydroxy-D-nicotine oxidase (*FGSG_03616*), involved in the production of hydrogen peroxide. In *F. oxysporum,* hydrogen peroxide has been shown to be directly involved in mediating peroxidase-stimulated hyphal chemotropism based on its biosynthesis by the NADPH oxidase (NOX) gene[91].

Further investigation of the DEGs revealed additional hits with more direct relevance to infection mechanisms, but of less potential relevance to chemotropism. These include up-regulation of the gene *FGSG_05147* which is related to SCRAMM family adhesin clumping factor ClfB. It is used primarily by bacterial species like *Staphylococcus* to promote attachment and invasion of host cells. A protein containing Ankyrin repeats (*FGSG_11438*) required for host-mediated nitric oxide production and known to promote virulence in *F. graminearum* was also upregulated[119]. Up-regulation of the gene *FGSG_04314* was also notable. It shares 36 % identity with a homologue of Clp protease, an ATP-binding subunit adaptor protein known to be involved

in the regulation of virulence genes in *S. aureus,* and 39 % identity with a homologue of ClpX in *S. cerevisiae* (Mcx1p), known to act as a molecular chaperone that contributes to thermotolerance. Also upregulated was *FGSG_07493,* related to the putative gacS sensor which is known to be involved in control of the production of secondary metabolites and extracellular enzymes involved in pathogenicity in *Pseudomonas*. In addition, it mediates production of acyl-homoserine lactones, responsible for quorum sensing in bacteria[120,121]. Though quorum sensing in pathogenic fungi has not been extensively studied, this raises a novel hypothesis that HRP may be involved in initiating transcription of genes that enable fungal communication. *FGSG_07493* also shares 90 % identity with *S. cerevisiae* nik-1, known to interact with Cdc28 and regulate cell cycle progression[122]. Finally, retinol dehydrogenase (*FGSG_01586*), known to oxidise retinol to retinal (a precursor for carotenoid biosynthesis and abscisic acid (ABA) production), was also upregulated[123–125]. The ABA phytohormone is well known to act as a fungal effector and accentuate fungal disease severity.

Four peroxisomal genes were identified as upregulated, including a peroxisomal targeting signal receptor (*FGSG_01174*), peroxisome biosynthesis factor 2 (*FGSG_00724*), a protein involved in peroxisome biosynthesis (*FGSG_07104*) and peroxisomal biogenesis factor 4 (*FGSG_05596*). Peroxisomes have been implicated as critical regulators of pathogenicity in *Fusarium*, harboring glutathione transferases that aid in the detoxification of host-derived proteins and maintenance of redox homeostasis. This highlights a possible mechanism for peroxide detoxification that is employed by *Fusarium* to deal with oxidative stress[126]. Peroxisomes also control secondary metabolism involving DON biosynthesis, siderophore biosynthesis and cell wall integrity in fungi[127].

A variety of mitochondrial genes were upregulated that included the mitochondrial amidoxime-reducing component 1 (MOSC1; *FGSG_11231*) and altered inheritance of mitochondria 32 (AIM32; *FGSG_12693*), the latter being a 2Fe-2S protein that functions in redox quality control[128]. As well, two mitochondrial carrier proteins: Fmp40 (*FGSG_05197*) found in the mitochondrial proteome and enoyl delta isomerase (*FGSG_01639*) were both upregulated. Although it is hard to predict what morphogenetic changes these mitochondrial proteins might be involved in, they are generally related to oxidative stress responses based on mitochondria being major centers for the generation of hydrogen peroxide and reactive oxygen species (ROS), which are later taken up by the peroxisome. However, mitochondrial proteins have also been shown to directly influence fungal pathogenicity through phenotypic changes that involve cell wall modification, polysaccharide capsule modulation, evasion of host immune response, and metabolic flexibility by alternating between carbon source utilization and controlling cAMP/PKA signaling[129,130].

Finally, gene enrichment analyses in Blast2GO and KOBAS **(Appendix A, Figure A6)** highlighted significantly upregulated genes (enrichment ratio 0.27) involved in the biosynthesis of branched chain amino acids (BCAA) valine, leucine and isoleucine. BCAAs have been shown to play very important roles during *Fusarium* pathogenesis with mutants of genes specifically involved in leucine biosynthesis such as *Fg*LEU2, *Fg*ILV2 and *Fg*ILV6, attenuated in infection potential, conidiation and mycelial development[131,132].Gene enrichment further revealed that biologically, the majority of DEGs are associated with membrane transport, transcription by RNA pol II, carbohydrate metabolic processes, proteolysis and cellular amino acid metabolic processes. With respect to molecular function, most DEGs fall into the oxidoreductase category/class, followed by hydrolases and nucleotide-binding.

Comparison 2: Fgste3Δ-3 strain versus wild-type strain, both treated with HRP The pairwise comparison of the effect of HRP in the presence and absence of *FgSTE3* was assessed to gain insight into the role of *Fg*Ste3 in mediating transcriptomic changes in *F. graminearum* cells exposed to peroxidase, and thus the mechanism underlying *Fg*Ste3's regulation of chemotropism. Interestingly, only 8 DEGs were deemed significant in this comparison based on our cut-off criteria (**Table 2-3**).

Table 2-3: List of differentially expressed genes in *Fgste3Δ* + HRP *vs* wild type + HRP comparison

Gene Identifier	Description	log_2 Fold Change	p-value
DOWNREGULATED			
FGSG_12829	Hypothetical protein	-4.828	6.09e-06
FGSG_04590	Averantin oxidoreductase	-2.094	1.60e-06
FGSG_04596	O-methyl transferase B	-1.877	3.13e-05
FGSG_05039	*Putative PTH 11*	*-0.959*	*0.1623589568*
UPREGULATED			
FGSG_06536	L-pipecolate oxidase	7.003	4.92e-06
FGSG_09354	N amino acid transport system protein	5.936	1.66e-05
FGSG_09118	Hypothetical protein	5.469	1.59e-05
FGSG_09001	Transcription factor	1.543	1.03e-05

Significantly downregulated genes included two genes related to the production of fungal toxins during the infection process, including a sterigmatocystin 8-O-methyltransferase (*FGSG_04596*) and a gene related to isotrichodermin C15 hydroxylase (*FGSG_04590*), a cytochrome P450 monooxygenase CYP65A1 which has been previously described to be part of C16 gene cluster involved in terpenoid biosynthesis[133]. The expression of these two genes have

been shown to increase dramatically 72 h post-inoculation (hpi) on barley and wheat and thus play an essential role in plant infection[133].

As well, and also notable, is the downregulation of *FGSG_05039*, which shares 79 % amino acid identity to a PTH11-like GPCR from *Hypocrea virens* (*Trichoderma*). PTH11 (*MGG_05871*) from *M. oryzae* is known to be involved in appressorium formation, contributing to the generation of turgor pressure and entry of fungal hyphae into the cells, thus potentially implicating HRP-stimulated *Fg*Ste3 directly in pathogenesis[72]. Although the $\log_2$ fold change was barely 1.0 for this hit, and its p-adjust was above the cutoff, it shows a consistent decrease in all replicates. GPCRs are generally expressed at very low levels making their transcriptional detection challenging[134]. For instance, even though *FgSTE3* was knocked out of the *Fgste3Δ-3* strain, because of its low constitutive expression in the wild-type strain, it did not fulfill the cut-off criteria that were set for this transcriptomic analysis and was not considered a downregulated gene compared to wild type.

Of the upregulated genes, only L-pipecolate oxidase (*FGSG_06536*) was noted as an enzyme linked to lysine catabolism and protection against hydrogen peroxide stress[135]. Thus, ultimately, while this pairwise comparison provides additional information on the potential regulatory roles of activated *FgSTE3* in infection, little insight was gained related to the mechanism underlying its role in chemotropism.

Comparison 3: Fgste3Δ-3 strain versus wild-type strain, both untreated. Finally, the pairwise comparison of *Fgste3Δ-3* to the wild-type strain in the absence of any treatment was assessed to obtain further insight into the constitutive role of *Fg*Ste3. Constitutive activity refers to any basal level of signaling activity that a GPCR elicits in the absence of ligand stimulation. Many GPCRs

are well known to elicit constitutive activity[136]. However, based on the cut-off criteria, only 5 genes were shown to be significantly differentially regulated upon deletion of *Fg*Ste3 (Table 4), suggesting that *Fg*Ste3 has minimal, if any, constitutive role under these assay conditions.

Table 2-4: List of differentially expressed genes in *Fgste3Δ uninduced vs wild type uninduced* comparison.

Gene Identifier	Description	log_2 Fold Change	p-value
DOWNREGULATED			
FGSG_12651	Conserved hypothetical protein	-4.068	5.77e-06
FGSG_11101	Hypothetical protein	-3.215	7.25e-06
FGSG_08852	Putative cryptochrome DASH	-2.474	6.23e-08
FGSG_04576	Conidial development transcriptional regulator fluffy	-1.033	3.35e-06
UPREGULATED			
FGSG_01936	Cutinase transcription factor 1 alpha	0.663	2.39e-05

Nonetheless, the one upregulated gene in the *Fgste3Δ-3* strain (albeit with a log_2 fold change of only 0.6) was a cutinase transcription factor 1-α (*FGSG_01936*), shown to be dispensable in *F. oxysporum* virulence[137]. Thus, the relevance of repression of this gene by constitutive *FgSTE3* remains enigmatic. With respect to the few downregulated hits detected, *FGSG_04576*, is a homologue of the major regulator of conidiation in *Neurospora crassa* known as Fluffy. Fluffy is also known to directly activate a developmentally-regulated hydrophobin gene, involved in osmotic stress tolerance[138]. Finally, a gene related to putative cryptochrome DASH (*FGSG_08852*), known to be involved in DNA photo repair and regulation of conidiation in the gray mold fungus *Botrytis cinerea*[139,140] was also downregulated. Together, these results point

toward a limited role for constitutive *Fg*Ste3 in stress sensing and regulation of conidiation and photoreception, although these findings remain to be validated functionally.

2.3 Discussion

F. graminearum is an aggressive pathogen of cereal crops that continues to adapt to the current line of antifungal agents[141]. Prior studies emphasized dual roles for Ste2 and Ste3 in many of the biological processes they regulate across fungal species[82,94,142]. The present study lends further evidence to this, demonstrating the involvement of the *Fg*Ste3 receptor in mediating chemotropism towards host-secreted peroxidases and virulence in its host, similar to activities previously documented for the opposite mating type receptors *Fg*Ste2, *Fo*Ste2 and *Vd*Ste2[46,59,143,144]

The underlying mechanisms mediating the chemotropic responses for either *Fg*Ste2 or *Fg*Ste3 remain somewhat enigmatic. Previously, peroxidase induction of the CWI-MAPK pathway was demonstrated for *F. graminearum, F. oxysporum and V. dahlia*[46,59,143,144]. Here, this was extended by confirming the involvement of *Fg*Ste2 and *Fg*Ste3 in mediating this signal from peroxidase to Mgv1 in the CWI-MAPK pathway, with observed decreases in Mgv1 phosphorylation for both peroxidase-stimulated mutant strains (**Figure 2-5**). With Mgv1 previously being shown to be important in fungal hyphal growth and pathogenicity[145], these results are consistent with the observed reduction in chemotropic responses[146] (**Figure 2-1**).

Further consideration of the chemotropic results emphasizes that the responsiveness of this homothallic *F. graminearum* fungus to pheromones is consistent with responses observed previously for the asexual *F. oxysporum*[59]. This includes the observation that receptor deletion strains respond only to the opposite pheromone. Furthermore, it is notable that each independent

deletion is close to fully effective in inhibiting peroxidase-directed chemotropism (**Figure 2-1**). Because only one of the two pheromone receptors is deleted in each mutant strain, it follows that the remaining receptor is incapable of mediating the peroxidase-stimulated chemotropic response, even a partial one, on its own. That is to say that neither of the two receptors can compensate for the loss of the other receptor. This raises the novel hypothesis that *Fg*Ste2 and *Fg*Ste3 work together to mediate the chemotropic response to peroxidases. Speculatively, this interdependence may be the result of independent signalling events elicited by each individual receptor. Although in this case, one might expect changes to chemotropic responses to be cumulative, rather than absolute, with single receptor deletion. As well, in that both receptors stimulate the CWI pathway, the interdependence could be consistent with a requirement for the formation of a peroxidase-stimulated heterodimer complex between *Fg*Ste2 and *Fg*Ste3 at the cell membrane. GPCR dimers (hetero and homo), as well as higher order oligomers, are well documented to play important roles in modifying GPCR signal transduction[147], including a prior report of Ste2p homooligomerization in yeast mating[148].

Host infection assays were used to assess the extent of fungal pathogenicity related to *Fg*Ste3 receptor. Coleoptile infection data showed a consistent and significant decrease in lesion development, yielding a reduction of almost 50 % compared to the wild type (**Figure 3**), similar to observations made previously for the *Fgste2Δ* strain[46]. In contrast, slightly decreased values for average infection of wheat heads and lower accumulations of DON for both *Fgste3Δ-3* and *Fgste2Δ-5* were not found to be statistically significant (**Appendix A, Figure A4**). While confirming the contribution of *Fg*Ste3 to virulence, comparison of results from wheat heads and wheat coleoptiles suggests that different routes of pathogenesis may be more or less reliant on *Fg*Ste2 and *Fg*Ste3 (i.e. potentially more prominent in stalk infection, than the wheat head

infection)[46]. As well, in plants, generally salicyclic acid (SA) defence is predominant against biotrophic pathogens and jasmonic acid and ethylene (JA/ET) allow resistance to necrotrophic pathogens. Both SA and JA/ET defence responses can also attenuate each other or work in a synergistic way[149,150]. Thus, with *F. graminearum* being a hemi-biotroph, plants could elicit a wide range of variable defense responses that potentially differ in wheat head and coleoptile tissues. Alternatively, the difference between wheat head and coleoptile infection results may simply be a product of the assay systems. With the conidia being deposited directly at the site of infection on the kernel of a wheat head with a pipettor, any significant need for chemotropism may be eliminated. In contrast, the coleoptile assay sees the conidia presented to the leaf indirectly on cotton fibres dipped in conidia suspensions and then wrapped loosely around the wound sites. As such chemotropism could be necessary for the hyphae to even make initial contact with the coleoptile leaf.

The results loosely linking DON accumulation to the pheromone receptors opens the question of the broader impact and roles of *Fg*Ste3 in *F. graminearum* infection. To glean further insight into the mechanisms related to peroxidase-induced, *Fg*Ste3-mediated chemotropism and virulence, a comparative transcriptomic study was completed. This is the first global transcriptomic RNA-seq study carried out in the context of peroxidase-mediated chemotropism of *Fusarium*, to our knowledge at the time of writing. Broadly speaking, the DEG analysis highlighted a somewhat limited, but fairly diverse array of modifications arising from treatment with peroxidase. Detailed DEG interpretations are largely included above in the results section. However, more generally, with respect to oxidation, as a known component of the plant pathogen defense response,[46,151] it is not surprising that *F. graminearum* would have multiple varied responses to treatment with the peroxidase. For example, transcription factors related to purine

utilization and cutinase enzyme used for plant cutin degradation were seen to be upregulated in wild type in response to peroxidase. As well, ornithine cyclodeaminase, which favors conversion of ornithine to proline during stress response was also upregulated. Notably, ornithine is an essential component in the synthesis of DON[152].

With respect to chemotropism, HRP induced a selection of genes involved in cell wall remodeling, with relevance to hyphal redirection during growth. Many additional changes linked to pathogenic transitions that contribute to the switch from benign phase to the beginning of the pathogenic phase, for penetration and obtaining nutrition, were also observed. Previous transcriptomic studies of *Fusarium* interactions with host plants have also highlighted up-regulation of peroxidases which in turn activate other ROS related genes[153]. In yeast, ROS stress is known to activate various signaling pathways and Rho GTPases, the guardians of the cell wall integrity pathway with Rho1 controlling cell polarity[154].

In contrast, only a very limited number of transcriptional changes were detected upon *Fg*Ste3 deletion. In the presence of HRP, genes involved in mycotoxin biosynthesis and appressorium formation were downregulated in the absence of *Fg*Ste3, linking important virulence-related events to this receptor. That this transcriptomic analysis did not reveal a connection to chemotropic-related machinery, such as CWI pathway components or cell wall modifying enzymes, may be due to underlying mechanisms acting at the post-transcriptional level, low expression levels of signal transduction machinery generally or strong general HRP effects masking weaker Ste3 related mechanisms. Alternatively, the 24-hour post HRP-induction time point selected for this transcriptomic analysis may not have been optimal for detection of *Fg*Ste3-related events.

Overall, this report demonstrates a role for *Fg*Ste3 in chemotropism and virulence. This is consistent with previous reports highlighting similar roles for Ste2[46,59,61]. While the transcriptomic analysis shed only limited light on the mechanisms by which *Fg*Ste3 might be mediating chemotropism, a clear relationship between HRP stimulation and cell-wall remodeling is highlighted. As well, potential roles for *Fg*Ste3 in mycotoxin production and appressorium formation are noted. Finally, evidence that *Fg*Ste2 and *Fg*Ste3 are interdependent on each other for perception of the peroxidase-derived signal and elicitation of the chemotropic response is highlighted. Experiments investigating the interdependence of the receptors' roles in chemotropism, along with elucidation of the nature of the peroxidase-derived ligand stimulating the receptors, are ongoing in our labs. Together, this research will enhance our understanding of how two related GPCRs can play so many different roles across mating, host perception and virulence.

2.4 Materials and Methods

Chemicals

All chemicals were obtained from Sigma-Aldrich (Burlington, MA, USA) unless otherwise indicated below.

2.4.1 Fungal strains, preparation of conidia and protoplast production

F. graminearum wild-type strain DAOM 233423 (also known as GZ 3639) was provided by C. Babcock of the Canadian Collection of Fungal Cultures (CCFC/DAOM), Agriculture and Agri-Food Canada, Ottawa. The *Fgste2Δ-5* deletion strain arose from wild type GZ 3639, and along with *Fgmgv1Δ,* are described in detail in our prior work[46]. Wild-type strain was inoculated

into 200 mL liquid carboxymethylcellulose (CMC) media from a frozen glycerol stock and grown in a rotating shaker at 180 rpm for 4 days at 28 °C in the dark. Macroconidia were harvested by filtering the culture through a double layer of sterile cheesecloth and followed by centrifugation for 10 min at 1500 *g* at 4 °C. The supernatant was discarded, and conidia washed twice with sterile water and then resuspended to obtain a concentration of approximately 7 x 10^8 conidia per mL, as measured by haemocytometer. For protoplast production, 1mL of the conidia solution was inoculated into 100 mL of Yeast Peptone Dextrose (YPD, BD Difco) media and grown for 8.5 h at 28 °C with shaking at 170 rpm. When germ tubes were observed to be approximately 1.5 times the length of the conidium, the mycelia were harvested by filtration through double layered Mira cloth and washed with 50 mL of sterile water and 30 mL of 1.2 M KCl. The mycelia were transferred to 20 mL of protoplasting solution (500 mg Driselase (Sigma, D-9515)**,** 200 mg Lysing enzyme (Sigma, L- 1412), 200 mg Yatalase (Takara Biotech, T017) dissolved in 20 ml 1.2M KCl). This solution was incubated at 28 °C with 170 rpm shaking and monitored every 10 minutes for progression. At 40 minutes, protoplasts were separated from the mycelial debris by overlaying the protoplast mixture with trapping buffer (0.6 M Sorbitol, 100 mM Tris- HCl, pH 7.5), followed by centrifugation at 1500 *g* for 10 min at 4 °C. The protoplast layer was transferred to a new tub and, washed three times with 30 mL of 1.2 M KCl with centrifugation at 1500 x g for 10 min at 4 °C between washes. The protoplasts were resuspended in 5 mL of 1 x STC buffer (1.2M Sorbitol, 10mM Tris-HCl (pH 8.0), 50 mM CaCl2), yielding a final concentration 10^7-10^8 per mL. DMSO (7 % final concentration) was added and aliquots (200 µL) were stored in 1.5 mL tubes at -80 °C.

2.4.2 Crispr/Cas9 knockout of *STE3* in *F. graminearum*

The entire coding sequence of *STE3* (GenBank accession: *FGSG_07270*) was deleted as described previously[155]. Briefly, a dual Cas9-gRNA was used, where two separate crRNAs C1 and C2 were designed to target selected protospacer sequences in the 5' and the 3' UTRs of *STE3* respectively (**Appendix A, Figure A1; Table 2-5)**. The chop chop tool (https://chopchop.cbu.uib.no) was used to identify the best protospacer adjacent motif (PAM) sites, recognized by the NGG sequence, upstream and downstream of the *STE3* start and stop codons respectively. A BLAST search for the selected protospacer sequences within the *F. graminearum* genome on ENSEMBL Fungi database (https://fungi.ensembl.org/) was conducted to ensure they displayed less than 15 base pairs (bp) of identity to any off-target loci in the genome. A selectable marker, hygromycin B (Hyg), was used to replace the STE3 gene in the Cas9 mediated gene deletion. A 1500 bp segment spanning a region of the pTrpC promoter and the hygromycin B phosphotransferase (hph) referred to as the hygromycin repair template was PCR amplified from the Prf-HU2 vector[156] using a designed primer set P1 and P2 (**Table 2-1)** and Phusion Hotstart polymerase (NEB, M0530S). The resulting PCR fragment was purified using the PCR purification kit (Qiagen, 28104), yielding the complete repair template composed of a Hyg cassette flanked by 50 bp microhomology regions targeting coding regions for the *STE3* gene. *In vitro* assembly of commercially available Alt-R-CRISPR-Cas9 components from Integrated DNA Technologies (IDT^{TM}) was carried out with Cas9 ribonucleoproteins (RNPs), the crRNAs and tracrRNA. *F. graminearum* strain DAOM 233423 protoplasts were thawed on ice and 200 µL transferred to a sterile 15 mL tube containing the reaction mixture of the dual RNPs targeting the 5' and 3' end of STE3 gene. Approximately 9 µg of purified hygromycin repair template (150 µL in volume) and 25 µL of polyethylene glycol (PEG)-$CaCl_2$ buffer (60 % *w/v* PEG 4000, 50 mM $CaCl_2.2H_2O$, 450

mM Tris-HCl, pH 7.5) were added and the mixture was incubated on ice for 50 min. Subsequently, 1.25 mL of PEG-$CaCl_2$ buffer was added and the mixture was incubated at room temperature for another 20 minutes. The mixture was diluted to a total volume of 4 mL by addition of TB3 molten media (3g/L yeast extract, 3g/L casamino acids, 200g sucrose/L) and incubated for 18 h at 25 °C at 150 rpm to allow for regeneration of fungal cell wall. Finally, 300 µL of the transformed protoplasts were mixed with 15 mL low melting point agar (Thermo fisher, 16520050) supplemented with 100 µg/mL hygromycin and spread onto culturing plates. The plates were incubated at 28 °C for 4 days until mycelium emerged from the surface. Putative transformants were picked and subjected to two further rounds of selection on Potato Dextrose Agar (PDA) plates supplemented with 150 µg/mL hygromycin. Individual colonies were picked, and conidia were obtained by growing in CMC media. Conidia were harvested and stored at -80℃.

Table 2-5: List of primers and crRNA sequences.

Name	Description	Sequence
P1*	5' Hygromycin repair template	ATATATACTCAACCACTCACTCAAGAGCCTCAAAAAGCCTCT TCCACATC**TCGACAGAAGATGATATTG**
P2*	3' Hygromycin repair template	AAAAAGGCACAAAAATCAAATAGGGTATCGCACGATGTACTT TTTGG**CCACTATTCCTTTGCCCTCGGACGA**
P3	Ste3 gene ORF-F	ATGGCCGATTCAATTCACTTG
P4	Ste3 gene ORF-R	CTAGCGTCGATATGTTTCCTC
P5	(*Fusarium*) ITS2 F	GTCGAGCTTCCATAGCGTAGTA
P6	(*Fusarium*) ITS2 R	CTACCTGATCCGAGGTCAACAT
P7	Arabidopsis PP2a (At 1G69960) F	AGTTCCAGAATCCAAACCAAC

P8	Arabidopsis PP2a (At 1G69960) R	CCTAGAGGCAACACAAACATC
C1	5'crRNA	AAAAAGCCTCTTCCACATCA
C2	3'crRNA	ATTCATCATCTATTCCGGGG

* the region in bold denotes hygromycin overlapping sequences

2.4.3 Fungal genomic DNA isolation and whole genome sequencing

Fungal conidia stocks of the transformants from -80℃ were thawed on ice and grown in Potato Dextrose Broth (PDB) media. Mycelia were collected from two-day-old *F. graminearum* liquid cultures by filtration, and ground into a fine powder in liquid nitrogen. Genomic DNA (gDNA) was then isolated from the ground tissue using the E.Z.N.A Fungal DNA Mini Kit (Omega Biotek, D3390-01) and eluted in sterile water. The deletion of the target *STE3* sequence was confirmed by PCR using primer set P1 and P2 for the hygromycin gene and P3 and P4 to show absence of *FgSTE3* (**Table 2-5)**. *FgSTE3* deletion was validated by whole genome sequencing performed on a NovaSeq 6000 PE100 (5M reads) platform following Illumina shotgun library preparation. FASTQ files were uploaded, and data analyzed using the QIAGEN CLC-Genomics platform (v. 21.0.5) following default settings. In brief, reads with an error probability of < 0.05 (corresponding to a Phred score of ~15) and with more than 2 ambiguous bases were trimmed. Terminal nucleotides were trimmed by 10 bases from the 5' end to limit sequencing bias, and IDT dual-index sequencing adaptors were removed, resulting in an average read length of 90.8 bases. Trimmed sequences were aligned to the reference genome (GCA_023242275.1) using the 'Map Reads to Reference' tool in CLC-Genomics Workbench with default settings, resulting in a 90.5% mapping efficiency to the reference and an average coverage of 308.95-fold. In total, 3,366 positions in the reference genome (0.009%) were covered by no sequencing reads, including the 1790 bp corresponding to the region of *FGSG_07270* (i.e. *FgSTE3*).

2.4.4 Quantitative chemotropism plate assays

Chemotropism plate assays were set up as described previously with minor modifications[46,111]. Chemoattractant solutions (50 µl) included either 4 µM horseradish peroxidase (HRP; Sigma, P8375) in water, or 378 µM chemically synthesized (Bio Basics) *F. graminearum* a-factor (QKPGYPLSCTVM) or α-factor pheromones (WCTWKGQPCW) dissolved in 50 % methanol (*v/v*), and were loaded in plate wells against solvent controls (water or 50 % methanol (*v/v)* respectively). The plates were incubated at 28 °C in the dark for 14 h. The directional growth of conidial germ tubes (hyphal tips) was quantified with a stereomicroscope (ZEISS Axiocam ERc 5s). The chemotropic index calculations were obtained using the formula $((N_{test} - N_{solv})/N_{total}) \times 100$), where N_{test} is the number of hyphae growing towards the chemoattractant solutions, N_{solv} is the number of hyphae growing towards the solvent control, and N_{total} is the total number of hyphae counted. For each interaction a minimum of 500 hyphal tips were scored. Plotted data is the average of 3 independent biological replicates (n = 500 hyphae / interaction / replicate; ** $p < 0.001$). Statistical analysis was conducted using the Student's *t*-test.

2.4.5 Wheat coleoptile infection assay

Infection of germinating coleoptiles with the wild type and *Fgste3Δ3* strains was carried out as previously described[46]. Briefly, 16 *Triticum aestivum* cultivar 'Roblin' seeds per *F. graminearum* strain to be tested were placed on 1⁄2 MS media in 0.7% (*w/v*) agar in water in autoclaved Magenta boxes and stratified overnight at 4 °C in the dark. The Magenta boxes were then placed in a growth chamber (Enconair chamber AC 60 with growth light and temperature conditions set to 20 °C day, 16 °C night, with a 16 h photoperiod (750 µmol photons/$m^2 \times s$), and

coleoptiles were grown to a height of 1 cm, with 12–16 seeds germinated per strain. Sterile scissors were used to cut 1 mm off the top of the coleoptile and cotton thread soaked in a macro conidial suspension (2×10^5 conidia per mL) was wrapped around the wound site. The magenta boxes were then placed back in the growth chamber to allow symptom development. After ten days, the length of infected lesions observed on the coleoptile stalks were measured for each strain. The averages of two independent biological replicate experiments are shown (compared to wild-type strain; n=18 for each experiment). Statistical analysis was conducted by one-way ANOVA.

2.4.6 *A. thaliana* detached leaf assay with fungal biomass quantification

Conidia concentrations for the wild type and knockout strains was adjusted to 1 x 10^4 conidia/mL. Briefly, 10 detached leaves from three-week old *A. thaliana* Col-0 plants were transferred onto a petri-plate containing 1 % agar. Wound inoculation on detached leaves of *A. thaliana* was done as previously described[157,158]. Plates were incubated in the dark at 28°C to simulate conditions required for infection. The progression of disease and lesion development on leaves was monitored for 3 days. Fungal DNA isolation from 2-days post infected *A. thaliana* leaves was performed using Phytopure plant DNA extraction kit, as per the manufacturer's instructions (Amersham biosciences, Quebec, Canada). DNA (30 ng) was applied to qPCR using PowerUP Syber Green Master Mix (Applied Biosystems). Primers of fungal rDNA-ITS region (P5 and P6) and *A. thaliana* PP2A (AT1G69960; P7 and P8) were used for normalization to calculate relative expression levels **(Table 2-1)**. Two biological replicate experiments were averaged (n=12 each) for the leaf assay, with 3 biological replicates averaged for the qPCR assay.

2.4.7 Wheat head infection assay

A pathology test was performed by point inoculation on a susceptible variety of wheat (*cv.* Roblin)[159]. Two independent biological repetition experiments were performed with 11-15 wheat spikelets/experiment.

2.4.8 DON quantification

DON (15 ADON) production was measured *in vitro* using a modified two stage media protocol[159]. Briefly, 5,000 conidia/mL were inoculated into 4 mL of 95 % putrescine second-stage media (6.2 mM Putrescine di-hydrochloride, 22 mM KH_2PO_4, 0.8 mM $MgSO_4 \cdot 7H_2O$, 85.6 mM NaCl, 116.8 mM sucrose, 108.6 mM glycerol v/v, pH 4.0), and 5% Glucose Yeast-extract Peptone first-stage media (GYEP; 56mM NH_4Cl, 8.1 mM $MgSO_4$ $7H_2O$, 0.23 mM $FeSO_4 \cdot 7H_2O$, 14.7 mM KH_2PO_4, 2 g/L Peptone, 2 g/L Yeast extract, 2 g/L malt extract and 111 mM glucose) per well, containing one sterile nylon filter (Millipore #NY1H). Culture plates were incubated at 28 °C and 160 rpm in the dark for 72 h. Mycelia were vacuum-dried and weighed. Culture supernatants were filtered (0.2 μM) and diluted to a final concentration of 15 % MeOH. Trichothecenes were analyzed on a Shimadzu Prominence LC-20AD (Mandel) with 100 μL injection on a Shimadzu SIL-20A HT Prominence autosampler. Samples were run using a 22.5 % isocratic methanol: water mobile phase at a rate of 1 mL/min for 20 min on a Restek Pinnacle DB C18 column (5uM, 150x4.6mm Cat#9414565). Trichothecenes (DON) was monitored by UV at 220 nm and reported as micrograms of toxin per milligram of mycelial tissue.

2.4.9 Western blotting of MAPKs

Approximately 10^5 *F. graminearum* conidia for each respective strain were grown in PDB for 24 h at 28 °C in the dark. HRP (0.05 μM) or an equivalent water control was then added to the growing culture and shaken for 1 h. The cells were lysed as previously described[160]. Total protein (20 μg) of each sample was loaded and resolved on a 12% SDS polyacrylamide gel and transferred to a polyvinylidene difluoride membrane (PVDF, Bio-Rad) by wet electroblotting at 100 V for 2 h. The membranes were blocked for 1 h in 5 % (*w/v*) non-fat dried skim milk in TBST buffer (50 mM Tris, pH 7.5, 150 mM NaCl, 0.05% (*v/v*) Tween 20) at 4 °C. The membranes were subsequently incubated with either anti-p44/42 MAP kinase (1:1,000 dilution, M5670, Millipore Sigma) or anti-phospho p44/42 MAP kinase (1:1,000 dilution, Cell Signaling Technology, 9101) primary antibodies. Following a wash step, membranes were incubated with HRP linked IgG secondary antibody for 1 h at room temperature for chemiluminescent detection (1:5,000 dilution, Cell Signal Technology, 7074S). For visualization, Enhanced Chemiluminescent Substrate (Thermo scientific, 32209) was added to the membranes and the emitted light was captured using a GelDoc Imager and Image lab software (Bio-Rad). The membrane was stripped and then re-probed for α-tubulin (1:1000, Santa Cruz Biotechnology, sc53030) as a loading control. Quantification was performed using ImageJ[161] (https://imagej.nih.gov/ij/, 1997-2018). Three independent biological repetitions of the experiment were averaged and analyzed by Student's *t*-test.

2.4.10 Total RNA extraction and differential RNA-Seq analysis

Approximately 2 x 10^5 conidia of both wild type and the *Fgste3Δ-3* strains were grown in 2 x 20 mL of PDB for 3 days at 28 °C in the dark. At this time, one culture of each strain type was induced with 0.05 µM of HRP while the other was left growing uninduced. After a further 24 hours the mycelia from all cultures was harvested. For RNA extraction, 1g of dried mycelial mass was frozen in liquid nitrogen and homogenized in 1 mL TRIzol reagent prepared according to the manufacturer's instructions (Thermo Fisher Scientific). The InviTrap Spin Universal RNA Mini Kit (Stratec molecular, Germany) was used to purify total RNA from the TRIzol aqueous phase, as per the manufacturer's protocol. The RNA concentration and purity was subsequently determined using a Nanodrop spectrophotometer ND-1000 (Thermo Scientific). RNA-seq libraries were prepared using TruSeq Stranded RNALT kit and sequenced on an Illumina HiSeq 2500 platform according to the manufacturer's guidelines (Illumina, USA). The *F. graminearum* RNA-Seq data was analyzed using CLC Genomics workbench version 11.0.1 (Qiagen Corp.). Raw data was trimmed using Trimmomatic v0.39 (http://www.usadellab.org/cms/?page=trimmomatic) based on default quality scores that were determined by the base caller error probability level ($P < 0.01$). To estimate the expression levels, high quality RNA sequences were aligned to the *F. graminearum* RR1.36 genome annotated with genes and transcripts using Salmon v1.2.1 (https://combine-lab.github.io/salmon/)[162]. Differential expression analysis was performed using SARTools v1.6.4, with the DESeq2 option and the parameters within their provided default template[163]. Differentially expressed transcripts over the threshold False Discovery Rate (FDR) [164] of corrected padj ≤ 0.05 were considered. Gene annotation and GO enrichment analysis for *F. graminearum* was accomplished within the FungiDB database (https://fungidb.org/fungidb/)[165] and KOBAS database

(http://kobas.cbi.pku.edu.cn)[166]. Full RNA-seq data is available from the NCBI (Bioproject ID PRJNA872394). Three biological replicates were used per condition.

Chapter 3

Fusarium graminearum Ste2 and Ste3 pheromone receptors undergo peroxidase induced heterodimerization

3.1 Abstract

*F. graminearum Fg*Ste2 and *Fg*Ste3 are G-protein coupled receptors (GPCRs) recently shown to play roles in mediating fungal hyphal chemotropism and plant pathogenesis in response to activity arising from host-released peroxidases. Here, we follow up on the previous observation that chemotropism is dependent on both *Fg*Ste2 and *Fg*Ste3; testing the possibility that this effect might be due to formation of an *Fg*Ste2-*Fg*Ste3 heterodimer. Initially the recombinant cell-surface expression of the *F. graminearum* GPCRs was validated in *S. cerevisiae* by confocal immunofluorescence microscopy. Using this system, bioluminescence resonance energy transfer analyses were conducted, where the addition of horse radish peroxidase (HRP) was found to increase the transfer of energy from the inducibly-expressed *Fg*Ste3-Nano luciferase (*Fg*Ste3-NLuc) donor, to the constitutively expressed *Fg*Ste2-yellow fluorescent protein (*Fg*Ste2-YFP) acceptor, compared to controls. A partial response was also detected when an HRP-derived ligand-containing extract was enriched from *F. graminearum* spores and applied to the *S. cerevisiae* BRET system directly after inactivation of the HRP. The selectivity of the interaction was demonstrated by comparison to treatment with pheromones as well as an unrelated bovine GPCR, rhodopsin, fused to YFP as acceptor, that yielded no response when co-expressed with *Fg*Ste3-NLuc. Finally, the peroxidase-stimulated heterodimerization was validated by affinity pulldown. Taken together these findings demonstrate the formation of HRP and HRP-derived ligand -stimulated heterodimers between *Fg*Ste2 and *Fg*Ste3. Outcomes are

discussed from the context of the roles of ligands and reactive oxygen species in GPCR dimerization.

3.2 Introduction

GPCRs represent the largest class of membrane proteins involved in cell signaling. They sense a broad range of environmental cues, referred to as ligands, and transduce these extracellular signals intracellularly. Classically, GPCRs form associations with heterotrimeric complexes consisting of hydrophilic guanine nucleotide binding (G-protein) alpha (α), beta (β) and gammas (γ) subunits[167]. Binding of ligands initiates conformation changes in the receptor leading to the dissociation of the α-subunit from the β- and γ- subunits, activating downstream signaling pathways.

Originally, it was believed that GPCRs functioned as independent entities. However, increasing evidence supports formation of functionally relevant receptor-receptor interactions. The process of two identical GPCRs interacting with one another is referred to as homodimerization and when two different GPCRs interact with one another, it is referred to as heterodimerization. Both of these processes have been shown to modulate differential ligand binding, GPCR trafficking and signaling pathway preferences [168,169]. These dimerization processes can occur on the membrane surface, or during protein synthesis and sorting in the endoplasmic reticulum. These receptor-receptor interaction events can change the cooperativity modulating ligand binding, where binding of one molecule of ligand influences the rate of binding of the other ligand molecule to the other GPCR, either positively or negatively[170].

Previous reports have highlighted the functional relevance of homodimerization and heterodimerization between GPCRs, with homodimerization being a more commonly observed phenomenon[171,172]. One example of heterodimerization between the same GPCR subtypes includes

the γ-aminobutyric acid (GABA) receptors, $GABA_BR1$ and $GABA_BR2$, where receptor functionality and cell sorting to the surface is dependent upon dimerization with each other[173]. Additionally, formation of heterodimers between different receptor subtypes, for example bradykinin B2 and angiotensin AT1 receptors, can yield changes in the type of G-proteins they couple, from Gi as homodimers, to Gq as heterodimers. Heterodimerization has also been shown to lead to alterations in endocytic properties in the cell[174].

Mechanistically, studies have shown dimerization-related structural rearrangements of transmembrane 4 (TM4) and TM5 as well as TM1 and TM7 to form the dimerization interfaces observed in GPCR dimer structures[147,175]. Additional interactions between the receptors can also be localized in either the N terminus (as observed for CCR5 homodimers)[176], C-terminal region (as seen in δ opoid homodimers)[177] or covalently linked dimers through cysteines located in extracellular domains (as reported for homodimerizing metabotropic glutamate receptor mGluR7 and the calcium sensing receptor CaR)[178,179]. In this vein, it is interesting to note that while the class D GPCR Ste2 has been shown to homodimerize for transmission of α-factor pheromone dependent signalling, evidence of heterodimerization in class D GPCRs is relatively sparse[180]. For Ste2 homodimerization a conserved GXXXG motif in TM1 was shown to be critical to dimer formation[43,148,181].

Previously, we and others demonstrated the involvement of *F. graminearum Fg*STE2 and *Fg*STE3 (encoding Class D GPCRs) in fungal hyphal chemotropism toward the product of a catalytic reaction completed by host-released peroxidases[46,143,182]. Δ*Fg*Ste2 and Δ*Fg*Ste3 deletion strains each individually lead to complete elimination of the chemotropic response to horse radish peroxidase (HRP). These individual deletions also both led to decreased pathogenicity on germinating wheat coleoptiles, underscoring the relevance of these receptors in mediating

infection[182]. Mechanistically, the receptor deletions individually led to decreased CWI-MAPK signaling compared to wildtype (WT) *F. graminearum*. Taken together, these findings highlight an enigma. How can two different receptors, each individually shown to modulate 100 % of chemotropic activity, show no activity in the absence of the other receptor? One possible explanation is that their activities are dependent on formation of a receptor heterodimer.

Here, we report the outcome of experiments testing the ability of *Fg*Ste3 and *Fg*Ste2 to form peroxidase-stimulated heterodimers. A combination of biochemical and biophysical approaches including confocal microscopy, bioluminescence resonance energy transfer (BRET) and affinity pulldowns to demonstrate and validate the specificity of the observed interaction were applied. BRET was also used to study the dynamics of heterodimer formation in response to the presence of peroxidase compared to an HRP-derived ligand-containing extract enriched from *F. graminearum* spores, in which the HRP was heat inactivated (referred to as the HRP-derived 'ligand'). The relevance of these findings to the molecular mechanisms underlying fungal chemotropism are discussed from the context of roles of receptor ligands and reactive oxygen species in GPCR dimerization.

3.3 Results

3.3.1 Confirmation of *Fg*Ste3-NLuc and *Fg*Ste2-YFP expression in *S. cerevisiae*

To confirm the recombinant expression of the *Fg*Ste3-NLuc and *Fg*Ste2-YFP fusion constructs, confocal imaging of the 'Test' strain (**Table 3-1**) was performed.

Table 3-1: List of yeast plasmids used in the study and different strains generated.

Vectors	**p415 GAL1: *LEU2,* GAL1 inducible promoter**
1	*Fg*Ste3-L-NLuc-L-YFP-FLAG-Stop
2	*Fg*Ste3-L-NLuc-FLAG-Stop
3	*Fg*Ste3-FLAG-Stop
	p416 GPD: *URA3,* GPD constitutive promoter
4	*Fg*Ste2-L-YFP-L-NLuc-FLAG-Stop
5	*Fg*Ste2-L-YFP-FLAG-Stop
6	*Fg*Ste2-FLAG-Stop
7	Rho-L-YFP-FLAG-Stop
Co-transformed vectors	**STRAIN NAMES**
1&4	Positive
2&5	Test
3&6	Negative (NR; no reporters)
2&6	Donor alone
2&7	Negative (Rho)

For *Fg*Ste2-YFP, whose expression was under the control of a constitutive p416 GPD promoter, a robust signal was observed in green (**Figure 3-1**). For detecting *Fg*Ste3-NLuc which was under the inducible p415 *GAL1* promoter, indirect immunofluorescence was employed. Following yeast cell wall digestion and permeabilization, anti-NLuc antibody followed by IgG secondary antibody conjugated to the fluorophore Alexa Fluor 647 (red color) were sequentially added to the cells. Significant red was observed concentrated at the shmoo regions and a more uniform, faint distribution was observed within the cell. It is worth mentioning that to avoid donor overexpression and detection of non-specific BRET signals, a low induction for the *Fg*Ste3-NLuc

donor protein expression was applied (at 2 % galactose compared to $BRET_{max}$ observed at 5.6 % galactose – see next section). Negative control (NR) strain (**Table 3-1**) treated with the same conditions was used to account for any autofluorescence background signal.

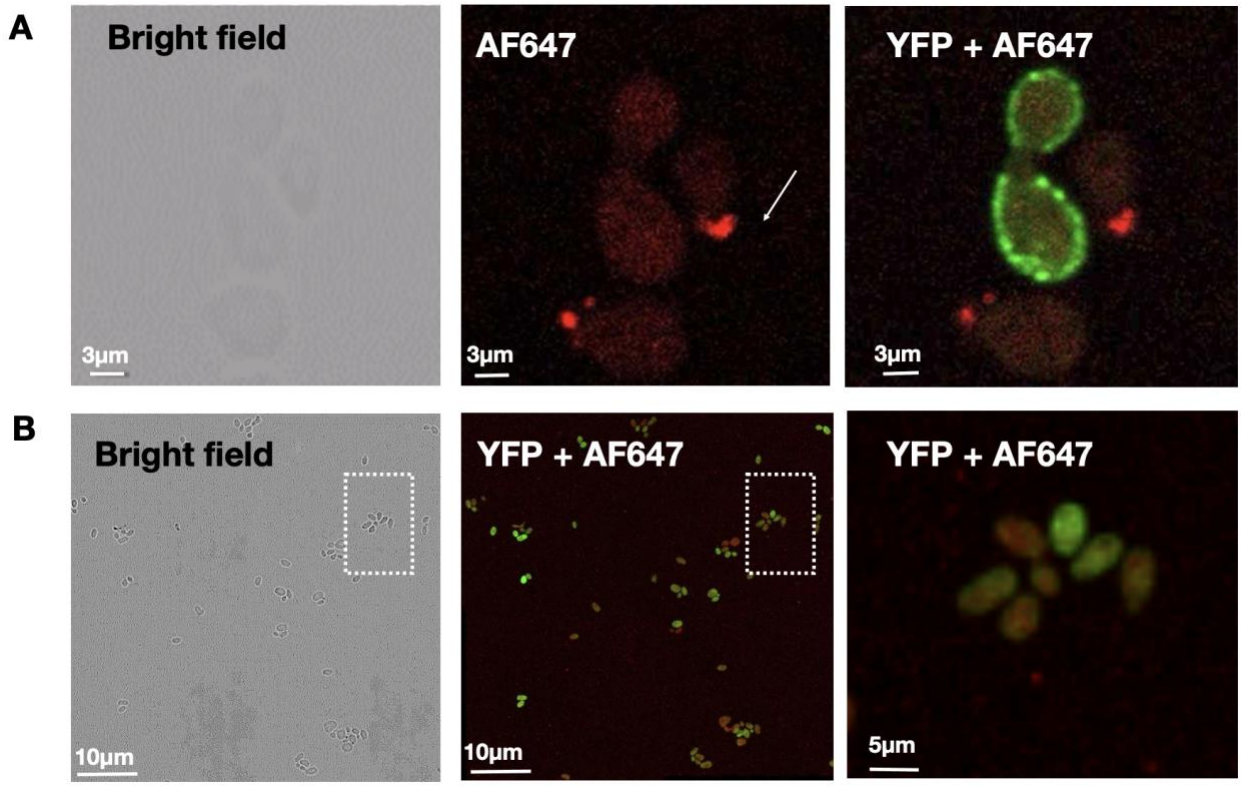

Figure 3-1. Expression analysis of *Fg*Ste3-NLuc and *FgS*te2-YFP in *S. cerevisiae*. A) Confocal microscopy analysis (3.1x zoom) of the BRET Test strain co-expressing *Fg*Ste3-Nluc and *Fg*Ste2-YFP. Expression of the donor *Fg*Ste3-NLuc was detected using immunofluorescence with AF647 and is shown in red and its concentration around the shmoo region depicted with an arrow. Expression of the acceptor *Fg*Ste2-YFP is shown in green. **B)** Heterogeneous population of transformed cells in 2x2 Mosaic Z stack images showing co-expression of *Fg*Ste3-NLuc and *Fg*Ste2-YFP in cell population. The white dashed box represents zoomed in view of *S.cerevisiae*

cells co-expressing both *Fg*Ste3-NLuc and *Fg*Ste2-YFP. NLuc refers to Nano luciferase and YFP refers to Yellow Fluorescent protein.

3.3.2 Optimization of BRET assay conditions

Initially galactose-induced *Fg*Ste3-NLuc donor expression levels in *S. cerevisiae* were optimised. Galactose saturation assays showed a hyperbolic curve (**Figure 3-2A**). With an inducible *GAL1* promoter employed to drive the expression of the donor *Fg*Ste3-NLuc protein, the BRET signal was found to increase, indicating an increase in donor expression and consequently receptor dimer formation, with saturation at 5.6 % galactose. This value, referred to as $BRET_{max}$, indicates the maximum BRET signal reached at receptor interaction saturation on the surface, where each donor interacts with an acceptor. To negate the possibility of detecting false signals due to donor protein overexpression, a $BRET_{50}$ value was calculated. $BRET_{50}$ is indicative of the probability of receptors forming complexes when they are co-expressed at the same time and in the same cell corresponding to the receptor-YFP/receptor-NLuc ratio giving 50 % of the maximal BRET signal reached upon saturation. It describes the relative affinity of BRET partners for each other. Here a $BRET_{50}$ value of 2 % galactose was obtained, which was subsequently used for all BRET assays. Thus, the observed hyperbolic curve indicates the receptors engaged in the formation of heterodimer indicating specificity of interaction between Ste3-NLuc and Ste2-YFP that increases on increasing donor expression and reaches a point of saturation. This is in contrast to the Ste3-NLuc co-expressed with Rho-YFP strain where no change in receptor engagement or BRET ratio is observed (**Appendix B, Figure B1**).

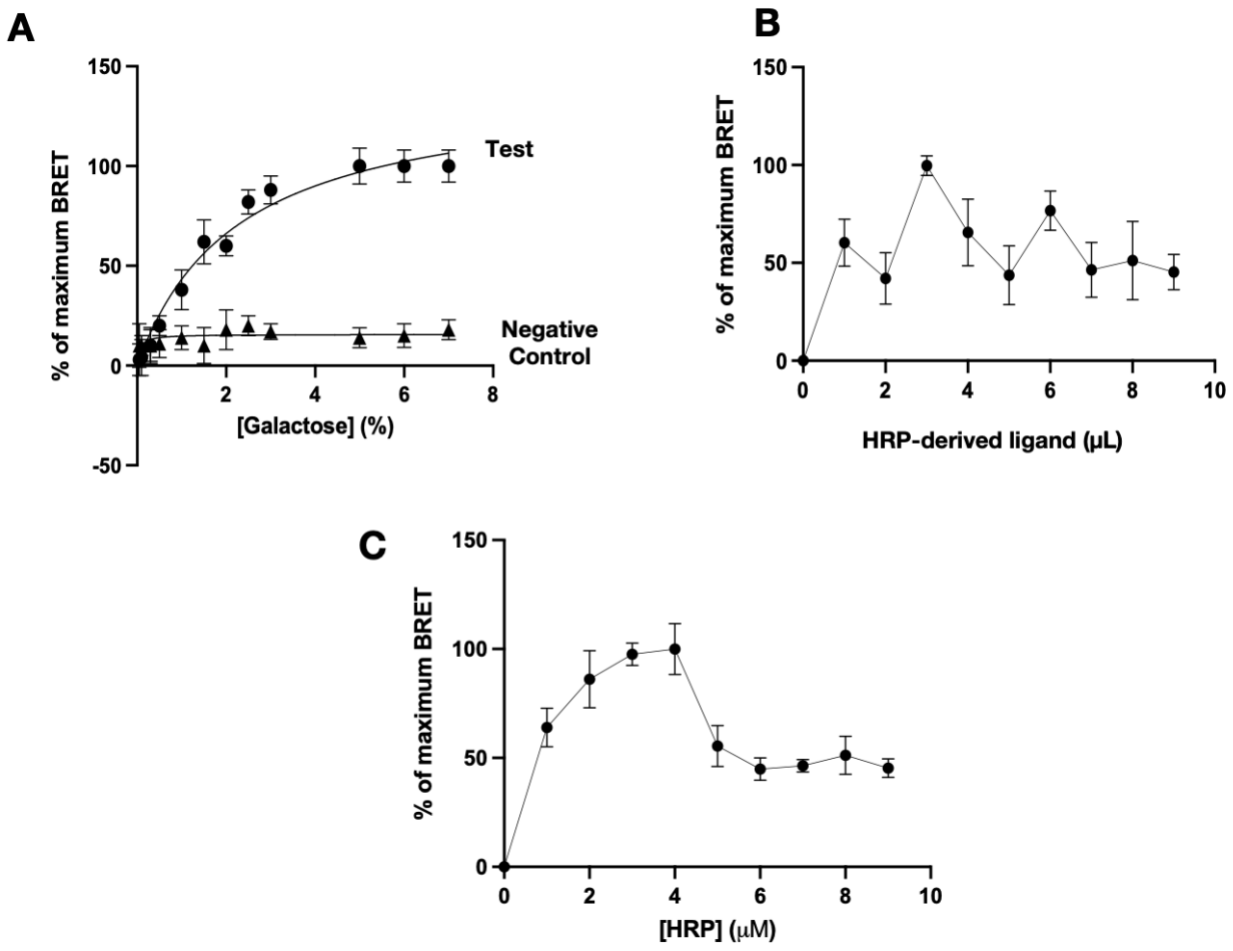

Figure 3-2. Optimization of BRET assay conditions. **A)** Galactose saturation assay: Galactose saturation assay was carried out at different concentrations of galactose (0-8%) with the Test strain (circles) co-expressing *Fg*Ste3-NLuc and *Fg*Ste2-YFP. The $BRET_{50}$ value was calculated from this to be 2 % galactose concentration that was used for subsequent experiments. Negative control strain-(Rho) (triangles) used here was *Fg*Ste3-NLuc co-expressed with Rho-YFP. **B)** Optimization of HRP-derived ligand application: The BRET response was investigated by treating the Test strain with HRP-derived ligand, by adding increasing volumes of the ligand sample from 1-10µL. **C)** Optimization of HRP application: Change in BRET signal was observed over a range of different concentrations of HRP added the Test strain. All data was plotted using Graph pad Prism version

9 (https://www.graphpad.com) and represents mean and SD of at least two independent experiments done in triplicate.

The optimal concentration of HRP or HRP-derived ligand was also investigated. Different concentrations of HRP-derived ligand or HRP were applied to the cell cultures and the effect on receptor interaction monitored by BRET. In the case of the HRP-derived ligand, while a response was detected indicating the presence of some heterodimer, whether there is any significant concentration-dependence remains to be better evaluated once the HRP-derived ligand is characterized and can be better quantified (**Figure 3-2B**). For HRP, a clear relationship between the concentration and increase in BRET was seen with receptor saturation achieved at 4 μM (**Figure 3-2C**). Thus, 4 μM HRP was selected and used for all subsequent BRET experiments. Beyond 4 μM, a steep decline was observed that could correspond to dissociation of the heterodimer upon internalization.

3.3.3 Exposure to HRP leads to *Fg*Ste2-*Fg*Ste3 heterodimerization

BRET analyses give the advantage of measuring protein interactions and proximity in real time. A significant BRET signal of 110 mBRET was observed in the Test strain on exposure to HRP (**Figure 3-3A**). This indicates heterodimerization between the *Fg*Ste2 and *Fg*Ste3 receptors. Significantly lower BRET signals were observed for the Negative controls, consisting of either No reporter (NR) or with co-expression of *Fg*Ste3-NLuc with RhoYFP (Negative-Rho) (**Table 3-1**). As well, the relative luminescence units (RLU) obtained were close to the background noise (**Appendix B, Figure B1**). An RLU of 5000 for donor and 2000 for acceptor was set as the threshold values above which signal was considered significant.

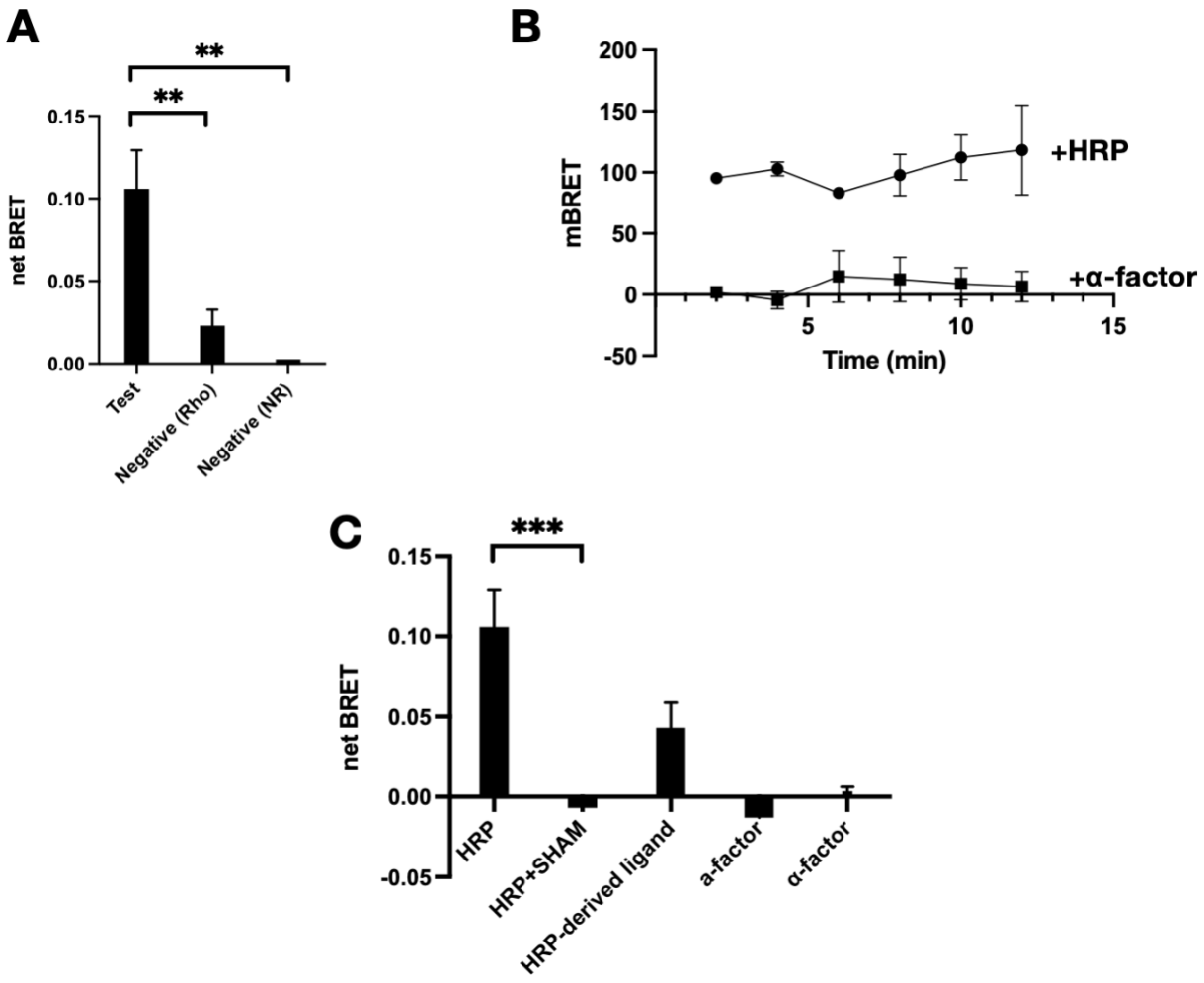

Figure 3-3. Characterization of *Fg*Ste2-*Fg*Ste3 heterodimer by BRET. A) netBRET is calculated for Test strain compared to the Negative (Rho) strain: The specificity of the interaction in presence of 4 μM HRP was validated using no reporter (NR) negative control and an unrelated GPCR, Rhodopsin (Rho) as a negative membrane protein control i.e *Fg*Ste3-NLuc was co-expressed with Rho-YFP (**p<0.01). **B)** Change in BRET with time: milliBRET (mBRET) were calculated for our Test construct *Fg*Ste3-NLuc co-expressed with *Fg*Ste2-YFP assayed against HRP and α-factor. Each data point represents the mean of ten technical replicates. **C)** BRET ratio of the Test strain under different treatment conditions: Final netBRET ratio was calculated for Test strain treated with 4 μM HRP, HRP deactivated by its inhibitor SHAM, 3μL fusarium spore

product, 1 μM Pheromone A and 1 μM Pheromone α (***p<0.001). Data was plotted using graph pad prism version 9 (https://www.graphpad.com) and represents mean and SD of at least two independent experiments done in triplicates.

To compensate for background emission of NLuc into the YFP emission spectra, emissions at 480 nm and 530 nm arising from the *Fg*Ste3-NLuc Donor alone expressing strain were used to calculate the BRET ratio and subtracted from the ratio obtained for the samples to calculate netBRET (**Figure 3A**). Specificity of the observed interaction was validated upon co-expressing *Fg*Ste3-NLuc with an unrelated GPCR construct, rhodopsin-YFP (Negative Control (Rho)). The Negative Control (Rho) strain showed no BRET above background levels (**Figure 3A**). The expression of Rho-YFP was confirmed through measurement of fluorescence for YFP with excitation at 513 nm and emission at 530 nm (**Appendix B, Figure B1-E, F,G**).

Finally, the ability of different ligands to stimulate formation of the heterodimer between *Fg*Ste2 and *Fg*Ste3 was investigated. A lack of time dependence suggested that under the conditions tested heterodimer formation was already saturated by the time the sample was first monitored after 5 minutes after adding the substrates **(Figure 3B)**. For the negative control α-factor, the time dependent BRET response was miniscule indicating no engagement of receptors upon its addition. The observed netBRET ratios (**Figure 3C**) upon addition of 4 μM HRP were compared to the those arising from treatment with pheromones a-factor and α-factor with their concentration optimized to 1 μM based on maximum donor response seen for concentrations tested from 0-10 μM. No evidence of BRET response was detected in the presence of the pheromones (**Figure 3C**). Furthermore, when HRP was treated with its inhibitor, 1 mM SHAM, the observed BRET response was completely lost. Interestingly, 3 μL of the HRP-derived ligand gave close to

half of the maximum response observed compared to the response upon HRP addition (**Figure 3C)**. Together these BRET results emphasize the specificity of the HRP and HRP-derived ligand - induced heterodimerization observed between *Fg*Ste2 and *Fg*Ste3.

3.3.4 Validation of the formation of a peroxidase-induced *Fg*Ste2-*Fg*Ste3 heterodimer by tandem affinity pull-down

To validate the receptor heterodimerization, a tandem affinity pulldown experiment was performed using the Test, Negative (NR) and Donor-alone strains (**Table 3-1**). After solubilization of the membrane receptors, the cell lysates were immunoprecipitated with anti-GFP agarose beads (known to also have affinity for YFP) and then probed for the presence of *Fg*Ste3-NLuc with anti-NLuc antibody by Western blot analysis. One prominent band at approximately 75 kDa (**Figure 3-4**) representing the monomeric form of recombinant *Fg*Ste3-NLuc was observed for the Test strain, compared to the predicted molecular weight of 73,460 kDa. The observed band was not observed in the Negative (NR) or Donor-alone strains, emphasizing that NLuc does not have any affinity for the Anti-GFP agarose beads itself.

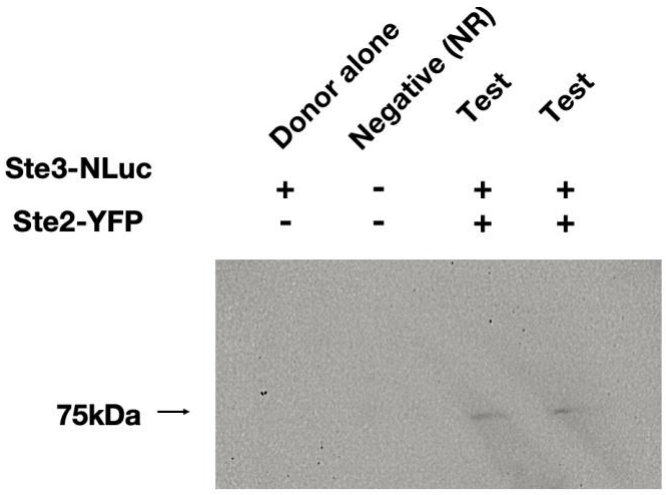

Figure 3-4. Validation of the *Fg*Ste3 and *Fg*Ste2 interaction using tandem affinity pulldown. The interaction between the receptors in the Test strain was confirmed using *Fg*Ste2-YFP as the bait protein and *Fg*Ste3-NLuc as prey protein. Anti-GFP agarose beads with specificity for YFP were used to pulldown interacting proteins. Western blot was performed using Anti-NLuc antibody that showed a band around 75 kDa corresponding to Ste3-NLuc protein. No bands are observed in the indicated Negative control (NR) and Donor alone.

3.4 Discussion

GPCRs are important signaling molecules that play a crucial role in numerous physiological processes in cells involving responses to external stimuli. GPCRs are known to be activated by the binding of a ligand and are thought to either work independently or form homodimers or heterodimers to initiate downstream signaling events. GPCR heterodimerization has been shown to control a wide range of cellular and physiological processes that differ from the functions of the monomeric versions of the receptors[167,168]. In the plant pathogen *F. graminearum*, we have demonstrated that two GPCRs, *Fg*Ste2 and *Fg*Ste3, are known to be involved in mediating

chemotropic responses to host derived peroxidases[68,182]. Individual deletions of each receptor abolished chemotropic response towards peroxidase, highlighting that each receptor was only active in the presence of the other. Now, through BRET assays and affinity pulldown using a recombinant *S. cerevisiae* system, we have demonstrated the formation of HRP and HRP-derived ligand stimulated heterodimers between *Fg*Ste2 and *Fg*Ste3. In terms of the mechanisms underlying the observed HRP and HRP-derived ligand -induced heterodimer formation, a number of different possibilities must be considered.

From the perspective that peroxidase is a notable component of a much larger Reactive Oxygen Species (ROS) system, possible broader roles of ROS are first considered. Common examples of ROS include superoxide anion ($\cdot O_2^-$), hydrogen peroxide (H_2O_2), hydroxyl radical ($\cdot OH$) and nitric oxide ($\cdot NO$). While high concentrations of ROS can cause damage to proteins, lipids, and nucleic acids, low levels of ROS are known to play a critical role in cellular signaling, including the regulation of ion channels, protein phosphorylation, and transcription factors. Thus, the idea of a ROS burst leading to heterodimerization of *Fg*Ste3 and *Fg*Ste2 receptors (**Figure 3-5A**) must be considered. The modification of lipids or other proteins in the membrane may impact their association with each other. At the same time, a large number of studies have shown that many different proteins form dimers in response to oxidative stress [183,184]. In this context, ROS have been shown to promote formation of disulphide bonds through modification of proteins by oxidation of cysteine residues leading to intramolecular disulphide linkages in the thiol groups[185–187]. Notably with relevance to MAPK pathways, Gotoh and Cooper demonstrated ROS dependent homodimerization of Apoptosis signal-regulating kinase 1 (ASK-1)[183,188,189], although whether the mechanism underlying this relates to disulfide formation remains enigmatic. Nonetheless, there is

no documented evidence of ROS stimulating GPCR dimerization (directly or indirectly) to date. Thus, in the absence of any precedence for this concept, we move on to other possibilities.

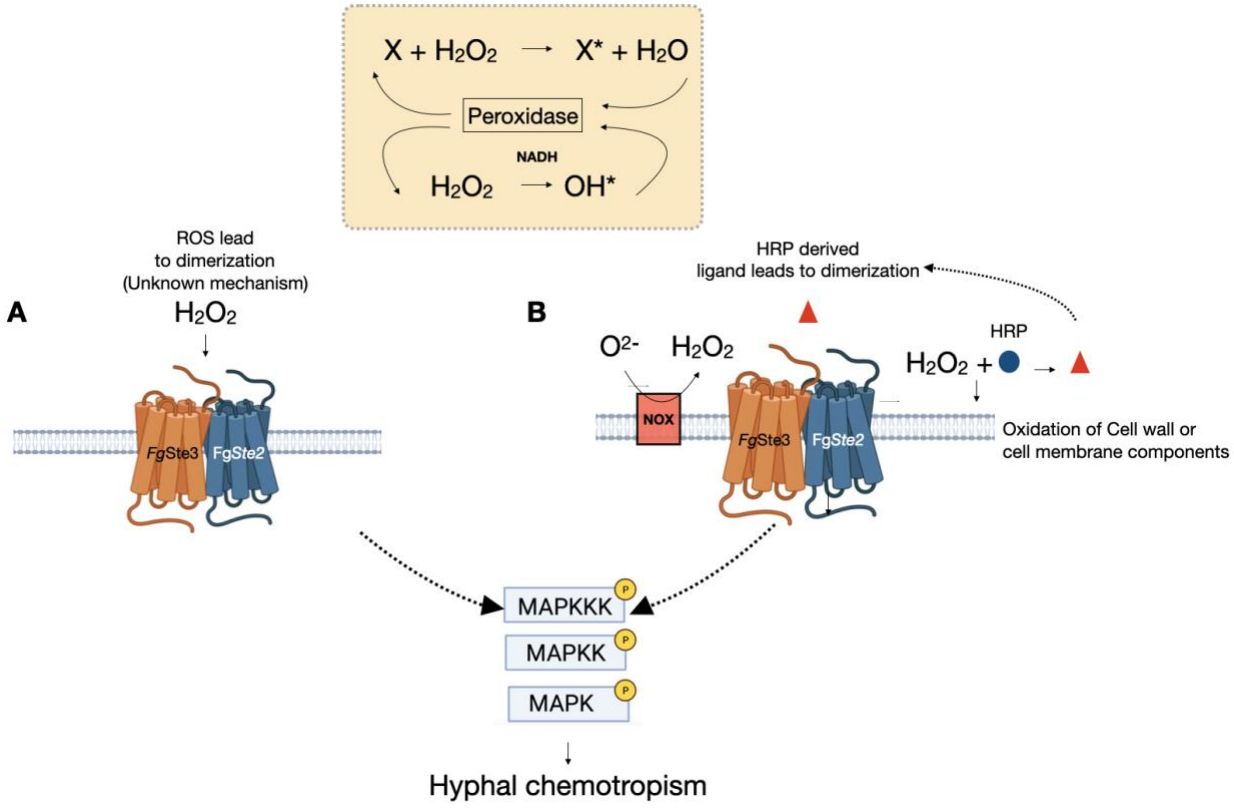

Figure 3-5. Putative model of mechanisms mediating heterodimerization of *Fg*Ste3 and *Fg*Ste2 receptors. **A**. This receptor dimer is activated through action of ROS generated through help of HRP further activating CWI-MAPK pathway. **B.** The heterodimer formation through action of HRP derived ligand that leads to dimerization of the receptors. Peroxidases are enzymes that typically use hydrogen peroxide (H_2O_2) as the electron acceptor in the catalysis of a number of oxidative reactions that involve a wide variety of organic and inorganic substrates from fungal cell wall or cell membrane.

Secondly, as it pertains specifically to the ROS H_2O_2, there is a possibility of a positive feedforward loop that involves NOX generating H_2O_2 that the HRP uses to make the HRP-derived ligand (**Figure 3-5B**). In this scenario, the ligand, derived from the action of peroxidase on the fungal cell wall induces receptor heterodimerization upon its binding to one or both of *Fg*Ste2 and *Fg*Ste3, where activation and dimerization of the receptors leads to up regulation of NOX expression, making more H_2O_2 and allowing HRP to make even more ligand.

With respect to the relationship between GPCRs and NOX, NOX expression has been shown to regulate chemotropic bending in *F. oxysporum* [91,182]. Specifically, deletion of *NOX* in *F. oxysporum* eliminated chemotropism, where addition of exogeneous H_2O_2 to *ΔnoxB* and *ΔnoxR* knockouts rescued chemotropic growth. These findings emphasize the importance of these enzymes and H_2O_2 in mediating chemotropism. However, H_2O_2 did not rescue chemotropism in a Δ*Foste2* strain, suggesting that H_2O_2 does not directly activate CWI-MAPK in this system[91]. Thus, this outcome suggests that the action of H_2O_2 is mediated via the receptor and the second model likely holds more relevance (**Figure 3-5B**). At the same time, transcriptomic analysis in WT *F. graminearum* on exposure to HRP shows upregulation of the NOX family gene, 6-hydroxy-d-nicotine oxidase (FGSG_03616), an effect not observed in the *Fgste3*Δ strain. This emphasizes a connection between NOX expression, peroxidase activity and *Fg*Ste3 signalling. Finally, it is interesting to note that beyond *Fusarium*, additional interactions between NOX and GPCRS have been detected[190]. For example, induction of both angiotensin (ANG) II and serotonin (5-HT) by ligand binding was found to induce the activation of a NOX-like enzyme, leading to the generation of intracellular ROS[190]. Accumulation of the ROS, in turn, led to activation of the p38 mitogen-activated protein kinase (MAPK) pathway mediating ANG II dependent cell hypertrophy[191,192]. Whether this example of ROS production-MAPK pathway crosstalk is relevant to the case of

*Fg*Ste2-*Fg*Ste3 heterodimerization remains enigmatic, as is the role of receptors in this example beyond initial NOX activation.

Our experiments testing HRP and HRP-derived ligand indicate a robust BRET response on HRP addition, with a weaker response observed for the ligand. The partial response to the ligand is indicative of an HRP-derived ligand stimulated heterodimer. However, lack of a clear concentration-dependence may pertain to our current inability to quantify the HRP-derived ligand (identity of the ligand being unknown at this time). In terms of investigations towards identifying the nature of the ligand, previous investigations from our lab have shown that the ligand being formed is of fungal origin, with the enzyme substrate presented either on the cell wall or cell membrane or both in *F. graminearum,* which are rich sources of peroxidases substrates[193,194]. Interestingly, low levels of ligand were also detected and isolated from *S. cerevisiae* cells[195]. Ligand induced heterodimerization has been demonstrated for a variety of GPCRs. For instance, CXCR4 and the δ-opioid receptor form dimer when induced with their respective agonists SDF1α and [d-Pen2,d-Pen5]enkephalin[196]. It is also possible that the peroxidase targets substrates that are displayed on *Fg*Ste2 and *Fg*Ste3 receptors as they are known to be highly glycosylated.

Structurally, although hydrophobic interactions are known to be the primary interactions underlying the dimerization interface, several studies have identified covalent bonds involved in GPCR dimerization. For example, heterodimerization of glutamate receptor and Calcium Sensing Receptor (CaSR) occurs via disulphide linkage between cysteine residues of the N-terminus. The dimerization is significantly altered (reduced) when those cysteine residues are mutated[197]. Six cysteine residues have been identified in *Fg*Ste2 and *Fg*Ste3 receptor. Future site directed mutagenesis studies will be used to identify the residues involved in formation of the heterodimer interface. Specifically, around the GXXXG motif known to facilitate GPCR dimerization and

oligomerization. This motif is identified in different transmembrane (TM) domains of various GPCRs including *Sc*Ste2, *Sc*Ste3. Additionally, studies involving identification of G-protein binding regions in both the receptors will be conducted as previously done for *Sc*Ste2 pheromone receptor where conserved GTPase domain residues were shown to mediate the interaction of Gα with the receptor.

Finally, it is interesting that other previous reports for these fungal pheromone receptors have also highlighted interdependence on each other. This includes for the yeast *S. cerevisiae* where the diffusible α-(WHWLQLKPGQPMY) and a-(YIIKGVEWDPA) mating factors bind their respective *Sc*Ste2p and *Sc*Ste3p receptors to mediate mating[142,180,198]. Moreover, membrane juxtaposition during mating elicited by pheromone stimulation of cross-membrane interactions between Ste2 and Ste3 receptor, have also been reported in *S. cerevisiae*[94]. In another example in *F. oxysporum*, the *Fo*Ste2 and *Fo*Ste3 receptors are known to work in an autocrine fashion to control conidial germination in a density dependent manner where the presence of a-factor can quench α-factor and lead to conidia repression[143,199]. However, the heterodimer formation between *Fg*Ste3 and *Fg*Ste2 in response to peroxidase highlighted in this study is the first of its kind.

In conclusion, heterodimers form unique signaling complexes augmenting the versatility of physiological responses and signaling pathways activated by GPCRs. Further investigations are required to characterize the molecular basis of the heterodimerization reported in this Chapter, through a combination of biophysical and structural studies. However, the possibility that both the action of peroxidase in the context of ROS burst activity as well as the HRP-derived ligand are needed to obtain a heterodimer that activates CWI-MAPK pathway, cannot be ignored. Studies involving Rho-dependent activation of downstream signal transduction events involved in the transmission of response from *Fg*Ste2 and *Fg*Ste3 in *F. graminearum* and possibly their individual

potential role in the formation of peroxidase-derived ligand are being carried out. In addition, experiments involving proximity biotinylation of *FgSte3* using TurboID to mine for adaptor proteins and identification of a possible peroxidase derived ligand are currently ongoing in our lab (**Appendix B, Figure B1 and B2**).

3.5 Material and Methods

3.5.1 Reagents D- (+) Raffinose hydrate (Cayman chemicals,16773). All other reagents were purchased from Sigma™ unless stated otherwise.

3.5.2 Vector constructs and *S. cerevisiae* strain generation

Yeast centromeric vectors p415 (*LEU*, *GAL1* inducible promoter) and p416 *(URA3, GPD* constitutive promoter) were used to express chimeric proteins. The vectors were a kind gift from Barbara Montanini (University of Parma, Italy)[200]. The coding sequence for *F. graminearum* STE3 sequence was codon optimized for expression in *S. cerevisiae*, synthesized and cloned into the p415 vector using commercial service offered by Biobasics™. It was tagged at the C-terminus with an engineered deep shrimp luciferase, NLuc generating a fusion protein. This p415-*Fg*STE3-NLuc vector is referred to as 'the Donor'. Similarly, *F. graminearum* STE2 coding sequence was subcloned into the p416 vector such that it was tagged with a C-terminal YFP, and thus p416-*Fg*STE2-YFP acted as 'the acceptor'[46]. Briefly, for generating fusion protein DNA constructs, the cDNA sequences were amplified without stop codons along with the respective reporter tags, NLuc for *Fg*Ste3 and YFP for *Fg*Ste2. They were followed by a glycine and serine rich linker molecule sequence (protein sequence: GGGGSGGGGS) that allowed

spatial flexibility. This was followed by a FLAG tag (amino acid sequence DYKDDDDK) and stop codon.

These constructs along with a number of others, were either expressed alone or were co-expressed in select combinations to create the Test, Positive control and Negative control *S. cerevisiae* strains needed for BRET analysis (**Table 3-1)**. Three notable Negative controls were employed. First the *Fg*Ste3-NLuc donor was expressed alone to account for any bleed through signal arising from the donor into the acceptor wavelength emission (Donor alone). Secondly, *Fg*Ste3-NLuc was co-expressed with an un-related GPCR, bovine rhodopsin, fused to YFP referred to as Rho-YFP[201] to produce the Negative (Rho) strain. Third, *Fg*Ste3 and *Fg*Ste2 were co-expressed in the absence of either of the two reporter fusions to account for background fluorescence, referred to as the Negative (NR (no reporters)) strain.

Fungal strain BY4741 YFL026W (*MATa his3Δ1 leu2Δ0 met15Δ0 ura3Δ0*) was grown in 50 mL of Yeast extract-Peptone-Dextrose (YPD) media and was used for transformation using the lithium acetate method as described with minor modifications[202,203]. Salmon sperm DNA (2mg/ml) was used as the carrier plasmid. The BY4741 YFL026W cells were transformed with the appropriate plasmids and the colonies were allowed to grow on SR/-Ura/-Leu plates (Synthetic Raffinose medium) for 2-3 days. For growth of transformants, single colonies were picked and individually grown in liquid SR/-Ura/-Leu at 29 ℃.

3.5.3 Confocal microscopy for studying Ste3-NLuc and Ste2 YFP expression and localization

The yeast 'Test' strain co-transformed to contain vectors encoding the NLuc and YFP tagged receptors was grown in SR/-Leu/-Ura media overnight and then induced with 2 %

galactose. The obtained cell cultures were treated with 4 μM HRP enzyme for 10 minutes (min) followed by centrifugation and subsequent washing in ice cold 1X Phosphatase Buffer Saline (PBS) consisting of 137 mM NaCl, 2.7 mM KCl, 10 mM Na_2HPO_4, 1.8 mM KH_2PO_4. They were fixed using 4 % paraformaldehyde for 20 min at 4°C. To enable antibody-based visualization of NLuc, Zymolase was added to the cell suspension for 1 hour (h) to digest the yeast cell wall. Following washing (3 times in PBS), cells were permeabilized with PBS containing 0.01 % Triton X-100 for 20 min. To reduce non-specific binding, cells were incubated in a blocking solution with PBS containing 1mg/mL Bovine Serum Albumin (BSA) for 30 min. Subsequently, cells were incubated with a 1:100 dilution of primary mouse anti-NLuc antibody (Promega, cat#7000) in PBS overnight at 4 °C. Following washing (3 times in PBS), cells were incubated with a 1:50 dilution of secondary rabbit IgG-antibody conjugated to Alexa fluor 647 (Thermo Fisher, A-21235) for 60 min at room temperature in the dark. Cells were then mounted using an anti-fading Mowiol media (Sigma, Cat# 81381), sealed and examined under the objective (HC PL APO CS2 40x/1.10) using a Stellaris 5 SR confocal laser microscope (Leica TCS NT, Heidelberg, Germany). WATER with Pinhole: 1AU and digital zoom of 3.1X was used. The sequential detection of YFP and Alexa 647 stained receptors was achieved using excitation laser lines at 488 nm (argon) at 2 %, Detection range: 493-620 nm, Gain:11 % for YFP. For Alexa 647 laser line at 638nm at 15%, Detection range: 643-750 nm, Gain:50 was employed. The fluorescence from the channels was collected sequentially, and images were produced using an 8-fold frame averaging a resolution of 102461024 pixels. Histogram stretching for images was done at 0-255 and for AF647 at 0-100.

3.5.4 Bioluminescence resonance energy transfer assay

This is a proximity assay based on radiative transfer of energy between Nano luciferase (NLuc) and yellow fluorescent protein (YFP), fused to *Fg*Ste3 and *Fg*Ste2 receptors respectively. NLuc was employed as the donor and YFP the acceptor construct as previously documented here.[200] Employing NLuc had the advantage of its smaller size and good separation between the NLuc and YFP emission spectra. Upon addition and oxidation of Nano-glo luciferase substrate (Promega, N1110) by NLuc, light is emitted with a peak at 480nm. YFP absorbs this if it is within the permissive distance (<100 Å) of the NLuc light emission and in turn emits fluorescence at with a peak at 530 nm.

Transformed fungal strains were grown for 2 days at 29 °C in SR/-Ura/-Leu media to O.D 0.7-1 (density of 2×10^3 cells per mL). Equal volume of culture (50 µL) was loaded in each well of a 96-well PerkinElmer ™ white optiplate, to which galactose was added at a final optimized concentration of 2 % (see below). The cells were incubated for 3 h at 29 °C for induction of the donor *Fg*Ste3-NLuc protein. Prior to recording the BRET reading, the cells were treated with HRP (final concentration 4 µM) dissolved in PBS and incubated at room temperature (RT) for 2 min. In cases where pheromones were applied, they were applied at a final concentration of 1 µM. Following this, 20µL of freshly diluted Nano-glo Luciferase Assay substrate (Promega ™, Madison USA, N1110) diluted to a ratio of 1: 1000 times in PBS was added. The relative luminescence units (RLU) readings were then acquired using a Spectra max M5^e multi-mode plate reader using the following emission filter settings for recording luminescence: NLuc: counting time 5 seconds; emission filter 480nm (±10nm) and YFP: counting time, 5 seconds; emission filter 530nm (±10nm). Measurements were performed on each well over time to measure the progress of reactions. Background luminescence detected in

i) wells containing donor alone transfected cells (expressing *Fg*Ste3 fused to NLuc and *Fg*Ste2 alone) and ii) the Negative (NR) strain (expressing *Fg*Ste2 and *Fg*Ste3 alone and lacking NLuc and YFP fusions (**Table 3-1**)) was subtracted. The experiments were performed with a minimum of three and maximum of ten replicates for each condition and repeated at least twice. The average of two independent experiments are represented in each graph. The BRET ratio was calculated by dividing the signal measured at 530 nm (YFP as acceptor) by the signal measured at 480 nm (NLuc as donor) after background emissions were subtracted. The netBRET was calculated by subtracting the ratio obtained for donor alone strain from the other strains being tested.

Expression levels of YFP tagged acceptor proteins were assessed using λex = 513 nm, λem = 530 nm prior to performing luminescence readings to make sure they were consistent across the samples and replicates. For quantification of the levels of donor protein, we used the sum of bioluminescence emission signal recorded from donor NLuc and acceptor YFP proteins as described previously[204]. Z factor values were calculated (>0.5) to optimize the feasibility of the assay for subsequent conditions tested[205].

3.5.5 Preparation of chemotropic ligands and applications to the BRET assay

The HRP-derived 'ligand' was obtained by treating 10 million *F. graminearum* spores with 0.05 µM concentration of HRP for 6 h at 28 °C. The spores were centrifuged at 6000 x g and the aqueous phase was collected and HRP was heat deactivated by incubating it at 95 °C for 10 min as demonstrated previously[47], leaving only the spore-derived product of the HRP reaction referred to herein as the 'ligand', and not HRP itself. The chemotropic activity of the ligand was confirmed in chemotropism plate assays[111], before being applied to the BRET assays. In other

experiments, intact HRP or pheromone itself was applied directly to the BRET assays. The correlation between concentration of ligand (or HRP, or pheromone) and receptor BRET saturation was studied by assaying increasing concentrations of the stimulants. HRP was assayed from 0-10 μM, pheromones (a-factor and α-factor) were assayed at 1-10 μM, while the ligand, which could not be quantified, was applied at increasing volumes from 0-10 μL.

3.5.6 Optimization of galactose concentration for expression from p415-*Fg*STE3-NLuc donor vector

A saturation assay was carried out for determining the galactose concentration at which donor saturation was observed ($BRET_{max}$). Samples (50 μL) of the yeast 'Test' strain culture were loaded in each well of a 96-well plate to which increasing concentrations of galactose were added from 0.01 to 8 % (in triplicate). The plate was incubated for 3 h (after optimization of induction time (see below)) at 29 ºC for induction of *GAL1* promoter driving *Fg*Ste3-NLuc (donor) protein expression. HRP (4 μM) was added followed by 20 μL of Nano-glo luciferase substrate (Promega, N1110) to each well. The luminescence data was collected as described above. The $BRET_{50}$ value was calculated and used going forward as the optimized concentration of galactose to be used for performing BRET assays. The expression of *Fg*Ste3-NLuc donor protein produced was also validated performing immunoblotting using anti-Nluc antibody (Promega cat#7000), see details below.

3.5.7 Temporal dynamics of heterodimer formation

With inducible expression of *Fg*Ste3-Nluc donor protein and constitutive expression of *Fg*Ste2-YFP acceptor protein ensuring that the receptors were expressed on the surface, the

observed BRET responses were relatively fast. The BRET response was measured using a kinetic assay over a period of time ranging from 0 min to 1 h after HRP or pheromone or 'ligand' and luciferase addition. Yeast cells expressing the Test constructs were grown for 2 days in SR/-Leu/-Ura media and induced to 2 % galactose concentration for 3 h. The cells (50 µL) were pipetted in each well of a white optiplate (Perkin Elmer) and assayed with 4 µM of HRP and 20 µL of Nano Glo luciferase substrate (Promega, N1110) diluted to 1:1000.

3.5.8 *Fg*Ste2 and *Fg*Ste3 interaction by tandem-affinity pulldown

The yeast Test strain, as described for BRET in **Table 1** was used. The cells were grown for two days in SR/-Ura/-Leu media in 2 % galactose and exposed to HRP for 10 min. The peroxidase treated cells were pelleted by centrifuging at 4000 x g for 10 min, resuspended in 5 mL of PBS and lysed by vortexing with glass beads following a previous protocol with minor modifications[206]. All the steps were performed at 4 °C unless indicated otherwise. The solubilized membrane proteins were diluted 1:1 in dilution buffer (10 mM Tris/Cl pH 7.5, 150 mM NaCl, 0.5 mM EDTA) and incubated with GFP trap beads (ChromoTek; AB_2631357; with 95 % efficiency to bind YFP tagged proteins) with end-over-end mixing overnight at 4 °C. The beads were washed three times in wash buffer (10 mM Tris/Cl pH 7.5, 150 mM NaCl, 0.05 % Triton-X, 0.5 mM EDTA) and allowed to settle by gravity each time. The supernatant was removed. Bound proteins were extracted from the beads using 50 µL of acidic elution buffer (200 mM glycine pH 2.5). SDS sample buffer (2X concentration, 10 µL; 120 mM Tris/Cl pH 6.8, 20 % glycerol, 4 % SDS, 0.04 % bromophenol blue, 10 % β- Mercaptaethanol) was added and samples were incubated at RT for 15 min. Solubilized proteins were resolved by SDS-PAGE (10% acrylamide) and transferred to nitrocellulose membrane using standard wet electroblotting protocol. The blot was probed with

1:1000 dilution of anti-NLuc antibody (Promega cat#7000) and the bands detected by chemiluminescent detection.

3.5.9 Statistical Analysis

All BRET experiments consisted of 3 minimum technical replicates and were replicated at least two times. One-way ANOVA and multiple mean separation modules of the Graph pad prism (version 9.0, Graphpad Software, San Diego, CA) were used to calculate statistical differences and compare the means, respectively. Curve fitting was performed using a non-linear regression equation assuming a single binding site. Multiple comparisons of the data were performed by ANOVA.

Chapter 4

Ongoing Long-term Projects

This chapter comprises a description of two projects that were initiated, but not completed, during my PhD candidacy. While they face the general topic of this thesis, and address longer-term associated goals, they represent unique investigations that do not strictly speaking fit with the work described in previous chapters. Their completion will require significant longer-term input from future researchers, going beyond the scope/timeframe of this dissertation. Section 4.1 represents the first steps toward conducting structural investigations of the *Fg*Ste3 receptor, focused on its high-yield recombinant production and purification using insect cell culture. These methods remain to be optimized for maximized yields at which time the obtained purified receptor will be applied to X-ray crystallographic and/or cryo-electron microscopy studies, along with similarly produced *Fg*Ste2[195]. Outcomes will shed light on the mechanisms underlying receptor activation, including heterodimer formation at the structural level. Section 4.2 describes my work with identification of an ABA biosynthetic gene homologue in *Fg* and details of its differential expression upon infection of wheat.

4.1 Recombinant Expression of *Fg*Ste3 GPCR in *Sf21* Insect cells and Its Purification for Future Structural Studies

4.1.1 Abstract

G-Protein Coupled Receptors (GPCRs) play crucial roles in sensing stimuli that lead to activation of signaling pathways and associated cellular responses. Ste3 and Ste2 GPCRs have

been shown to modulate chemotropic sensing and pathogenicity in *Fusarium graminearum*. Structural elucidation of these GPCRs is essential for understanding their complex functional mechanisms, including heterodimer formation and as they may represent targets for designing novel anti-fungals in the future. Structural studies are challenging because of the need to obtain highly pure and functional protein in its correctly folded state in milligram quantities for X-ray crystallography and Cryo-EM studies. In this study, we test the *Sf21* insect cell expression system (known to be an optimal platform for production of GPCRs), for the production of *Fg*Ste3. *Sf21* cells offer several advantages including eukaryotic post-translational modifications, high expression levels, proper protein folding, and scalability. Here, the recombinant expression, solubilization and purification of an *Fg*Ste3-mCherry fusion protein was carried out, with outcomes verified by confocal microscopy and Western blotting.

4.1.2 Introduction

GPCRs represent a diverse class of membrane proteins that play key roles in cellular signaling. Recently, GPCRs from *F. graminearum*, *Fg*Ste2 and *Fg*Ste3 have been shown to mediate fungal chemotropism and infection mediated responses which makes them attractive targets for drug development[47,111]. Structural elucidation of GPCRs provides insights into their ligand recognition, activation, and conformational dynamics. Determining high-resolution structures of GPCRs is a challenging task due to their complex architecture and inherent flexibility[207,208].

Generally, GPCR consists of a single polypeptide chain that crosses the membrane seven times. It includes an N-terminus (-NH2) that is located extracellularly and a C terminus (-COOH) that is intracellular. The transmembrane segments are alpha helices (H) that are labelled from helix 1

(H1) to H7. These helices are connected through loops that can be intracellular loops (ICL) or extracellular loops (ECL). The arrangement of helices creates a pocket that is a binding site for ligands. The binding of ligands leads to conformational changes (re-orientation of the helices with respect to each other) that induces activation of downstream pathways through the activity of heterotrimeric G-proteins, the latter composed of α, β and γ subunits[209].

Recently structures of the first class D fungal GPCR from *S. cerevisiae* for Ste2 (*Sc*Ste2) receptor was determined using cryo-EM[35]. An insect cell expression platform consisting of High Five insect cells was employed for recombinant production of the *Sc*Ste2 receptor[35]. A modified yeast G-α protein was engineered, capable of capturing the active state of *Sc*Ste2. At the same time, purification and assembly techniques for the necessary components were developed and then cryo-EM was used to decipher the structure. Ultimately an activated *Sc*Ste2 homodimer structure linked to two G-α subunits was obtained. Interestingly, a novel active state conformation was discovered, that has not been observed in other GPCRs belonging to other classes. In its inactivated state, the H7 helix blocks the G-protein coupling site by occupying space in between H1 and H6. Upon binding of the pheromone ligand, outward movement of H6 and H7 is observed on the cytoplasmic side of the membrane, opening access to the G-protein coupling site. This enables activation of the heterotrimeric G-protein subunits Gpa-1, Ste-4, and Ste-18. The homodimer interface was found to be comprised of the N-terminus, ECL1, H1 and H7[35,210].

Using the appropriate expression systems for GPCR production should ensure proper protein folding, stability, and functional behavior. Various platforms, including yeast-based *Pichia pastoris*, mammalian, and insect cells, have been employed for this purpose. Our aim was to find a robust recombinant expression system to recombinantly express and produce milligram

quantities of *Fg*Ste3 to perform structural studies in the future. Some GPCRs have been reported to achieve yields of up to 10 mg/L of media in mammalian and insect cell systems[211–213].

The use of mammalian cell expression systems is limited due to high costs, challenges in scaling up, and long experimental cycles. In contrast, insect cells, despite sharing some of these disadvantages, have proven to be more successful hosts in terms of yields. The post translational modifications (PTMs) differ between yeast, mammalian and insect cell systems, which matter when correct modifications are necessary to aid in interactions of the proteins with their lipid environment in the membrane. Mammalian cells have N-linked glycosylation that is lacking in insect cells as they add terminal sialic acid residues to proteins. These PTMs, including glycosylation, phosphorylation, and disulfide bond formation, are often critical for GPCR stability and function. Previous experiments in our lab involving recombinant expression and purification of *Fg*Ste2 in *Pichia pastoris* yielded only very low quantities of protein and hence that system was not followed up. However, subsequent efforts expressing *Fg*Ste2 in *Sf21* insect cells, were much more successful[214,215].

Sf21 cells allow for high-level expression of GPCRs, enabling the scaling up and production of milligram quantities of the protein. Though the High Five cell line has 5-10 fold higher levels of recombinant protein produced compared to *Sf21* and slightly faster doubling time (less that 18-24 hours compared to 24-30 hours for *Sf21*), it is more preferred for secreted recombinant proteins[216]. This is particularly advantageous for structural studies, as large amounts of purified GPCRs are required for optimization of crystallization conditions or cryo-EM sample preparation. *Sf21* cells provide a favorable environment for proper folding and stability of Ste3 GPCR, minimizing structural heterogeneity and facilitating high-resolution structure determination.[215]

The baculovirus expression vector system (BEVS) has been widely adopted for infection of insect cells and recombinant protein production. The infection process involves the transduction of the viral genome into the host cell nucleus, where it is replicated and expressed. Its genome consists of double stranded circular DNA and a nucleocapsid. Gene transcription in BEVS is controlled by the constitutively active very late polyhedrin p10 promoter and is used to control expression of the target gene. BEVS is highly versatile, as it can be used for both transient and stable expression of recombinant proteins. Transient expression involves infecting cells for a short period, typically 48-72 hours, to produce a high level of recombinant protein quickly. Stable expression, on the other hand, involves generating cell lines that maintain the recombinant gene stably integrated into the host cell genome, allowing long-term production of the desired protein. Polyhedrin protein itself is generated in abundant quantities (up to 20% of total synthesized proteins) in a natural manner and is not crucial for the spread of the virus in cell culture. Hence, it can be substituted with any desired gene[217,218].

Here I describe the recombinant expression of an *Fg*Ste3-mCherry fusion protein in *Sf21* cells using the BEVS transient expression system. Its expression was validated by confocal microscopy and Western blot analysis.

4.1.3 Results

4.1.3.1 *in-silico* evaluation of the *Fg*Ste3 structure

Toward the longer term objective of understanding structural aspects of the *Fg*Ste3 receptor mechanism of action an *in-silico* evaluation was conducted based on its known amino acid sequence.

To assess the homology of Ste3 orthologs in fifteen *Fusarium* species, their sequences were compiled and aligned by BLAST and analyzed using Jalview. The homology analysis revealed a

minimum identity of 80% between all orthologs, indicating a high degree of similarity within this genus. Notably, it shared maximum homology with *F. pseudograminearum* (96.27%) and *F. culmorum* (96.49%). The highest degrees of conservation are seen in TM1, TM3 and E1 and L2 loop hinting towards their important role in mediating activation of the receptor. The alignment is shown in **Figure 4-1-1**.

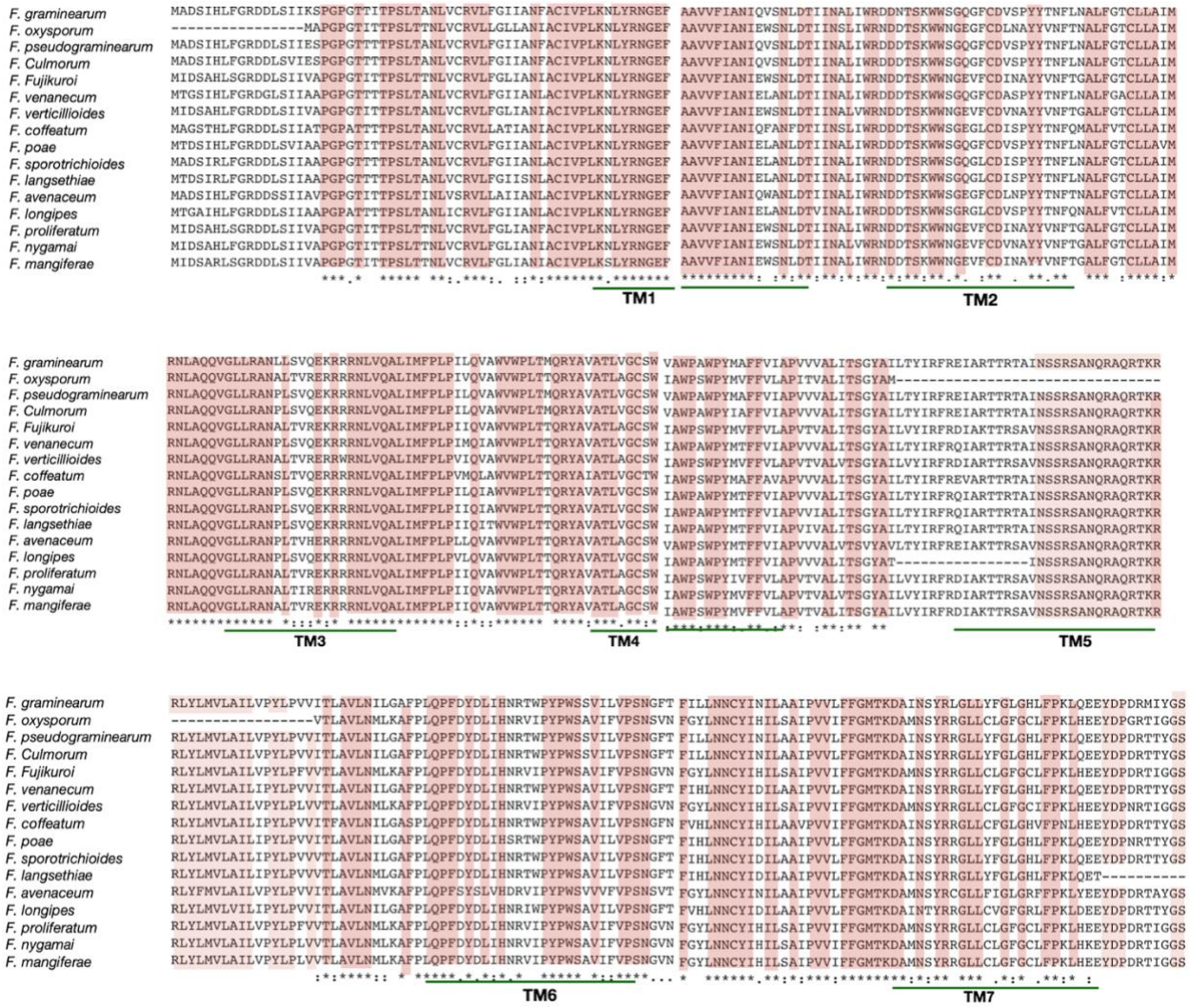

Figure 4-1-1. Ste3 sequence conservation in *Fusarium* species. Alignment of Ste3 sequence was performed using BLAST and Jalview. Dark peach denotes sites of 100 % conservation across all species evaluated. The transmembrane regions are denoted by green underlining. A single, fully conserved residue is denoted by an asterisk (*), while conservation between groups

of weakly similar properties is indicated by a period (.) with scoring =< 0.5 and > 0 in the Gonnet PAM 250. Conservation between groups of strongly similar properties, equivalent to scoring higher than 0.5 in the Gonnet PAM 250 matrix, is denoted by a colon (:)

The transmembrane regions and extracellular loops were predicted using the online tool TMHMM that showed seven transmembrane topologies expected for GPCRs connected through intracellular and extracellular loops. A serpentine scheme representing the 2-dimensional structure showing the membrane and loop regions is shown in **Figure 4-1-2 A**, made using Protter offered by ETH Zurich (https://wlab.ethz.ch/protter/start/). *Fg*Ste3 is predicted to consist of an N-terminus which is 28 amino acid residues long and C-terminus that is 133 amino acid residues long. There are 5 predicted N-glycosylation sites found in full length *Fg*Ste3 sequence with 2 of them in the C terminus. Three-dimensional structure predictions of *Fg*Ste3 were conducted using Alphafold (**Figure 4-1-2 B)**. A connecting alpha helix loop is present in between TM3 and TM4. TM4 and TM5 are connected via beta sheets. The predicted structure of *Fg*Ste3 using Phyre2 shares the highest homology with Human β-2 andregenic receptor (19% identity with 97% confidence as calculated by Phyre2. The length of the transmembrane segments varies between the two receptors, but the overall structural homology was present.

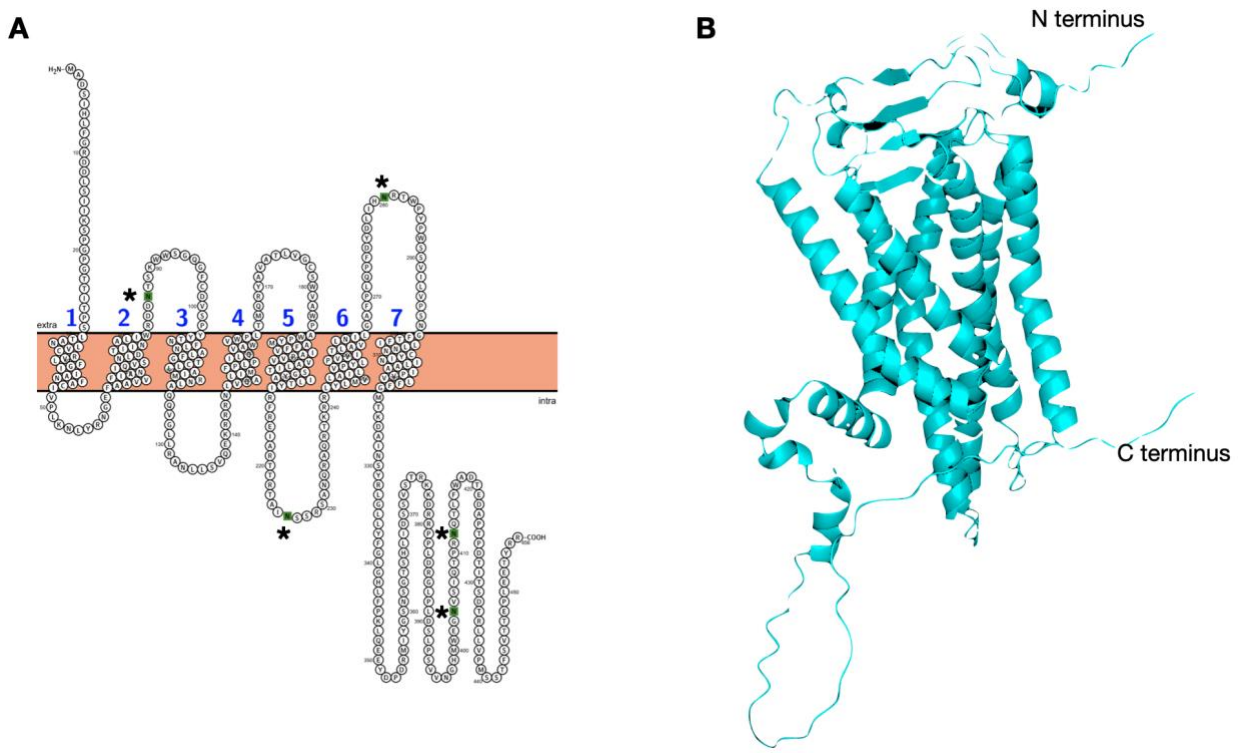

Figure 4-1-2. Prediction of *Fg*Ste3 structure. A. *Fg*Ste3 consists of serpentine schematic representation of 7 transmembrane regions and loops representing a two-dimensional arrangement made using Protter online tool. The N-terminus is outside the membrane and consists of amino NH_2 terminal and the C terminus containing carboxy (-COOH) terminus is inside the cell. The starts denote position of N-glycosylation sites. **B.** Three-dimensional structure prediction of Ste3 was carried out using Alphafold. The models were subsequently visualised using Pymol v2.1.0.

Though improvements in protein modeling and artificial intelligence models are being made, prediction techniques fall short in accurately reproducing the original protein structure due to challenges in exploring the vast conformational space, limitations in template-based approaches, difficulties in accounting for environmental factors, and the inherent complexity of protein folding. Approximations and computational algorithms used in modeling introduce errors, while the

dynamic nature of proteins and their interactions further complicate accurate predictions. Experimental methods like X-ray crystallography and NMR spectroscopy remain superior in providing detailed and precise protein structures.

4.1.3.2 *Fg*Ste3-mCherry recombinant expression and purification

Baculovirus mediated transfection of *Sf21* cells was carried out using MOI=5 (optimized previously for *Fg*Ste2 and gave high protein yield at 72 hours post infection[195]). The STE3 gene was cloned under the control of a strong polyhedrin promoter which led to large amounts of protein being formed. The protein expression was monitored by visualization of mCherry through fluorescence microscopy compared to the uninfected control (**Figure 4-1-3 A**). The appearance of bright red coloring confirms the mCherry expression and as part of the *Fg*Ste3-mCherry fusion protein in *Sf21* cells. In addition, mCherry fluorescence in transfected and non-transfected cells was verified using a microplate reader using fluorescent settings. Outputs showed significantly higher fluorescence observed in transfected cells compared to control wells containing uninfected cells. Following normalization with SFM media, relative fluorescence units were plotted using a bar graph as shown in **Figure 4-1-3 B**.

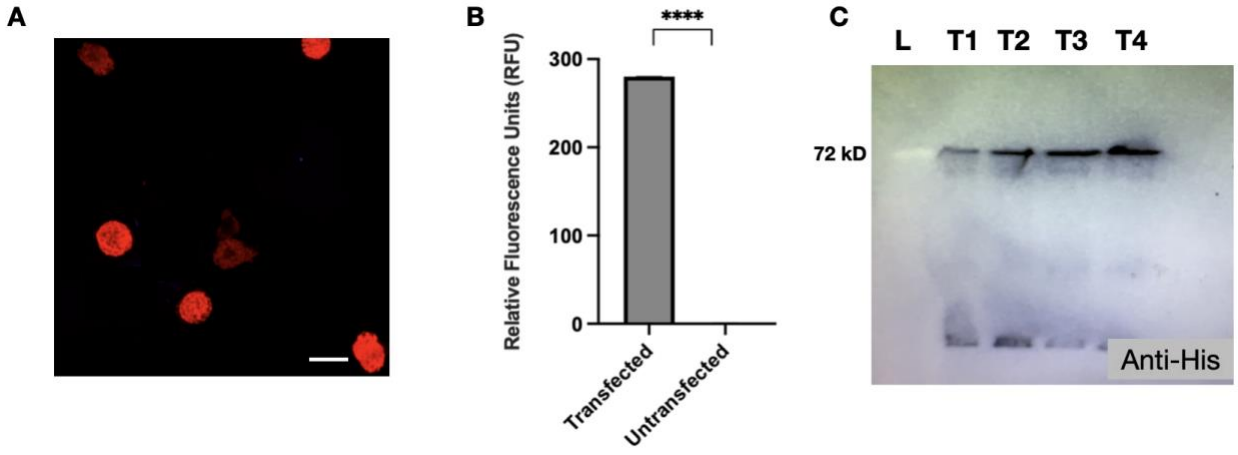

Figure 4-1-3. Confirmation of *Fg*Ste3 expression in Sf21 insect cells. **A.** Expression confirmation of *Fg*Ste3-mCherry construct was done using confocal microscopy Bright red hue denotes presence of Ste3 protein. *Sf21* cells infected with P2 baculovirus at an MOI of 5. Cells were imaged at 40x magnification 48 h after infection. Scale bar represent 50 μM **B.** The bar graph shows presence of Ste3 protein detected by measuring Relative Fluorescence Units (RFU) in transfected vs untransfected cells. The fluorescence measurement using a multiplate reader at eh excitation and emission wavelength of mCherry. **C**. The total cell lysate extracted was solubilized using a detergent cocktail of 0.1% SDS, 1% Triton X and 0.1% sodium deoxycholic acid. The monomeric form of *Fg*Ste3 was seen at the expected molecular size of 81kDa is shown in replicates as T1, T2, T3 and T4.

The solubilization of *Fg*Ste3 from insect cell membrane fractions was carried out using two different detergent conditions. First, non-ionic DDM detergent was used at a 1 % concentration for overnight solubilization at 4°C. Solubilization with DDM yielded multiple bands with higher molecular weight bands detected at 150 kDa that probably correspond to SDS-resistant *Fg*Ste3 dimers (**Figure 4-1-4 A, B**). A band close to the expected size of Ste3-mCherry at 81 kDa was seen. Additional bands were observed at around 50 kDa that most likely correspond to folded versions of the receptor or that lack full post translational modifications[219]. In comparison, a solubilization was also carried out using a combination of 3 detergents in a single cocktail: 0.1 % SDS, 0.1 % Deoxycholic acid and 1 % Triton-X. This yielded a single band detected at the expected size at 81 kDa corresponding to *Fg*Ste3-mCherry fusion protein (**Figure 4-1-3 C**). While the cocktail was useful for SDS-PAGE analysis, DDM is widely recognised for solubilization of

membrane proteins due to its milder nature in maintaining the functionality of the proteins which is required for structural elucidation.

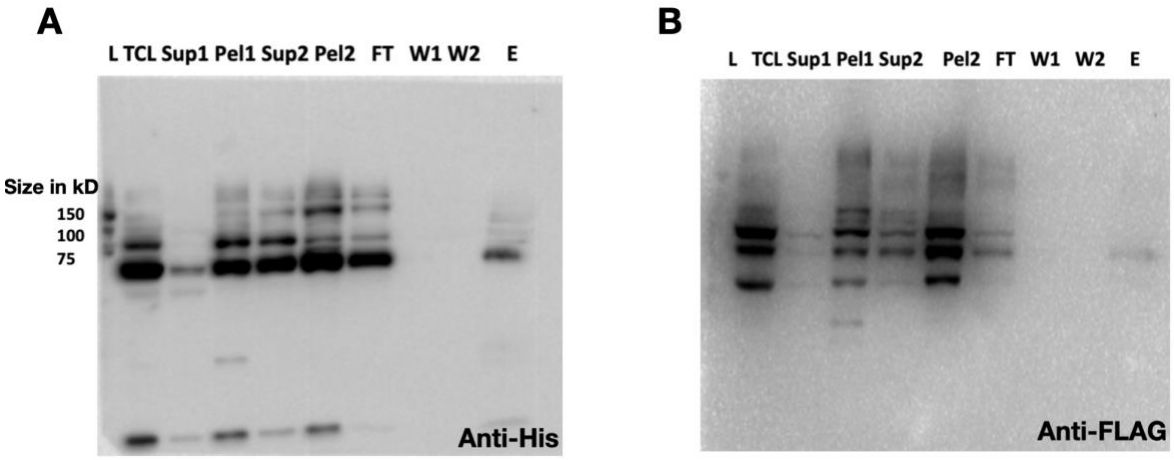

Figure 4-1-4. Western blot analysis to confirm expression of *Fg*Ste3 from *Sf21* insect cells. Cell lysis followed by 1% DDM solubilization was performed followed by purification using Ni-NTA for capturing his tagged *Fg*Ste3 fusion protein. Following detergent solubilization, samples were clarified, and supernatant (Sup) and pellet (Pel) fractions were resolved using SDS-PAGE and western blotted using Anti-His antibody (**A**) for His tag (on the C terminus) and anti-FLAG antibody (**B**) for FLAG tag (on N terminus) present in the fusion protein (two sample tubes were there and hence 2 supernatant and pellet fractions). Wash and Elution fractions are denoted by W and E. Expected molecular weight of the monomeric form of Ste3 protein is around 81kDa. Different forms of *Fg*Ste3 receptor were observed on the gel with a band detected at 81kDa and doublet band seen at 50 kDa. FT represents flow through fraction and TCL represents total cell lysate.

The purification of *Fg*Ste3 was carried out using Ni-NTA based affinity resin. Three wash and elution fractions were collected for each experiment. These fractions were run on an SDS-PAGE gel then transferred to the PVDF membrane for Western blotting. Upon immunoblotting with anti-His antibody, the majority of the protein was detected in the pellet representing the membrane fraction, with significantly lower concentration detected in the supernatant (**Figure 4-1-4 A, B**). The protein band corresponding to the monomeric form of the *Fg*Ste3 fusion protein was observed at about 72 kDa running slightly below its expected molecular size of 81 kDa. Baculovirus harbouring our expression construct was used for transfection of Sf21 insect cells that yielded 10 μg of protein per mL from a small-scale purification experiment done in T25 flasks.

GPCRs are known to not run at exact molecular weight due to their complex folded nature and post translational modifications showing anomalous patterns[220,221]. Additional protein bands can be seen in the 90-150 kDa range which correspond to higher order oligomers that are resistant to SDS. Interestingly, most of the protein bands appeared in the flow through with some protein detected in elution fractions. This could be due to problem in protein binding to resin (due to aggregation), His tag sequestered in a fold within a protein that would not let it interact with the resin or adjusting the pH of the elution and wash buffers by further optimization to prevent protein loss.

4.1.4 Discussion

Filamentous fungi GPCRs control important cellular events like fusion, morphogenesis, chemotaxis, virulence establishment, pathogenic development, and secondary metabolite production. Various fungi, including *Aspergillus nidulans*, *Magnaporthe grisea*, *Cryptococcus neoformans*, *Neurospora crassa*, *Verticillium spp*., and *Trichoderma spp*., have been identified to encode GPCRs. Notably, Family D, exclusive to fungi, consists of fungal pheromone receptors Ste2 and Ste3[222–224].

Our work with the recombinant expression of *Fg*Ste2 and *Fg*Ste3 highlights the feasibility of employing the baculovirus overexpression system to produce large quantities of fungal GPCRs in insect cells, which can then be purified for structure determination[35,195]. Recently, the first structure of a class D GPCR Ste2, a pheromone receptor found in *S. cerevisiae* yeast was resolved. This structure serves as a blueprint for comprehending other class D GPCRs and designing novel drugs that target fungal GPCRs. The successful use of an insect cell expression system in this study lays the groundwork for unraveling the structure and function of other fungal GPCRs, including Ste3. The investigations from our lab with previous utilization of *P. pastoris* system for GPCR expression and purification did not yield sufficient quantities of proteins. High Five insect cells have faster doubling time and produce almost 10 times higher quantities of protein that *Sf21*, but the cells are formed irregularly and are multilayered making them hard to visualize under the microscope. Thus we initially used an *Sf21* insect cell system which grew and passaged well[225,226]. Further optimization of purification methods like using mCherry specific agarose beads, TALON resin (IMAC resin charged with Cobalt, Co^{2+} and is more specific for binding His tagged proteins) should be employed in the future to ensure maximum capture of the *Fg*Ste3 protein.

Mild detergents and cholesterols are commonly utilized to solubilize receptors, with detergents shielding the transmembrane helices and cholesterols exerting lateral pressure to stabilize them. Initially the solubilization with DDM overnight yielded multiple bands, which could represent SDS resistant dimers. A combinatorial approach was applied where a cocktail of anionic, zwitterionic detergent yielded a single band at the correct molecular weight corresponding to the monomeric form of *Fg*Ste3 receptor. Though successful, the functionality of the extracted receptor in these micelles requires further investigation. The quality of the solubilized receptor can be confirmed through techniques such as SEC coupled to Multiangle Light Scattering (MALS) and Differential scanning calorimetry (DSC) to assess homogeneity and thermal stability of the protein.

Although there remains a significant amount of work to obtain an high resolution structural map of FgSte3, *in-silico* structural prediction provides a short term alternative. Modelling was performed for *Fg*Ste3 using AlphaFold and Phyre2. Phyre2 showed highest amino acid sequence identity of *Fg*Ste3 to Human β-2 androgenic receptor at 19% identity, with 97% confidence. Thus, perhaps owing to a higher resolution structure for β-2 andregenic receptor and more similarity to its protein folds, it was the preferred choice for modelling. Compared to the *Sc*Ste2 structure, the predicted Ste3 structure differs in the arrangement of its TM7 which appears like a helix turn helix on the bottom left (**Figure 4-1-2 B)**. In addition, the presence of beta sheet region connecting TM4 and TM5 is more prominent in *Fg*Ste3 structure that perhaps plays an important role.

The nature of ligands controlling receptor activity, controls its confirmational changes. In the case of *Sc*Ste3, a-factor ligand must diffuse in and out of the receptor's binding pocket. Consequently, possibly the hairpin structure formed by β-sheets possibly acts as a lid to shield it from hydrolysis and create a hydrophobic pocket for the ligand to bind. Due to their low solubility

in water and a large N-terminal domain plug obstructing access from the extracellular milieu, hydrophobic ligands reach the receptor binding site through the lipid bilayer. In the case of endogenous hydrophobic ligands of lipid receptors, like anandamide and sphingosine-1-phosphate, membrane components synthesize the ligand when needed which are metabolized by membrane-penetrating enzymes such as fatty acid amide hydrolase. As a result, a swift and efficient signalling process is regulated without the ligands leaving the membrane environment[227].

Previous investigations on the *Sc*Ste3 receptor revealed that substituting leucine-194 with glutamine in the receptor's third cytoplasmic loop led to a 20-fold increase in pheromone sensitivity and hyperactivation of the response pathway. These findings indicate the involvement of the third cytoplasmic loop in maintaining a non-signaling state of the receptor. Furthermore, a mutation that truncates a significant portion of the receptor's C-terminal domain also resulted in a 20-fold increase in pheromone sensitivity, suggesting that this domain is involved in the negative regulation of the receptor. These individual mutations independently affect receptor activity, as evidenced by the 400-fold increase in pheromone sensitivity observed in the double mutant[228]. These studies provided information about ligand-specific conformational rearrangements in general terms but did not offer direct information at the atomic level on the binding modes of the ligands or how these ligands could stabilize distinct conformations leading to different signalling pathways. The high-resolution structures obtained from the crystallized proteins will start providing answers to these questions.

It is plausible that *Fg*Ste3 operates via a mechanism akin to that of *Sc*Ste2 though they share low sequence homology; nevertheless, the precise process by which its peroxidase-generated ligand binds to *Fg*Ste3 or *Fg*Ste2 leading to pathogenicity is yet to be determined. Additionally,

the intracellular effector proteins that get activated in response to peroxidase in this scenario remains unidentified, underscoring the necessity for comprehensive structural analyses.

While software like AlphaFold can predict GPCR structures, there have been instances where predicted models and experimental structures exhibited disparities in the shape and conformation of ligand-binding pockets and transducer-binding interfaces, limiting the use of predicted models for structure-based drug design. Nevertheless, with a greater availability of representative experimental structures, structure-prediction algorithms are expected to improve and can complement experimental approaches in gaining comprehensive insights during drug development. This will facilitate the development of drugs with enhanced efficacy and potency[229–231]. Determining structures of proteins less than or equal ~50kDa using cryo-EM presents significant challenges. Generally, proteins larger than 200kDa are considered more favorable targets. Accurate alignment of particles is required to obtain a structure, which can be more difficult with small proteins. Larger targets with more discernible features are easier to identify and align during the reconstruction process. The evidence that *Fg*Ste2 and *Fg*Ste3 form a heterodimer to transduce the signal from the peroxidase-generated ligand would make the heterodimer complex of the right size for CryoEM studies.

Ultimately, elucidation of fungal GPCRs structure will enable us to study their ligand binding pocket and binding mode for designing targeted drugs. Future studies involving testing the functionality of the purified *Fg*Ste3receptor will be carried out. Usage fungal mini-G proteins, to stabilize the active state of GPCRs and the "pre-stabilization of a GPCR by weak association" (PSGWAY) methodology to stabilize ligand-free GPCR states for structural analysis has been deemed successful in recent studies. The purification of GPCRs can pose challenges, influenced by factors such as detergent compatibility, receptor solubilization, and accessibility of affinity tags,

all of which impact the capture of the receptor. Minimizing buffer and temperature changes during purification can help maximize the purification of the receptor. This will enable the development of optimized *Sf21* insect cell platforms for efficient recombinantly expression and purification of Ste2 and Ste3 protein for structural studies.

4.1.5 Material and Methods

All materials were obtained from Sigma^{TM}, unless otherwise indicated below.

4.1.5.1 Homology sequence analysis of Ste3 across fungal species

A BLAST search was conducted using the protein sequence of *Fusarium graminearum* STE3 (Accession ID: FGSG_07270) across 15 *Fusarium* species. The sequence alignment was performed using Clustal omega and the obtained alignments were viewed using Jalview. The full proteins sequences for *Fusarium* species Ste3 receptors were retrieved from NCBI.

4.1.5.2 *In-silico* analysis of Ste3 structure

An analysis of Ste3 secondary structure was carried out using *in-silico* tools for protein structural prediction. PSIPRED (https://bio.tools/psipred) and TMHMM (https://services.healthtech.dtu.dk/services/TMHMM-2.0/) were used to predict transmembrane helices and extracellular and intracellular loops. Protter (https://wlab.ethz.ch/protter/) was used to generate a serpentine scheme and identify N-linked glycosylation sites in Ste3. The 3D structure of Ste3 was predicted using Alpha Fold[232].

4.1.5.3 Design of Ste3 expression construct for *Sf21* insect cells

A recombinant baculovirus was generated where the *Fg*Ste3 gene was synthesized, and codon optimized for expression in insect cells. It was integrated into the viral genomic DNA under the control of the polyhedrin promoter that controls the expression of viral capsid. The expression construct for transfection of *Fg*Ste3 protein in *Sf21* insect cells were designed as shown in **Figure 4.1-5**. The expression construct was created, and sequence verified by Genscript™. The construct consisted of a FLAG tag on the N-terminus of the protein followed by STE3 fused to mCherry. A tobacco etch virus (TEV) cleavage site consisting of Glu-Asn-Leu-Tyr-Phe-Gln-(Gly/Ser) residues that cleaves between the Gln and Gly/Ser residues was added to enable removal of the mCherry tag to potentially address any arising concerns about the impact of affinity tags on the structure of the *Fg*Ste3 protein. Typically, target proteins are separated from the fusion protein by site-specific proteolysis after affinity chromatography. The TEV cleavage site is followed by mCherry and a 10X Histidine tag for fluorescence microscopy detection and purification purposes. Baculoviral P2 stock in high titre (2 x10^8) harboring the construct was obtained from Genscript™ for carrying out the transfection.

Figure 4-1-5. Expression construct design for expressing *Fg*Ste3 in *Sf21* insect cells. *Fg*Ste3 was fused to a FLAG tag on the N terminus followed by TEV-cleavable mCherry and a 10XHis tag at the C-terminus.

4.1.5.4 Insect cells maintenance and passaging

The *Sf21* insect cells were provided by Dr. Zongchao Jia from Queen's University. The cells were cultured in SF-900TM II SFM media in either T-25 or T-75 cell culture flasks at 27 °C and passaged until 80-90 % confluency was observed. The media was aspirated off and the cells were detached using mechanical tapping. Cell counting was performed using a hemocytometer and cell viability was assessed using trypan blue. The cells were assessed using a Nikon SMZ1000 microscope. The cells were either readily transfected or stored for future use in a liquid nitrogen storage facility.

4.1.5.5 Freezing insect cells

A freezing medium containing a cryopreservation buffer (Fetal Bovine Serum, DMSO, SF-900TM II SFM) was used for storing insect cells. Cell suspensions, in range of 1-10 million cells per milliliter, were transferred into cryovials in desired volumes (1 mL aliquots). Care was taken to ensure proper sealing to prevent contamination and leakage. The cryovials were then placed in a controlled-rate freezing container (Mr.Frosty, ThermoFisher Scientific) allowing the cells to gradually cool at a controlled rate (1°C/minute) and kept overnight in -80°C. Once adequately frozen, the cryovials containing *Sf21* insect cells were transferred to a liquid nitrogen storage tank (-80°C). Proper labeling of the storage containers with essential information, including cell line name, passage number, and freezing date, was ensured. To revive the cells, they were quickly thawed under running water or agitated in water bath at 37°C for 30-40 seconds till completely thawed and suspended in 1mL of fresh SF-900TM II SFM media. This was followed by centrifuging the cells and resuspending them in freshly T-25 flasks at 27°C.

4.1.5.6 Transfection of *Sf21* insect cells with *Fg*Ste3

Sf21 cells in T-75 flasks were grown until they reached 80-90% confluency, at which time the cells were detached and counted. The virus stock was diluted to achieve desired Multiplicity of Infection (MOI) of 5. MOI refers to the ratio of number viral particles to the number of cells. It is calculated using the following formula:

Volume of Baculovirus to use= (MOI*Number of target cells) / (Viral titre of P2 stock)

The growth medium in the cell culture dish was replaced with the calculated volume of baculovirus stock in SF-900 SFM media. Subsequently, the dish was incubated at 27°C and monitored at 24 h and 48 h time points to allow for efficient virus-cell interaction. After the incubation period, the virus-containing medium was carefully aspirated, and cells were released by mechanical tapping. The cell suspension was centrifuged at 4000 x g for 20 minutes to harvest the cells and the excess media was removed.

4.1.5.7 Expression analysis of *Fg*Ste3

Sf21 cells expressing *Fg*Ste3 protein were visualized and imaged using an Olympus IX83 inverted microscope equipped with a 20x objective lens and an Andor Zyla 4.2 plus camera. The imaging was performed using cellSens software. To visualize the mCherry-tagged *Fg*Ste3 protein within the cells, a red filter was utilized during imaging. In addition, the expression was tested through fluorimetry comparing mCherry fluorescence in transfected and non-transfected cells in 96-well white optiplates (PerlkinElmer). mCherry was excited at a wavelength of 587 nm and the emission was read at a wavelength 610 nm using Spectramax m5e microplate reader with fluorescence acquisition settings.

4.1.5.8 Isolation of membrane fraction and protein solubilization conditions

Lysis buffer (10 mM HEPES at pH 7.5, 1 mM Ethylenediaminetetraacetic acid (EDTA), 10 mM MgCl2, 2 mM phenylmethylsulfonyl fluoride (PMSF), 1 uL of Benzonase and a Protease Inhibitor Cocktail (PIC, Roche) was added to the cells. Cell lysis was carried out using sonication (Sonics & Materials, vibra-cell) performed on ice for 2.5 minutes with intervals of 10 seconds on/40 seconds off at 65 watts. The obtained lysate was centrifuged first at 5000 x g for 5 minutes to remove cellular debris. Following this, the cells were ultracentrifuged at 50,000 x g for one hour to isolate the membrane fraction. The membrane pellet was resuspended in solubilization buffer (20 mM HEPES at pH 7.5, 100 mM NaCl, 20% Glycerol, 10 mM $MgCl_2$, 1% w/vn-Dodecyl-B-D-Maltoside (DDM), 0.1% w/v Cholesteryl Hemisuccinate Tris Salt (CHS), 2 mM phenylmethylsulfonyl fluoride (PMSF),1 uL of Benzonase and Protease Inhibitor Cocktail (PIC, Roche) followed by passing the suspension through an 18 gauge syringe to get rid any aggregates. The resulting samples were rotated end over end overnight at 4°C. A second solublization buffer was used which consisted of 20 mM HEPES, pH 8.0, 20 % glycerol, 100 mM NaCl, 10 mM MgCl2, 0.1% SDS, 1% Triton-X and 0.1% Sodium deoxycholic acid.

4.1.5.9 Purification of Ste3-mCherry protein from the membrane fraction

The purification column consisted of Ni-NTA resin. Wash Buffer (20 mM HEPES at pH 7.5, 300 mM NaCl, 20% Glycerol, 10 mM MgCl2, and 40 mM Imidazole) was added to calibrate the column. The solubilized membrane fraction was added to the column and allowed to bind in batch mode for 10 minutes with end over end shaking. Washing was performed thrice 3x the column volume to get rid of non-specific proteins and flow throughs were collected. Subsequently, the protein was eluted with 1x column volume of elution buffer three times (20 mM HEPES at pH

7.5, 100 mM NaCl, 20% glycerol, 10 mM MgCl2, and 300 mM Imidazole). The elution fractions were collected and stored on ice.

4.1.5.10 Detection of *Fg*Ste3 expression through immunoblotting

For Western blotting analysis, the following procedure was employed. The total protein content in the cell lysates was determined using Bradford assay[233]. Equal amounts of protein were loaded onto a 10 % SDS-PAGE gel and electrophoresed at 150V until the loading dye reached the end of the gel. Subsequently, the proteins were transferred onto a pre-activated PVDF membrane via wet electroblotting at 100 mA for 2 hours on ice, using transfer buffer. After transfer, the PVDF membranes were blocked in 5% skim milk in TBST for 1 hour at 4 °C with gentle agitation. Following the blocking step, the membranes were incubated overnight at 4 °C with gentle agitation in a 1:1000 dilution of anti-6x His antibody (Abcam, ab1187) prepared in 5% skim milk in TBST. The next day, the membranes were washed three times with TBST and then treated with Pierce™ ECL Western Blotting Substrate for band detection. To probe for the FLAG tag, the membranes were stripped using a stripping buffer and incubated for 1 hour at 4 °C with rabbit anti-FLAG antibody (Sigma A8592) diluted 1:1000 in 5% skim milk in TBST. The blots were washed three times with TBST followed by visualization using enhanced chemiluminescent substrate (Thermo Scientific, 32209) emitted light was captured using a GelDoc Imager and the Image Lab software package (Bio-Rad).

Chapter 4.2: A Role for an Abscisic Acid Biosynthetic Gene in *Fusarium graminearum* during its early Infection of Wheat

4.2.1 Abstract

The genome of *Botrytis cinerea* encodes five genes that have been characterized as comprising an abscisic acid (ABA) biosynthetic gene family. In pathogenic fungi, fungal derived ABA has been shown to accentuate disease severity with a potential role in contributing to disease pathogenesis. To date, no such ABA biosynthetic genes have been characterized in *F. graminearum* (*Fg*). Here, we report for the first time, identification of an ABA biosynthetic gene homologue in *Fg* and details of its differential expression upon infection of wheat. Initially, the sequences of known members of the fungal ABA biosynthetic pathway from *B. cinerea* were used to BLAST against *Fg* sequences in NCBI and ENSEMBL databases. A single hit was obtained with 75.8 % identity to *Bc*CPR1, a known ABA biosynthetic cytochrome p450 oxidoreductase from *B. cinerea*. This gene is referred to as *Fg*CPR1-like heretofore. It consists of a conserved NADPH cytochrome p450 reductase (CYPOR) domain. Subsequently, a pre-existing global transcriptomic RNA-seq dataset for the *Fg*-susceptible *Triticum aestivum* L. cultivar 'Fielder' in the presence or absence of *Fg* challenge, upon treatment with ABA and an ABA receptor antagonist (AS6) was mined. *Fg*CPR1-like was found to be expressed under all tested conditions, with co-application of *Fg* + AS6 leading to some downregulation compared to *Fg* alone. More broadly, comparison of differentially regulated *Fg* genes in the *Fg* + ABA and *Fg* + AS6 conditions highlighted changes in activity of hydrolases, organic substance metabolic process (20%) and membrane components (24%). Together these results suggest that expression of *Fg*CPR1-like is relevant at the 24 h time point after *Fg* infection.

4.2.2 Introduction

Abscisic acid (ABA) biosynthesis and signaling is believed to be an ancient process found in early unicellular eukaryotes which followed divergent evolution. Currently, while primarily associated with plant development and stress responses, several phytopathogens have now been found to also possess the ability to synthesize ABA. With respect to fungal pathogenesis, most of the ABA is secreted and believed to be a host mimicry response to manipulate or hijack host hormone homeostasis[234,235]. *P. syringae* has been shown to utilize a secreted 'effector' molecule, modulating the endogenous ABA biosynthesis and response pathways in the host plant[236][. An ABA gene family was discovered in *B. cinerea* that consisted of *BcABA1*, *BcABA2*, *BcABA3*, *BcABA4* and *BcCPR1*. Similarly, the rice blast fungus *Magnaporthe Oryzae*, which depends on the same ABA biosynthesis pathway as *B. cinerea*, relies on ABA for virulence and to form appressoria for infection[237–240].

The fungal ABA biosynthesis pathway is distinct from that of plants and is referred to as the "direct" or "mevalonate" pathway, in contrast to plants that produce ABA via cleavage of large C-40 carotenoid molecules. The "direct" fungal pathway is via sesquiterpenes (C15) intermediates and occurs in the cytoplasm of the cell. In this pathway, a C-5 metabolite, isopentenyl diphosphate (IPP) is produced from the MVA pathway, which is condensed to form the C-15 farnesyl diphosphate (FPP) also called as farnesyl diphosphate (FDP). Subsequently, the FDP undergoes several steps of modification to generate ABA (**Figure 4-2-1**). Isomers of ionylideneethanol (IE) and/or ionylideneacetic acid have been identified from several fungi and are proposed to be the endogenous precursors of ABA in fungi[241,242]. In *B. cinerea* and *C. pini-densiflorae*, α-ionylideneethane as α-IE is likely the predominant precursor whose endogenous levels are correlated with ABA synthesis while 1′,4′-trans-dihydro-γ-ionylideneacetic acid (DH-IAA) is

thought to be simply an intermediate of ABA biosynthesis. During the conversion from ionylidene ethanes to ABA, atmospheric oxygen is incorporated into ABA at C-1, C-1′, and C-4′ in *C. cruenta* and *B. cinerea*. A P450 has been shown to be involved in these hydroxylation and oxidation steps which is proposed to be *BcCPR1*, a cytochrome p450 oxidoreductase enzymes since P450 inhibitors can effectively block ABA production.[241–243]

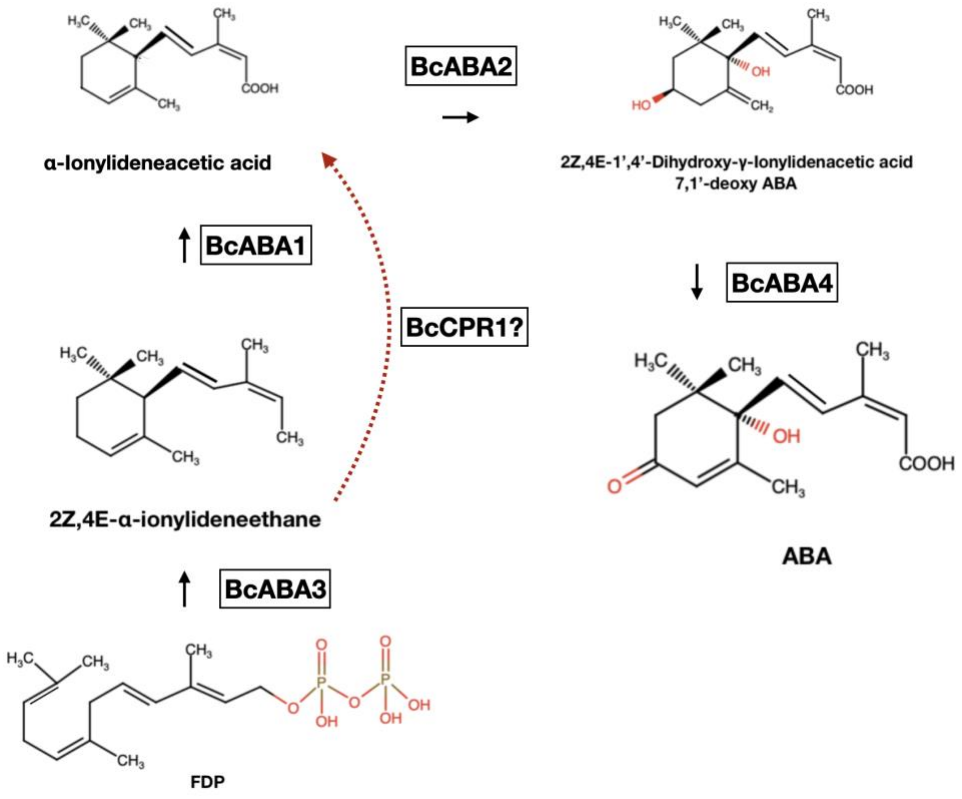

Figure 4-2-1. Pathway for ABA biosynthesis in fungi. Reactions catalyzed by enzymes (boxes) from *B. cinerea* that form the ABA gene cluster (Pathway based on Takino *et al.*)[244].

An ABA biosynthetic gene cluster was first identified in *B. cinerea.* It consists of 4 primary genes. First is *BcABA1* which is a P450 monooxidase gene. Downstream of *BcABA1* is *BcABA2*,

a second P450 mono-oxygenase-encoding gene. On-going 3.7 Kb upstream of *BcABA1* is *BcABA3*, an unknown protein[245,246]. In an RNA-seq experiment involving the addition of the ABA precursor, mevalonic acid, a significant and persistent expression was seen for *BcABA1* after 90 min, expression was also detected for *BcABA2*, starting after 60 min. Expression of *BcABA3* was likewise enhanced at 60 and 90 min after the addition of MVA but declined again after 120 min, whereas *BcABA4* was constitutively expressed at a low level. Surprisingly, another gene, not considered part of the gene subfamily was induced up to 120 min only under the conditions of ABA biosynthesis. It was a cytochrome P450 (CYP) oxidoreductase and hence was referred to as *BcCPR1* gene[247]. Deletion of *BcCPR1* led to significant decrease in ABA production (from 2927 nmol/L in WT to 2.14 nmol/L in *BcCPR1* deletion mutant)[248].

Cytochromes P450 are haem containing monooxygenases that catalyze a wide variety of reactions; e.g. hydroxylation, epoxidation, oxidation, reduction, deamination, dehalogenation, dealkylation, dehydrogenation and demethylation[249,250]. Nonetheless, they all insert one atom of molecular oxygen into an organic substrate. To perform this reaction, they must activate molecular oxygen that requires the sequential delivery of electrons to the haem cofactor in the CYP active site. The source of electrons is coenzymes NADH or NAD(P)H[251–253]. We aim to look for elements of ABA biosynthetic pathway in *F. graminearum* based on previous reports of ABA contributing to disease pathogenesis.

4.2.3 Results

4.2.3.1 *F. graminearum* encodes a homologue of the *Bc*CPR1 gene, while the presence of other ABA biosynthetic genes remains enigmatic

To identify potential ABA homologues in *F. graminearum*, known genes involved in the ABA biosynthetic pathway from phytopathogenic ascomycete *B. cinerea* were retrieved from NCBI and used for BLAST analysis in the ENSEMBL database against *F. graminearum* (http://fungi.ensembl.org/Fusarium_graminearum/). For *BcABA1*, the highest homology was seen for FGSG_12534 at 22.2 % sequence identity. For *BcABA2*, FGSG_08023 was detected with 37.2 % identity, as well as FGSG_12534 with 38.4 % identity and FGSG_03540 with 36.7 % identity. For *BcABA4*, the closest identity was seen for FGSG_04826 at 30.2 % and FGSG_10025 at 30.2 %. The highest identity at 75.8 % identity was obtained for the gene FGSG_09786 (FGRAMPH1_01T26277) against *BcCPR1*, a known cytochrome p450 oxidoreductase in *B. cinera* proposed to play a role in ABA biosynthesis by incorporating molecular oxygen during the conversion of Ionylidene ethanes to ABA helping *BcABA1*[248] (**Figure 4-2-1**). This gene is referred to as *FgCPR1*-like going forward.

```
Bcin12g03180.1        MGGQLDVLDIVVLGVLALGTIAYFTKGKYWGVVKDPYATSYAATNGNKPAKTRNITEKMD     60
FGRAMPH1_01T26277     -MAELDTLDVIVLGVIFLGTVAYFTKGKLWGVTKDPYANGFAAGGAAKPGRTRNIVEAME     59
                        .:**.**::****: ***:******* ***.*****..:** .. **.:****.* *:

Bcin12g03180.1        ESNKNCVVFYGSQTGTAEDYASRLAKEGKSRFGLETMVADLEDYDYDTLDTFGEDKVAIF     120
FGRAMPH1_01T26277     ESGKNCVIFYGSQTGTAEDYASRLAKEGKSRFGLNTMIADIEDYDFDSLDTVPNDNVVMF     119
                      **.****:**************************:**:**:****:*:***. :*:*.:*

Bcin12g03180.1        VLATYGEGEPTDNAVDFYEYFMNEDVEFSSGE-KSLANLKFVAFGLGNNTYEHYNSMVRN     179
FGRAMPH1_01T26277     VLATYGEGEPTDNAVDFYEFITGEDATFNEGNDPPLGNLNYVAFGLGNNTYEHYNAMVRK     179
                      ********************:: .**. *..*:   *.**::***************:***:

Bcin12g03180.1        VTKAFEKLGATRIGEAGEGDDGAGTMEEDFLAWKDPMWTALAEKMGLQEREAVFEPVFAI     239
FGRAMPH1_01T26277     VDQALEKFGAHRIGEAGEGDDGAGTMEEDFLAWKDPMWESLAKKMGLEEREAVYEPIFAI     239
                      * :*:**:** *************************** :**:****:*****:**:***

Bcin12g03180.1        TDREELTKDSSEVYLGEPNKMHLEGTSKGPYNAHNPYIAPISESKELFTVKDRNCLHLEI     299
FGRAMPH1_01T26277     NERDDLSPESNEVYLGEPNKLHLEGTAKGPFNSHNPYIAPIAESYELFSAKDRNCLHMEV     299
                      .:*:!*: :*.*********:*****:***:*:********:** ***:.*******:*:

Bcin12g03180.1        DISGSNLSYQTGDHIAVWPTNAGREVDRFLDVTGLSSKKDSVITVKALDSTAKVPFPTPT     359
FGRAMPH1_01T26277     DISGSNLKYETGDHIAIWPTNPGEEVNRFLDILDLSGKQHSVITVKALEPTAKVPFPNPT     359
                      *******.*:*******:**** *.**:****: .**.*:.********: *******.**

Bcin12g03180.1        TYDAIVRYHMEICAPVSRQFLATLAAFAPNDAIKAEMEKLGGDKDYFHQKISNNYLNIAQ     419
FGRAMPH1_01T26277     TYDAILRYHLEICAPVSRQFVSTLAAFAPNDSIKAEMNRLGSDKDYFHEKTGPHYYNIAR     419
                      *****:***:**********::*********:*****:::**.*******:* . :* ***:

Bcin12g03180.1        VLQEVGGQEKWSAIPFSAFIEGLGKIQPRYYSISSSSLVQKKKISITAVVESTDIPGRTD     479
FGRAMPH1_01T26277     FLSSVSKGEKWTTIPFSAFIEGLTKLQPRYYSISSSSLVQPKKISITAVVESQQIPGRDD     479
                      .*..*.  ***::********** *:************** ********** :**** *

Bcin12g03180.1        ALKGVTTNYLLALKQKQHGDEHPDPHGLTYEITGPRNKYDGIHVPVHVRHSNFKLPSDPS     539
FGRAMPH1_01T26277     PFRGVATNYLFALKQKQNGDPSPAPFGQTYELTGPRNKYDGIHVPVHVRHSNFKLPSDPG     539
                       ::**:****:******:**  * *.* ***:**************************.

Bcin12g03180.1        KPVIMIGPGTGVAPFRAFVQERAAQAKAGENVGRTILFFGCRKSTEDFMYKDEWKEYEEA     599
FGRAMPH1_01T26277     KPVIMIGPGTGVAPFRGFVQERAKLARDGVEVGKTLLFFGCRKPSEDFMYEKEWQEYKEA     599
                      ****************.******  *: * :**:*:******* :*****:.**:**:**

Bcin12g03180.1        LGDKFSLITAFSREGKEKVYVQHRLKEHAKEINDLLMQKSYFYVCGDAANMAREVNTVLG     659
FGRAMPH1_01T26277     LGDKFEMITAFSRESAKKVYVQHRLKERAQEVSDLLSQKAYFYVCGDASNMAREVNTVLA     659
                      *****.:*******. :**********:*:*:.*** **:********:**********.

Bcin12g03180.1        QIISEQRGIPESKAEDIVKSMRSANQYQEDVWS        692
FGRAMPH1_01T26277     QIIAEGRGVSEAKGEEIVKNMRSANQYQEDVWS        692
                      ***:* **: *:*.*:***.**************
```

Figure 4-2-2. Multiple sequenced alignment of *BcCPR1* and putative *FgCPR1* genes (FGSG_09786 or FGRAMPH1_01T26277). Clustal omega was used to align and calculate the percentage identity between the amino acid sequence of the CPR1 gene from *B. cinerea* and *F. graminearum*. The stars indicate the identical protein sequence residues.

4.2.3.2 Conserved NADPH oxidase domain detected

The gene structures of the *FgCPR1* gene family were first analyzed by determining the exon-intron arrangement. The length of the putative *FgCpr1* protein is 692 amino acid residues with the predicted molecular weight and PI of 77 kDa and 5.08, respectively. This is similar to *BcCPR1* whose amino acid sequence is 692 bp long, molecular weight is 77 kDa and PI is 5.21. The subcellular localization tool predicted the presence of *Cpr1* in the cytoplasmic or in endoplasmic reticulum. A total of 2 conserved domains designated CYPOR (NADPH cytochrome p450 reductase) and Flavodoxin_1 were identified with length varying from 273 bp to 691 bp and 67bp to 212 bp respectively in putative *FgCPR1*-like sequence (**Figure 4-2-3**).

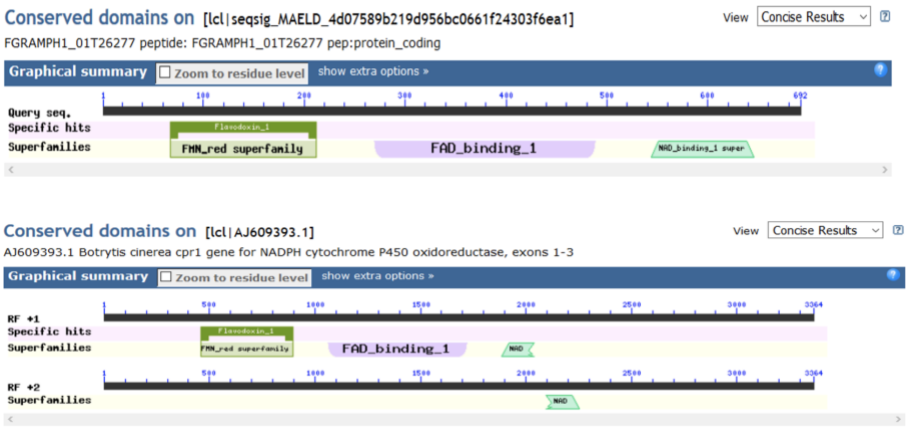

Figure 4-2-3. Identification of conserved NADPH oxidase domain. A conserved FAD containing, and NADPH oxidase domain was detected in *FgCPR1*-like sequence (on top) similar to the one present in *BcCPR1* (bottom) using Conserved Domain Database (CDD).

4.2.3.3 *FgCPR1*-like expression is differentially regulated upon treatment with AS6 inhibitor

The differential expression pattern for putative *FgCPR1* gene was observed in treatment under different conditions involving ABA and AS6 co-applied with *Fg* spores compared to FHB/WT (or *Fg* alone). The log_2FC for putative *FgCPR1* gene was investigated through transcriptomic data analysis that shows its expression in FHB/WT condition when *F. graminearum* spores are applied to the wheat leading to initiation of *Fg* infection, showing its relevance in disease state (log_2FC of 7.1933, padj of 9.60E-19). Upon exogenous co-application of ABA with the *Fg* spores, the activity of the gene is reduced (log_2FC of 1.0125, padj of 8.14E-01) indicating its activity is no longer required (**Figure 4-2-4)**. Finally, on co-application of AS6 with the spores, where AS6 is an inhibitor of ABA signalling, we also observed downregulation of the gene, potentially indicating specificity of this gene in ABA dependent responses (log_2FC of 1.14, padj of 3.57E-01).

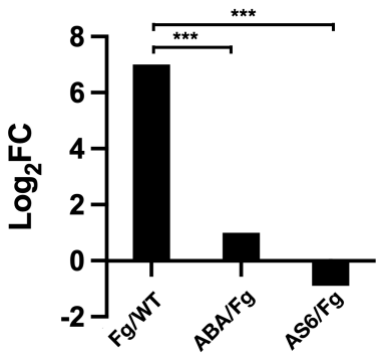

Figure 4-2-4. Log$_2$FC values for putative *FgCPR1* expression. Log$_2$FC values for the *FgCPR1*-like gene detected in *F. graminearum*. Global transcriptomic profiling was carried out in the FHB-susceptible wheat cultivar 'Fielder' to map the regulatory responses effected upon treatment with ABA, or an ABA receptor antagonist (AS6), in the presence of *Fusarium graminearum* (*Fg*) challenge.*** $P \leq 0.001$

4.2.4 Discussion

Abscisic acid (ABA) is a plant hormone primarily associated with regulating plant physiology, but has also been found to play roles in regulating fungal pathogenesis. On the one hand, ABA influences plant immune responses including the activation of defense genes and closure of stomata. These responses indirectly affect the susceptibility or resistance of plants to fungal infections[240,254]. ABA has also been shown to participate in plant-fungal communication, with ABA produced by stressed plants potentially acting as a signal that triggers fungal responses or influences fungal growth and development. Additionally, there is evidence to suggest that fungal pathogens themselves produce ABA, as demonstrated for *B. cinerea* and *M. oryzae*[246,255]. ABA serves as a virulence factor produced by numerous phytopathogenic fungal pathogens, and certain mutualistic host-microbe interactions also depend on ABA.

In terms of the ABA biosynthetic gene family in *B. cinerea*, knock-out experiments have provided confirmation that *BcABA1, BcABA2, BcABA3, BcCPR1* play a crucial role in ABA production in *B. cinerea*, whereas BcABA4 contributes to the pathway but is not deemed essential [248]. Three ABA biosynthetic gene homologs (*MoABA1, MoABA2 and MoABA4*) have also been identified in *M. oryzae* though no homolog has been identified for CPR1 yet[246,255,256]. Deletion of *MoABA4* yielded gene knockout mutants that are impaired in their ability to form lesions on rice. For establishing virulence, the ability of the pathogen to form appressorium (a specialized infection structure that accumulates high turgor pressure forming a penetration peg that enters the rice cuticle) is important. It was observed in *M. oryzae* that the germination and appressorial formation was enhanced in spores exposed to higher concentrations of ABA (50 or 100 μM) compared to untreated controls. Interestingly, a GPCR has also been identified that has been proposed to act as a receptor for ABA in *M. oryzae* on chromosome 3 but further investigations are needed to confirm this[239]. With respect to the level of ABA observed in the cells, the deletion mutants of both *MoABA4* and the *GPCR* produced approximately half the amount of ABA that was produced by wild type.

Following upon on the reported evidence of fungal pathogens producing ABA, we wanted to investigate first, whether *Fg* encodes an ABA biosynthetic pathway, and then whether expression of members of this pathway are modulated during infection, or by the presence of ABA. The ENSEMBL data base was used to retrieve the sequences of the 5 major ABA biosynthesis gene family in *B. cinerea* that have been well characterized. In *F. graminearum*, the highest identity hit at 75.8 % was obtained against *BcCPR1*. The homology for the other genes was around 30 % which was low according to the identity threshold of 50 % that was set, and they were not followed up. As mentioned above, the evidence of *BcCPR1* playing an important role in ABA

synthesis in fungi is well documented its expression only induced during ABA biosynthesis and with the deletion knockout showing significant reduction in ABA levels [246,257,258].

In the realm of the transcriptomic studies by our lab, the effect of co-application of ABA with *Fusarium* spores on the susceptible wheat cultivar "Fielder" was studied. The relevance of *FgCPR1* expression in *F. graminearum* was observed at the 24-hour time point. This indicated its possible role in mediating early infection based responses on wheat that decreased upon co-application of exogenous ABA with the spores, and co-application of ABA inhibitor AS6[259,260]. On the one hand, being that we did not detect homologues for other ABA genes, we could argue that perhaps *Fusarium* uses *FgCPR1* to modulate the plant ABA that is bioavailable and utilize it according to its needs. The fungal cells producing ABA are known to have a high cell wall permeability to aid in easy uptake and release of ABA anions through the membrane. AS6, also known as 3′-hexylsulfanyl-ABA, is an ABA inhibitor and possesses a six-carbon alkyl substitution (**Figure 4-2-5**). It effectively binds PYL like receptors, similar to ABA, and hampers the ABA-induced PYL-PP2C interactions that elicits ABA dependent signalling. Therefore, AS6 binds PYR1's ligand-binding pocket and disrupt PP2C binding. This hindrance occurs due to direct steric interference caused by the S-hexyl chain of AS6, resulting in the inhibition of plant ABA responses[261].

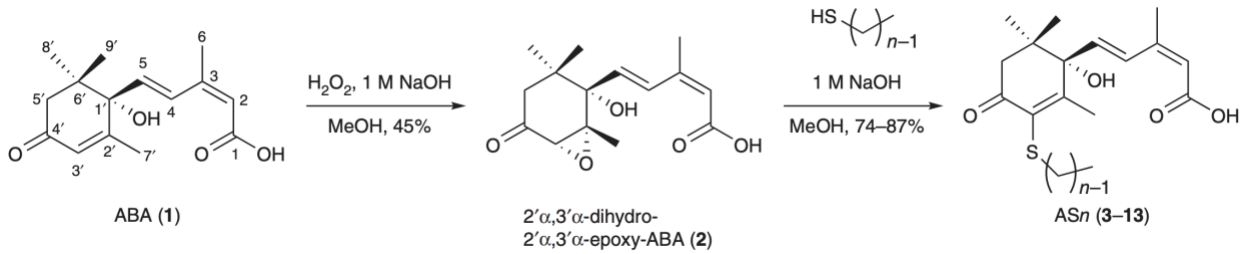

Figure 4-2-5. Structure of AS6 synthesized from ABA. ABA's ring positions at 2', 3', and 4' in gate closure through hydrophobic contacts with the gate loop has been observed. Multiple X-ray structures of PYL-ABA complexes have shown that gate closure results in the formation of two small solvent-exposed tunnels near ABA's 3'-CH and 4'-C=O groups. Based on these findings, a series of 3'-alkylsulfanyl ABAs (3-13) were designed by adding alkyl thiolate to the 2',3'-epoxide 2, which was derived from ABA. These compounds, referred to as the ASn compound series, where n represents the alkyl chain length, were expected to bind to the ligand-binding pocket of PYR1 and disrupt PP2C binding.

Roles for the non-classical defense phytohormone ABA in both resistance and susceptibility have been emphasized, indicating alternative mechanisms underlying the interaction between the host and pathogen[125,262]. This study highlights a fungal ABA biosynthetic cytochrome P450 homologue expressed under conditions containing *F. graminearum*, further supporting the proposition that fungal-derived ABA functions as an effector of infection. This comes from the recent reports suggesting that non-classical defense phytohormones are also synthesized by the pathogen itself[263].

Future studies involving knockout of the *BcCPR1* and identification of any ABA sensing GPCR homologue (*from M. oryzae*) and their corresponding impact on *F. graminearum* infection

and virulence will be carried out. This will aid in understanding the biological significance of these transcriptome responses in the interaction between wheat and *F. graminearum*. However, the significance of these findings and their relevance to pathogenesis will require further investigation. Altogether these observations will pave the way for development of a consolidated model that provides insights into the disease response and severity in a more unified manner.

4.2.5 Material and Methods

4.2.5.1 Homology search for ABA genes in *F. graminearum*

To identify potential members of the ABA biosynthesis gene subfamily in the *Fg* genome, known sequences of fungal ABA biosynthetic genes from *Botrytis cinerea* were retrieved and used for BLAST (protein) analysis against the *Fg* genomic databases; ENSEMBL (https://fungi.ensembl.org/Fusarium_graminearum) and NCBI (https://www.ncbi.nlm.nih.gov/assembly/GCF_000240135.3/). After retrieval of the coding sequence (CDS) sequences, the percentage identity between the genes was calculated by using multiple sequence alignment software, Clustal omega (https://www.ebi.ac.uk/Tools/msa/clustalo/).

4.2.5.2 Identification of conserved domains and motifs

The conservation and divergence of motifs in ABA biosynthetic genes were identified using NCBI-Conserved Domain Database (CDD) (https://www-ncbi-nlm-nih-gov.proxy.bib.uottawa.ca/cdd/) and Multiple Expectation Maximization for Motif Elicitation (MEME) version 4.11.4 (http://meme-suite.org)[264,265]. The following parameters were specified to

run MEME: maximum motif width, 50; minimum motif width, 6; and maximum number of motifs, protein parameters were assessed using ProtParam tool (https://web.expasy.org/protparam/).

Chapter 5
General Discussion

The ascomycete group of phytopathogenic fungi are commonly responsible for causing root rot, seedling blight, and foot rot diseases. This thesis has focused on one member of this family, *F. graminearum*. *F. graminearum* is the causative agent of Fusarium Head Blight (FHB), characterized by the premature bleaching of the wheat heads, leading to significant annual losses in yield and quality, amounting to $50-100 million in annual economic losses in Canada alone. In addition to physical damage to crops, fungi produce a mycotoxin called deoxynivalenol (DON) that contaminates the wheat. Apart from its immediate toxicity, DON's ability to be a potential carcinogen is under investigation[266,267].

5.1 Intricate interplay between host and pathogen

Host-pathogen interaction ns are complex in nature involving recognition and responses on both sides. Plants have developed two immune systems, called pattern-triggered immunity (PTI) and effector-triggered immunity (ETI), through coevolution with natural pathogens. PTI is activated by specific microbial patterns, (comprising of proteins like chitin, flagellin, peptidoglycan or lipopolysaccharides) recognized by host receptors on the cell membrane, while ETI is triggered by pathogen-secreted effectors (proteins or small molecules), detected through alternate intracellular receptors. These two immune systems work together, leading to immune responses such as calcium influx, ROS signaling, MAPK activation, and gene reprogramming on detecting an invading pathogen. Peroxidases released by host plants serve as critical components of the plant innate immune response, contributing to the elimination of invading pathogens[268,269].

During evolution pathogens have evolved their own mechanisms to also use host signals to their advantage by using effector molecules[270,271]. For example: In the fungal phytopathogen *Magnaporthe oryzae,* the effector protein NIS1 suppresses the complex hypersensitive response of oxidative burst in barley and rice that is known to induce local cell death at the site of pathogen entry to contain its spread. The overexpression of effector UV_1261 in *Nicotiana benthamiana* and *Arabidopsis* resulted in the inhibition of flg22-triggered ROS burst[272,273].

Through the studies described in this thesis, the sensing of host-plant released peroxidases by *F. graminearum* and how *Fusarium* uses Ste3 receptor (traditionally known to be only involved in mating in *S. cerevisiae*) to mediate chemotropic sensing towards the host are investigated.

5.1.1 Peroxidase-mediated activation of pheromone receptors: a mechanism for regulation of chemotropism

Through the studies described in Chapter 2, the roles of peroxidases and the GPCR *Fg*Ste3 in mediating fungal hyphal chemotropism in *F. graminearum* was explored. GPCRs are essential in sensing extracellular signals and activating intracellular pathways to generate appropriate responses. For a long time, Ste2 and Ste3 GPCRs were only regarded as pheromone mating receptors in *S. cerevisiae*[274]. These pheromone receptors are essential in the mating and survival of heterothallic fungi. Through evolution from diploid heterothallic fungi (that need a sexual partner for mating) to haploid homothallic fungi like *F. graminerum* which are self-fertile (a single individual is capable of sexual reproduction by possessing both mating alleles in the same organism), these organisms adapted the pheromone peptides and receptors for alternate functionalities[274].

Ste3, traditionally considered a Pheromone A receptor in yeast mating, has been shown to also control Ste3 receptor endocytosis and recycling in yeast. *Cryptococcus neoformans*, a pathogenic fungus, employs Ste3, along with GPR4 and GPR5 GPCRs in various virulence mechanisms, notably in the morphological transition to giant or Titan cells (known as Titanization). Pheromone α has been shown to modulate biofilm formation in *Candida albicans*[275]. In *F. oxysporum*, *Fo*Ste2 and *Fo*Ste3 are known to mediate density dependent control of conidial germination and thus control fungal development[199,276]. Turra *et al.* also showed how secreted class III peroxidases serve as reporters of wounded sites for adapted pathogens to track and enter host tissue using *Fo*Ste2 receptor. This is not surprising as GPCRs have been known to be highly versatile receptors that mediate multiple functions[62,80,277]. Indeed, other studies in closely related fungal species have established *Fg*Ste2 and *Fg*Ste3 gene orthologues in *F. oxysporum* (for *Fo*Ste2), *Verticillium dahliae*, *Trichoderma reesei* (*Fg*Ste2 and *Fg*Ste3 orthologues Hpr1 and Hpr2) as the primary mediators responding to host released peroxidases, and initiating chemotropism[59,61,144]. Through our work in Chapter 2, we showed that in *F. graminearum* the homologue of a-factor pheromone receptor, *Fg*Ste3 mediates chemotropic growth towards host released peroxidases. Prior investigations from our lab have shown similar response for *Fg*Ste2[68]. Together these results emphasized that, knocking out *Fg*Ste3 and *Fg*Ste2 receptors individually respectively each led to complete elimination of the chemotropic response towards peroxidase. In addition, significant decreases in pathogenicity on germinating wheat coleoptiles and Arabidopsis leaves was observed in the knockout strains underscoring the correlation between chemotropism and pathogenesis[47,68].

This hyphal chemotropic bending has been shown to be mediated through activation of the CWI-MAPK pathway, though in *V. dahliae* the mTOR pathway regulation by Rag GTPase Gtr1 is also involved[47,59,68,143]. Through our investigations in *ΔFgste3* and *ΔFgste2* strains, we showed

significant decrease in phosphorylation of Mgv1 protein belonging to CWI-MAPK pathway that plays a crucial role in maintaining the cell wall integrity in fungi. Nonetheless, while the involvement of mTOR has not been investigated in *F. graminearum* yet, the possibility of cross talk between CWI and mTOR cannot be ignored. Finally, while not related to Ste2 or Ste3, the cytosolic pH (pHc) has been shown to induce activity of the three conserved MAPKs in *F. oxysporum* chemotropism[47,92].

It is also worth highlighting that the generation of ROS is closely associated with mediation of the chemotropic response. In *F. graminearum*, chemotropism has been shown to be mediated through the action of peroxidases, where the ROS H_2O_2 acts as a co-substrate in the generation of a ligand (as yet uncharacterized) that stimulates the Ste2 receptor[195]. The sources of H_2O_2 in this host-pathogen interaction has been shown to be fungal, with the conversion of other ROS (like oxide or superoxide radicals) into H_2O_2 by superoxide dismutase (SOD) and NOX B with its associated NADPH oxidase enzymes. Thus together this ROS pathway plays a crucial role in chemotropism in *F. oxysporum*[91]. In *F. graminearum* through transcriptomic analysis, upregulation of a NOX homologue 6-hydroxy-D-nicotine oxidase (Log2FC 46.8) was detected 24 h after peroxidase treatment in WT *F. graminearum*[47]. Homologues for NOXA, NOXB and NOXR have been identified in *F. graminearum,* with prior studies demonstrating their role in affecting pathogenicity, growth and development, stress response, and mycotoxin production[278]. Previous transcriptomic studies have also shown upregulation of peroxidases in wheat up to 48 hours after infection with *F. graminearum* and *Puccinia triticana*[279,280]. Furthermore, a prior investigation conducted by our research team demonstrated a notable increase in the expression of three out of the four wheat peroxidases discovered in the 'Roblin' exudate when wheat plants were infected with *F.* graminearum[124], implying the importance of ROS processes in infectious responses. Thus

altogether, we can speculate that the contribution of ROS and H_2O_2 generation and utilization by peroxidase for chemotropism in *F. graminearum* might be similar to *F. oxysporum*, but future studies assessing loss of NOX genes in relation to chemotropism are required to validate this.

Regarding the production of Ste2 and Ste3 ligand(s) by peroxidases, peroxidases are enzymes that catalyze oxidation reactions by utilizing hydrogen peroxide (H_2O_2) as a substrate. While peroxidases primarily function within cells, they have also been shown to act on the cell membrane and cell wall components including oxidize phenolic compounds, hydroxycinnamic acids, lignin, and alkaloids[194]. Prior mass spectrometry analysis detected a 400 Da peak, unique to peroxidase treated conidia extracts (predicted molecular formula $C_{14}H_{24}O_{13}$). Further studies to confirm the identity of the ligand compound are being carried out[195].

Looking beyond the immediate *Fg*Ste3 related chemotropic response system, genome-wide expression profiling analysis 24 hours post induction with HRP of wildtype *F. graminearum* compared to untreated wildtype *F. graminearum* revealed that peroxidase also leads to upregulation of genes that are involved in infection mediated responses and cell wall remodeling. These included a range of enzymes that help in pathogen attachment to host cells, secondary metabolism gene clusters that are induced before penetration and during biotrophy, followed by upregulation of MFS transporters, hydrolases and enzymes involved in cell wall reorganization[46,47,111]. At the same time, upregulation of a variety of peroxisomal and mitochondrial enzymes that have been shown to possess various antioxidant defense and infection mediated responses is also notable. For example, deletion of *Fg*Pex5 and *Fg*Pex6 led to decreases in reactive oxygen species (ROS) metabolism, slower vegetative growth on fatty acid-rich media, reduced sexual development, and diminished pathogenicity[281–284]. Ultimately the contributions of these other HRP-related effects to *Fg*Ste3 ligand generation and other pathogenic-related

responses cannot be ignored. Overall, we conclude that the observed chemotropic and pathogenic responses linked to *Fg*Ste3, and peroxidase are likely the result of a complex network of signaling and responses, some of which we have gleaned insight into here, but also others that remain to be fully characterized and mapped in the future.

Future strategies to uncover the missing mechanisms could involve identification of regulators, possibly adaptor proteins preceding the CWI MAPK activation. Investigations of additional characteristics that could be common in plant and fungal systems could throw light on chemotropic systems as the interactions in nature are usually complex and interdependent.

In *F. oxysporum*, there have been reports of indirect evidence suggesting a potential interplay between TOR and the Fus3 homolog, Fmk1, in the regulation of virulence in response to nitrogen sources[285]. Similarly, the mechanism underlying the distinct signaling outcomes of NOXB in chemotropism and invasive growth remains unclear, particularly regarding how these outputs are transmitted to the CWI and invasive growth MAPK cascades, respectively, and whether there is a possibility of involvement of cross talk between two pathways will be explored in future studies in *F. graminearum*. Quantitative western blot, proximity biotinylation studies and gene knockout studies will be performed in the future to ascertain the answers to these questions.

5.2 GPCR Dimerization: Its Role in Mediating the Chemotropic Response to Peroxidase

GPCRs were previously thought to work in an independent fashion, but in the early 2000s, dimeric complexes of GPCR were observed. The formation of GPCR homodimers or heterodimers expands the physiological responses that can be controlled by these receptors individually. Dimerization enables allosteric modulation, where conformational changes in one subunit affect the other, influencing ligand binding and signaling. It diversifies signaling by forming

heterodimers between different GPCRs that expand the range of signaling pathways that can be affected. It also enhances signaling efficiency by facilitating efficient coupling to downstream effectors. It impacts receptor trafficking, localization, stability, and subcellular targeting and ligand binding[286,287].

In Chapter 3, the possibility of the *Fg*Ste2 and *Fg*Ste3 receptors undergoing ligand induced heterodimerization for transmission of chemotropic response was investigated. Our rationale for heterodimerization was based on the findings that both *ΔFgste2* and *ΔFgste3* strains were each completely compromised in their chemotropic response to HRP, meaning that neither of the receptors could compensate for the loss of the other. How can knocking out one receptor completely abolish the response that is also controlled by another receptor? In the context of GPCR biochemistry, the most likely explanation is if they are interacting with each other as a dimer. Through BRET and tandem affinity pull down, we showed the formation of peroxidase induced heterodimer between *Fg*Ste2 and *Fg*Ste3. Though the exact mechanism that leads to this is enigmatic, the following possibilities could explain the observed phenomenon.

First, ROS burst has been shown to lead to heterodimerization of various proteins through as yet unknown mechanisms. While, there is no precedent in the literature for ROS burst-mediated GPCR dimer formation, there is precedent for other proteins that dimerize due to ROS induced stress[184]. Mechanistically, ROS is known to lead to oxidation of thiol residues ($-SH_2$) promoting formation of disulphide bonds in between corresponding cysteines. ROS stress is also known to modulate membrane microdomains generating spatial proximity of the receptors. Major components of the membrane include cholesterols, unsaturated fatty acids, phosphatidyl choline and lipids, all of which are known to be oxidized through action of peroxidases[288,289]. Whether any or all of these

effects might be contributing to formation or stabilization of the *Fg*Ste3-*Fg*Ste2 heterodimer remains to be determined.

Alternatively, and more in keeping with mechanisms known to induce GPCR homo- and hetero- dimers more broadly, is the possibility of ligand induced dimerization. For instance, CCR2 and CCR5 when stimulated with MCP-1, RANTES or equimolar concentrations of both form a heterodimer[290]. Similarly, CXCR4 and the δ-opioid receptor form dimer when induced with their respective agonists SDF1α and [d-Pen2,d-Pen5]enkephalin[196].

In this model, the putative 400 Da ligand produced by the action of peroxidase would bind to one or both receptors leading to conformational changes that increase their affinity for each other. In some respects, one might argue that this is still ROS-related, being that ligand production in this case requires generation of the ROS H_2O_2, that is utilized by peroxidase to make the peroxidase-derived ligand. But we separate this out here as distinct from other ROS mechanisms, based on the well characterized mechanism of ligand induced dimerization.

Although there are numerous structures available for GPCR homodimers, including *Sc*Ste2, within the Protein Data Bank (PDB), there is a scarcity of heterodimer structures that have been resolved. The $GABA_BR$ heterodimer exhibits significant conformational changes in its transmembrane domains (TMDs) during activation, as evidenced by recent cryo-EM structures. In the inactive state, there is an interface between TM3-TM5/TM3-TM5, which transitions to a TM6/TM6 interface in the active state[291,292]. The existence of phospholipids within the core of each transmembrane domain (TMD) suggests their potential role in stabilizing and/or regulating the arrangement of TMDs, and thus the potential impact of ROS modification of lipids on dimer formation. A model of the adenosine A2AR-Dopamine D2R heterodimer, featuring a TM-IV/V interface, has also been constructed using protein-protein docking, followed by refinement through

molecular dynamics simulations. The predicted interface was subjected to mutational analysis, which revealed reduced A2AR-D2R interactions in BRET (bioluminescence resonance energy transfer) experiments, along with altered allosteric modulation[293].

Thus, in conclusion, the observed heterodimer between *Fg*Ste2 and *Fg*Ste3 is consistent with the observation that neither receptor alone can mediate chemotropism and may provide a mechanistic explanation of this effect. However, heterodimer formation remains to be directly correlated with chemotropism and signal transduction in *F. graminearum* in the future. As well, teasing out additional details related to specific aspects of the structural implications of heterodimer formation and residues responsible for mediating the heterodimerization between the *Fg*Ste2 and *Fg*Ste3 receptors are pending. A comprehensive analysis involving protein modeling using *in-silico* techniques, site-directed mutagenesis studies, and structural investigations will be required.

5.3 Significance: new potential targets for anti-fungal compound generation

Agricultural pathogens pose a significant threat to global food security. Diseases caused by pathogens lead to reduced crop yields, crop losses, and lower quality produce. The estimated worldwide economic impact of pathogens and pests on annual crop yield loss is approximately US $220 billion[294,295]. By studying these pathogens, researchers can develop strategies to prevent, control, and mitigate their impact, thereby safeguarding food production and ensuring an adequate food supply for the growing population.

With respect to the structural investigations alluded to above, Chapter 4 (Section 1) showcases the feasibility of utilizing the baculovirus overexpression system to generate large

quantities of fungal Ste3 protein in *Sf21* insect cells, which can be subsequently purified for structural analysis.

Structural elucidation of receptors is necessary for designing novel drugs against them (or anti-fungals in the case of Ste2 and Ste3). On the human disease side more broadly, various other GPCRs are being explored as targets for drug development as a variety of features makes them an excellent choice. These include their functional diversity and specificity, their essentiality in fungal survival as well as their conservation across fungal species, their druggable nature enabling the development of selective small molecule modulators, and finally their potential for combination therapy. Exploiting these features through targeted anti-fungal discovery and development efforts holds promise for the design of effective and innovative treatments against fungal infections. By harnessing the wealth of structural data, researchers have been able to discover previously unknown binding sites. Out of the 826 human target GPCR structures listed on the GPCR network (http://zhanglab.ccmb.med.umich.edu/GPCR-EXP/), a total of 115 unique receptor structures have been successfully resolved. Among these structures, 84 have utilized the baculovirus system for protein expression, with 64 employing the *Spodoptera frugiperda* (*Sf*) cell line and 20 utilizing *Trichoplusia ni*. Employing insect cells for membrane protein overexpression offers several advantages, including high production yields, relatively straightforward setup of large-scale cultures, and the capability to facilitate most post-translational modifications.

Target validation is essential before designing receptor agonists. As our research has shown, knocking out GPCR receptors *Fg*Ste2 and *Fg*Ste3 individually led to complete elimination of chemotropism and significant reduction in infection potential of *F. graminearum*[46,47]. In addition, mycotoxin biosynthesis genes were downregulated in the *ΔFgste3* knockout strain. Though we did not see absolute loss of virulence, a combinatorial approach of blocking receptor

signaling and using broadly ranging anti-fungals could still be a robust strategy. We could also design inhibitors that inhibit each individual receptor as a classical antagonist as has already been initiated *in silico*[296], or block the dimerization event or add agonists to induce unstable receptor conformations. Agonists that can bind to inactive receptors and interfere with their activation for example as seen for the action of eticlopride in Dopamine D2 and D3 receptors[24,297].

The current line of anti-fungal compounds include azole based molecules that inhibit ergosterol, a component of the fungal cell membrane by inhibiting 1,4 α-lanosterol demethylase encoded by yeast ERG11 gene. The echinocandins class of anti-fungal compounds target β-1,3-glucan which is an essential fungal cell wall component[298,299]. However, resistance is rapidly developing against these existing compounds which necessitates the need for novel targets. In addition to anti-fungal compounds, various biocontrol agents are also being explored to target fungal infestation on crops. ASPERELLO® T34 Biocontrol® is a bio fungicide which contains the antagonistic fungus *Trichoderma asperellum* strain T34[300,301]. *Clonostachys rosea* is another biocontrol agent that detoxifies DON through production of glucosyltransferases[302].

A variety of other GPCR targets are also under investigation as potential targets for anti-fungal compound generation. These include in *Candida spp*., where activation of the GPCR GPR1 is crucial for regulating the yeast-to-hypha switch, promoting tissue invasion, and expressing the pore-forming toxin candidalysin (Ece1p) for cytolysis of human cells[303]. Also in *Aspergillus fumigatus* the GPCR GprK, known to be activated by sensing pentose sugars, plays multiple roles in asexual development, carbon sensing, stress responses, and the production of gliotoxin, which is the most potent toxin produced by *A. fumigatus*[304].

Overall, targeting GPCRs allows for the disruption of critical signaling pathways and virulence mechanisms, ultimately impairing the survival and pathogenicity of fungal pathogens.

The diversity and specificity of GPCR signaling networks in different fungal species offer the potential for the development of highly targeted anti-fungal compounds with minimal impact on host cells. Advancements in understanding fungal GPCR structure, function, and signaling pathways, coupled with techniques such as protein modeling, structural studies, and high-throughput screening, will enhance our ability to design specific GPCR-targeting compounds.

Beyond GPCRs, the machinery of ROS detoxification might also serve as a target for preventing plant diseases, as few anti-ROS-scavenging compounds have been developed. For example, in the model system *B. cinerea*, antagonist compounds targeting secretion of the cytochrome c-peroxidase, *BcCcp1* (that removes plant-produced H_2O_2 and promotes pathogen invasion) have shown promise. As well, disruption of either BcTol1 or BcCcp1 through quinone based compounds led to dramatically reduced virulence of *B. cinerea*. An urgent need exists in disease control for fungicides that specifically target pathogenicity-related genes, due to global concerns about anti-fungal resistance arising due to targeting housekeeping genes and off-target effects induced by the existing solutions[305,306].

Finally, going beyond pathogenic fungi, the role of ROS, and thus relevance of drugs targeting ROS components, has also been established in mammalian systems where they are known to be involved in chemotaxis of leukocytes, antigen cross presentation and secondary messengers[307].

5.4 Future Directions

Herein, that loss of *Fg*Ste3 leads to complete elimination of chemotropic response to peroxidase, as already established for *Fg*Ste2[46,47], is demonstrated. In addition, upon assaying the activation of the Mgv1 protein in the CWI-MAPK pathway (implicated in infectious responses

and virulence), both the knockouts showed significant decrease in pathway activation. Following up on these observations, the presence of peroxidase induced *Fg*Ste2 and *Fg*Ste3 heterodimer was discovered that could account for the overlapping mode of action of both the receptors. Though experiments directly linking the heterodimer to chemotropism are lacking, considering their individual roles in mediating chemotropic sensing, the dimer could explain why none of the receptors can work individually. Future experiments to demonstrate this could involve CRISPR mutagenesis of individual receptors in *F. graminearum* one at a time, to see if that leads to corresponding loss of chemotropism. Alternatively, since *Sc*Ste2 receptor structure is known, development of compounds that can inhibit its activation can be tested in *F. graminearum* system to see if it impedes dimer formation and retroactively shows loss in chemotropism in *F. graminerum*.

Proximity biotinylation experiments (e.g with TurboID) to mine for activating G-proteins and other adaptors proteins associated with the *Fg*Ste3 receptor activation have been developed (**Appendix B, Figure B2 and B3**), but will require extensive future optimization due to the challenging nature of applying this method to membrane proteins and GPCRs in particular. Nonetheless their completion will throw light to help us understand the downstream activation mechanism involving adaptor proteins or 14-3-3 proteins that control transmission of responses from the G-proteins and leading to MAPK pathway activation.

Furthermore, baculovirus based *Sf21* insect cell expression was carried out making it an effective system for recombinant protein production and purification of *Fg*Ste3 for structural studies[35]. Future studies involving large scale purification of protein and functionality testing based on its ability to bind to corresponding G-protein subunit would be carried out. Following that, we

will start crystallography trials using Lipid Cubic Phase (LCP) method or perform cryoEM in case the protein is difficult to crystallize.

Structural studies of GPCRs have revealed important features such as the ligand-binding pocket, extracellular loops, transmembrane helices, and intracellular signaling domains. This structural information guides the design of ligands with improved selectivity, potency, and therapeutic efficacy. By studying the receptor structure, scientists can identify key residues and interactions necessary for ligand binding and activation, enabling the development of drugs that can either activate or inhibit GPCR signaling pathways.

The changing global distribution of pathogens is a cause for concern, as emerging evidence indicates that pathogens tend to inflict greater damage in newly invaded regions and on new hosts compared to their native regions and hosts. Some agricultural pathogens have zoonotic potential, meaning they can infect both animals and humans. Understanding these pathogens and their transmission pathways is critical for preventing disease outbreaks and protecting public health. By studying agricultural pathogens, researchers can contribute to early detection, surveillance, and effective control measures, and minimizing the risk of zoonotic infections. Existing organizations like the Consultative Group for International Agricultural Research (CGIAR) and the Food and Agriculture Organization of the United Nations (FAO) have an important role to play in this regard.

Bibliography

1. RS Goswami, H. K. Heading for disaster: Fusarium graminearum on cereal crops. *Mol. Plant Pathol.* **5**, 515–525 (2004).
2. Chin, T. *et al.* A status update on fusarium head blight on Western Canadian wheat. *Can. J. Plant Pathol.* (2023). doi:10.1080/07060661.2023.2177352
3. Lee, J., Leslie, J. F. & Bowden, R. L. Expression and Function of Sex Pheromones and Receptors in the Homothallic Ascomycete Gibberella zeae. *Eukaryot. Cell* **7**, 1211 (2008).
4. Trail, F. For Blighted Waves of Grain: Fusarium graminearum in the Postgenomics Era. *Plant Physiol.* **149**, 103–110 (2009).
5. Gilbert, J. & Tekauz, A. Review: Recent developments in research on fusarium head blight of wheat in Canada. *https://doi.org/10.1080/07060660009501155* **22**, 1–8 (2009).
6. Saharan, M. S. & Naef, A. Detection of genetic variation among Indian wheat head scab pathogens (Fusarium spp./isolates) with microsatellite markers. *Crop Prot.* **27**, 1148–1154 (2008).
7. Powell, A. J. & Vujanovic, V. Evolution of Fusarium Head Blight Management in Wheat: Scientific Perspectives on Biological Control Agents and Crop Genotypes Protocooperation. *Appl. Sci. 2021, Vol. 11, Page 8960* **11**, 8960 (2021).
8. Powell, A. J. & Vujanovic, V. Evolution of Fusarium Head Blight Management in Wheat: Scientific Perspectives on Biological Control Agents and Crop Genotypes Protocooperation. *Appl. Sci. 2021, Vol. 11, Page 8960* **11**, 8960 (2021).
9. Somma, S. *et al.* Impact of fungicide application to control T-2 and HT-2 toxin contamination and related Fusarium sporotrichioides and F. langsethiae producing species in durum wheat. *Crop Prot.* **159**, 106020 (2022).

10. Feksa, H. R. *et al.* Pre- and postinfection application of strobilurin-triazole premixes and single fungicides for control of fusarium head blight and deoxynivalenol mycotoxin in wheat. *Crop Prot.* **117**, 128–134 (2019).

11. CHEN, A. hai, ISLAM, T. & MA, Z. hua. An integrated pest management program for managing fusarium head blight disease in cereals. *J. Integr. Agric.* **21**, 3434–3444 (2022).

12. Palazzini, J. M., Ramirez, M. L., Torres, A. M. & Chulze, S. N. Potential biocontrol agents for Fusarium head blight and deoxynivalenol production in wheat. *Crop Prot.* **26**, 1702–1710 (2007).

13. Baldwin, T. *et al.* Silencing efficiency of dsRNA fragments targeting Fusarium graminearum TRI6 and patterns of small interfering RNA associated with reduced virulence and mycotoxin production. *PLoS One* **13**, e0202798 (2018).

14. Werner, B. T., Gaffar, F. Y., Schuemann, J., Biedenkopf, D. & Koch, A. M. RNA-Spray-Mediated Silencing of Fusarium graminearum AGO and DCL Genes Improve Barley Disease Resistance. *Front. Plant Sci.* **11**, 483792 (2020).

15. Worth the wheat: new durum wheat line shows intermediate resistance to fusarium head blight, a first for Canada and the world - agriculture.canada.ca. Available at: https://agriculture.canada.ca/en/news-agriculture-and-agri-food-canada/scientific-achievements-agriculture/worth-wheat-new-durum-wheat-line-shows-intermediate-resistance-fusarium-head-blight-first-canada-and. (Accessed: 16th July 2023)

16. Bargués-Ribera, M. & Gokhale, C. S. Eco-evolutionary agriculture: Host-pathogen dynamics in crop rotations. *PLoS Comput. Biol.* **16**, (2020).

17. Kikukawa, T. Unique Cl– pump rhodopsin with close similarity to H+ pump rhodopsin. *Biophys. Physicobiology* **18**, 317 (2021).

18. Sakmar, T. P. Introduction: G-protein coupled receptors. *Chem. Rev.* **117**, 1–3 (2017).

19. Yang, D. *et al.* G protein-coupled receptors: structure- and function-based drug discovery. *Signal Transduct. Target. Ther. 2020 61* **6**, 1–27 (2021).

20. Brown, N. A., Schrevens, S., Van Dijck, P. & Goldman, G. H. Fungal G-protein-coupled receptors: Mediators of pathogenesis and targets for disease control. *Nat. Microbiol.* **3**, 402–414 (2018).

21. Schrick, K., Garvik, B. & Hartwell, L. H. Mating in Saccharomyces cerevisiae: The role of the pheromone signal transduction pathway in the chemotropic response to pheromone. *Genetics* **147**, 19–32 (1997).

22. Alhosaini, K., Azhar, A., Alonazi, A. & Al-Zoghaibi, F. GPCRs: The most promiscuous druggable receptor of the mankind. *Saudi Pharm. J. SPJ* **29**, 539 (2021).

23. Cao, J. *et al.* Evolution of the class C GPCR Venus flytrap modules involved positive selected functional divergence. *BMC Evol. Biol.* **9**, (2009).

24. Hauser, A. S., Attwood, M. M., Rask-Andersen, M., Schiöth, H. B. & Gloriam, D. E. Trends in GPCR drug discovery: new agents, targets andindications. *Nat. Rev. Drug Discov.* **16**, 829 (2017).

25. Hu, G. M., Mai, T. L. & Chen, C. M. Visualizing the GPCR Network: Classification and Evolution. *Sci. Rep.* **7**, (2017).

26. Basith, S. *et al.* Exploring G Protein-Coupled Receptors (GPCRs) Ligand Space via Cheminformatics Approaches: Impact on Rational Drug Design. *Front. Pharmacol.* **9**, (2018).

27. Gether, U. Uncovering Molecular Mechanisms Involved in Activation of G Protein-Coupled Receptors. *Endocr. Rev.* **21**, 90–113 (2000).

28. Vizurraga, A., Adhikari, R., Yeung, J., Yu, M. & Tall, G. G. Mechanisms of adhesion G protein–coupled receptor activation. *J. Biol. Chem.* **295**, 14065–14083 (2020).

29. Zhou, Q. *et al.* Common activation mechanism of class A GPCRs. *Elife* **8**, (2019).

30. Franklin, J. M. & Carrasco, G. A. Cannabinoid receptor agonists upregulate and enhance serotonin 2A (5-HT2A) receptor activity via ERK1/2 signaling. *Synapse* **67**, 145–159 (2013).

31. Mafi, A., Kim, S.-K., Iii, W. A. G., De Vivo, M. & Jacobson, K. A. The mechanism for ligand activation of the GPCR-G protein complex. (2022). doi:10.1073/pnas

32. Semenkovich, K. *et al.* Prescription Opioid Analgesics Increase Risk of Major Depression: New Evidence, Plausible Neurobiological Mechanisms and Management to Achieve Depression Prophylaxis. *Mo. Med.* **111**, 148 (2014).

33. Jean-Charles, P. Y., Kaur, S. & Shenoy, S. K. GPCR signaling via β-arrestin-dependentmechanisms. *J. Cardiovasc. Pharmacol.* **70**, 142 (2017).

34. Raote, I., Bhattacharya, A. & Panicker, M. M. Serotonin 2A (5-HT2A) Receptor Function: Ligand-Dependent Mechanisms and Pathways. *Serotonin Recept. Neurobiol.* 123–150 (2007). doi:10.1201/9781420005752-11

35. Velazhahan, V. *et al.* Structure of the class D GPCR Ste2 dimer coupled to two G proteins. *Nature* (2020). doi:10.1038/s41586-020-2994-1

36. Seo, -a *et al.* The gprA and gprB genes encode putative G protein-coupled receptors required for self-fertilization in Aspergillus nidulans. *Mol. Microbiol.* **53**, 1611–1623 (2004).

37. Chung, K. S. *et al.* Isolation of a Novel Gene from Schizosaccharomyces pombe: Stm1 Encoding a Seven-transmembrane Loop Protein that May Couple with the Heterotrimeric

Gα2 Protein, Gpa2. *J. Biol. Chem.* **276**, 40190–40201 (2001).

38. Kraakman, L. *et al.* A Saccharomyces cerevisiae G-protein coupled receptor, Gpr1, is specifically required for glucose activation of the cAMP pathway during the transition to growth on glucose. *Mol. Microbiol.* **32**, 1002–1012 (1999).

39. Galagan, J. E. *et al.* The genome sequence of the filamentous fungus Neurospora crassa. *Nature* **422**, 859–868 (2003).

40. Zhang, F. *et al.* The microbial opsin family of optogenetic tools. *Cell* **147**, 1446–1457 (2011).

41. Gehret, A. U., Bajaj, A., Naider, F. & Dumont, M. E. Oligomerization of the Yeast-Factor Receptor IMPLICATIONS FOR DOMINANT NEGATIVE EFFECTS OF MUTANT RECEPTORS *. *J. Biol. Chem.* **281**, 20698–20714 (2006).

42. Brosig, B. & Langosch, D. The dimerization motif of the glycophorin A transmembrane segment in membranes: importance of glycine residues. *Protein Sci.* **7**, 1052–1056 (1998).

43. Overton, M. C., Chinault, S. L. & Blumer, K. J. Oligomerization, biogenesis, and signaling is promoted by a glycophorin A-like dimerization motif in transmembrane domain 1 of a yeast G protein-coupled receptor. *J. Biol. Chem.* **278**, 49369–49377 (2003).

44. Hu, J. & Spiegel, A. M. Structure and function of the human calcium-sensing receptor: insights from natural and engineered mutations and allosteric modulators. *J. Cell. Mol. Med.* **11**, 908–922 (2007).

45. Rozenfeld, R. *et al.* AT1R–CB1R heteromerization reveals a new mechanism for the pathogenic properties of angiotensin II. *EMBO J.* **30**, 2350 (2011).

46. Sridhar, P. S. *et al.* Ste2 receptor-mediated chemotropism of Fusarium graminearum contributes to its pathogenicity against wheat. *Sci. Rep.* **10**, (2020).

47. Sharma, T. *et al.* Fusarium graminearum Ste3 G-Protein Coupled Receptor: A Mediator of Hyphal Chemotropism and Pathogenesis . *mSphere* **7**, (2022).

48. Hoffman, C. S. Except in Every Detail: Comparing and Contrasting G-Protein Signaling in Saccharomyces cerevisiae and Schizosaccharomyces pombe. *Eukaryot. Cell* **4**, 495 (2005).

49. Zhao, X., Mehrabi, R. & Xu, J. R. Mitogen-Activated Protein Kinase Pathways and Fungal Pathogenesis. *Eukaryot. Cell* **6**, 1701 (2007).

50. González-Rubio, G., Fernández-Acero, T., Martín, H. & Molina, M. Mitogen-Activated Protein Kinase Phosphatases (MKPs) in Fungal Signaling: Conservation, Function, and Regulation. *Int. J. Mol. Sci. 2019, Vol. 20, Page 1709* **20**, 1709 (2019).

51. Jiang, C., Zhang, X., Liu, H. & Xu, J. R. Mitogen-activated protein kinase signaling in plant pathogenic fungi. *PLOS Pathog.* **14**, e1006875 (2018).

52. Yin, T. *et al.* The cyclase-associated protein FgCap1 has both protein kinase A-dependent and -independent functions during deoxynivalenol production and plant infection in Fusarium graminearum. *Mol. Plant Pathol.* **19**, 552 (2018).

53. Jiang, C. *et al.* TRI6 and TRI10 play different roles in the regulation of deoxynivalenol (DON) production by cAMP signalling in Fusarium graminearum. *Environ. Microbiol.* **18**, 3689–3701 (2016).

54. Gong, C., Xu, D., Sun, D. & Zhang, X. PKR Protects the Major Catalytic Subunit of PKA Cpk1 from FgBlm10-Mediated Proteasome Degradation in Fusarium graminearum. *Int. J. Mol. Sci.* **23**, (2022).

55. Jenczmionka, N. J. & Schäfer, W. The Gpmk1 MAP kinase of Fusarium graminearum regulates the induction of specific secreted enzymes. *Curr. Genet.* **47**, 29–36 (2005).

56. Gu, Q., Chen, Y., Liu, Y., Zhang, C. & Ma, Z. The transmembrane protein FgSho1 regulates fungal development and pathogenicity via the MAPK module Ste50-Ste11-Ste7 in Fusarium graminearum. *New Phytol.* **206**, 315–328 (2015).

57. Xu, M. *et al.* Combatting Fusarium head blight: advances in molecular interactions between Fusarium graminearum and wheat. *Phytopathol. Res. 2022 41* **4**, 1–16 (2022).

58. Segorbe, D., Di Pietro, A., Pérez-Nadales, E. & Turrà, D. Three Fusarium oxysporum mitogen-activated protein kinases (MAPKs) have distinct and complementary roles in stress adaptation and cross-kingdom pathogenicity. *Mol. Plant Pathol.* **18**, 912 (2017).

59. Vangalis, V. *et al.* Components of TOR and MAP kinase signaling control chemotropism and pathogenicity in the fungal pathogen Verticillium dahliae. *bioRxiv* 2022.06.20.496898 (2022). doi:10.1101/2022.06.20.496898

60. Turrà, D., Segorbe, D. & Di Pietro, A. Protein kinases in plant-pathogenic Fungi: Conserved regulators of infection. *Annu. Rev. Phytopathol.* **52**, 267–288 (2014).

61. D Turrà, M. G. F. R. A. Pietro. Fungal pathogen uses sex pheromone receptor for chemotropic sensing of host plant signals. *Nature* **527**, 521–524 (2015).

62. Vitale, S., Di Pietro, A. & Turrà, D. Autocrine pheromone signalling regulates community behaviour in the fungal pathogen Fusarium oxysporum. *Nature Microbiology* **4**, 1443–1449 (2019).

63. Goldman, G. H. *et al.* Deletion of FgHOG1 Is Suppressive to the mgv1 Mutant by Stimulating Gpmk1 Activation and Avoiding Intracellular Turgor Elevation in Fusarium graminearum. (2019). doi:10.3389/fmicb.2019.01073

64. Zheng, D. *et al.* The FgHOG1 Pathway Regulates Hyphal Growth, Stress Responses, and Plant Infection in Fusarium graminearum. *PLoS One* **7**, e49495 (2012).

65. Liu, N. *et al.* Lipid droplet biogenesis regulated by the FgNem1/Spo7-FgPah1 phosphatase cascade plays critical roles in fungal development and virulence in Fusarium graminearum. *New Phytol.* **223**, 412–429 (2019).

66. Yu, F. *et al.* The TOR signaling pathway regulates vegetative development and virulence in Fusarium graminearum. *New Phytol.* **203**, 219–232 (2014).

67. Inoki, K., Li, Y., Xu, T. & Guan, K. L. Rheb GTPase is a direct target of TSC2 GAP activity and regulates mTOR signaling. *Genes Dev.* **17**, 1829–1834 (2003).

68. Sridhar, P. S. *et al.* Ste2 receptor-mediated chemotropism of Fusarium graminearum contributes to its pathogenicity against wheat. *Sci. Rep.* **10**, 10770 (2020).

69. Hao, Z. *et al.* Genome Sequence Analysis of the Fungal Pathogen Fusarium graminearum Using Oxford Nanopore Technology. *J. Fungi* **7**, 699 (2021).

70. Dilks, T., Halsey, K., De Vos, R. P., Hammond-Kosack, K. E. & Brown, N. A. Non-canonical fungal G-protein coupled receptors promote Fusarium head blight on wheat. *PLoS Pathog.* **15**, (2019).

71. Jiang, C. *et al.* An expanded subfamily of G-protein-coupled receptor genes in Fusarium graminearum required for wheat infection. *Nat. Microbiol.* **4**, 1582–1591 (2019).

72. Kou, Y., Tan, Y. H., Ramanujam, R. & Naqvi, N. I. Structure-function analyses of the Pth11 receptor reveal an important role for CFEM motif and redox regulation in rice blast. *New Phytol.* **214**, 330–342 (2017).

73. Ismael, A. *et al.* Gβ promotes pheromone receptor polarization and yeast chemotropism by inhibiting receptor phosphorylation. *Sci. Signal.* **9**, ra38 (2016).

74. Beccaccioli, M., Scala, V. & Reverberi, M. Communication With Plants. *Encycl. Mycol.* 114–122 (2021). doi:10.1016/B978-0-12-819990-9.00051-2

75. Bary, A. de, Balfour, I. B. & Garnsey, H. E. F. Comparative morphology and biology of the fungi, mycetozoa and bacteria. *Comp. Morphol. Biol. fungi, mycetozoa Bact.* (1887). doi:10.5962/BHL.TITLE.56861

76. Robinson, P. M. Chemotropism in fungi. *Trans. Br. Mycol. Soc.* **61**, 303-IN13 (1973).

77. George Massee, B. & Bo, R. G. On the Origin of Parasitism Fungi.

78. Turrà, D., Nordzieke, D., Vitale, S., El Ghalid, M. & Di Pietro, A. Hyphal chemotropism in fungal pathogenicity. *Semin. Cell Dev. Biol.* **57**, 69–75 (2016).

79. Karathia, H., Vilaprinyo, E., Sorribas, A. & Alves, R. Saccharomyces cerevisiae as a Model Organism: A Comparative Study. *PLoS One* **6**, (2011).

80. Haber, J. E. Mating-Type Genes and MAT Switching in Saccharomyces cerevisiae. (2012). doi:10.1534/genetics.111.134577

81. Versele, M., Lemaire, K. & Thevelein, J. M. Sex and sugar in yeast: two distinct GPCR systems. *EMBO Rep.* **2**, 574 (2001).

82. Alvaro, C. G. & Thorner, J. Heterotrimeric G protein-coupled receptor signaling in yeast mating pheromone response. *Journal of Biological Chemistry* **291**, 7785–7798 (2016).

83. Guo, M. *et al.* The Yeast G Protein α Subunit Gpa1 Transmits a Signal through an RNA Binding Effector Protein Scp160. *Mol. Cell* **12**, 517–524 (2003).

84. Takeshita, N. Coordinated process of polarized growth in filamentous fungi. *Biosci. Biotechnol. Biochem.* **80**, 1693–1699 (2016).

85. Jones, L. A. & Sudbery, P. E. Spitzenkorper, exocyst, and polarisome components in Candida albicans hyphae show different patterns of localization and have distinct dynamic properties. *Eukaryot. Cell* **9**, 1455–1465 (2010).

86. Jones, L. A. & Sudbery, P. E. Spitzenkörper, exocyst, and polarisome components in

Candida albicans hyphae show different patterns of localization and have distinct dynamic properties. *Eukaryot. Cell* **9**, 1455–1465 (2010).

87. Li, Y. B. *et al.* Magnaporthe oryzae fimbrin organizes actin networks in the hyphal tip during polar growth and pathogenesis. *PLOS Pathog.* **16**, e1008437 (2020).

88. Xie, Y. *et al.* Polarisome scaffolder Spa2-mediated macromolecular condensation of Aip5 for actin polymerization. *Nat. Commun. 2019 101* **10**, 1–18 (2019).

89. Li, X., Ferro-Novick, S. & Novick, P. Different polarisome components play distinct roles in Slt2p-regulated cortical ER inheritance in Saccharomyces cerevisiae. *Mol. Biol. Cell* **24**, 3145 (2013).

90. Bhattacharyya, A., Chattopadhyay, R., Mitra, S. & Crowe, S. E. Oxidative Stress: An Essential Factor in the Pathogenesis of Gastrointestinal Mucosal Diseases. *Physiol. Rev.* **94**, 329 (2014).

91. Nordzieke, D. E., Fernandes, T. R., El Ghalid, M., Turrà, D. & Di Pietro, A. NADPH oxidase regulates chemotropic growth of the fungal pathogen Fusarium oxysporum towards the host plant. *New Phytol.* **224**, 1600–1612 (2019).

92. Fernandes, T. R. *et al.* Cytosolic pH Controls Fungal MAPK Signaling and Pathogenicity. *MBio* **14**, (2023).

93. Brand, A. & Gow, N. A. Mechanisms of hypha orientation of fungi. *Curr. Opin. Microbiol.* **12**, 350–357 (2009).

94. C Shi, S. K. S. C. M. L. A role for a complex between activated G protein-coupled receptors in yeast cellular mating. *Proc. Natl. Acad. Sci. USA* **104**, 5395–5400 (2007).

95. CG Alvaro, J. T. Heterotrimeric G protein-coupled receptor signaling in yeast mating pheromone response. *J. Biol. Chem.* **291**, 7785–7798 (2016).

96. CL Jackson, J. K. L. H. cerevisiae alpha pheromone receptors activate a novel signal transduction pathway for mating partner discrimination. *Cell* **67**, 389–402 (1991).

97. Haber, J. Mating-type genes and MAT switching in Saccharomyces cerevisiae. *Genetics* **191**, 33–64 (2012).

98. SK Jones, R. B. Fungal mating pheromones: Choreographing the dating game. *Fungal Genet. Biol.* **48**, 668–676 (2011).

99. EK Manavathu, D. T. Chemotropism of Achlya ambisexualis to methionine and methionyl. *Microbiology* **131**, 751–756 (1985).

100. Jones, S. W., Donaldson, S. P. & Deacon, J. W. Behaviour of zoospores and zoospore cysts in relation to root infection by Pythium aphanidermatum. *New Phytol.* **117**, 289–301 (1991).

101. Musgrave, A., Ero, L., Scheffer, R. & Oehlers, E. Chemotropism of Achlya bisexualis germ hyphae to casein hydrolysate and amino acids. *J. Gen. Microbiol.* **101**, 65–70 (1977).

102. H-B Jansson, T. J. B. N.-H. A. T. G. O. Chemotropic growth of germ-tubes of Cochliobolus sativus to barley roots or root exudates. *Trans. Br. Mycol. Soc.* **90**, 647–650 (1988).

103. Zentmyer, G. A. Chemotaxis of Zoospores for Root Exudates. *Science* **133**, 1595–6 (1961).

104. Andrew Brown, N., Schrevens, S., Dijck, P. & Henrique Goldman, G. Fungal G-protein-coupled receptors: mediators of pathogenesis and targets for disease control. *Nat. Microbiol.* (2018). doi:10.1038/s41564-018-0127-5

105. Lottersberger, F. The Saccharomyces cerevisiae 14-3-3 proteins are required for the G1/S

transition, actin cytoskeleton organization and cell wall integrity. *Genetics* **173**, 661–675 (2006).

106. H El-Defrawy, M. M. & El-Latif Hesham, A. G-protein-coupled Receptors in Fungi. (2020). doi:10.1007/978-3-030-41870-0_3

107. Martínez-Soto, D. & Ruiz-Herrera, J. Functional analysis of the MAPK pathways in fungi. *Rev. Iberoam. Micol.* **34**, 192–202 (2017).

108. Zheng, D. *et al.* The FgHOG1 Pathway Regulates Hyphal Growth, Stress Responses, and Plant Infection in Fusarium graminearum. *PLoS One* **7**, (2012).

109. HK Kim, T. L. S. Y. A putative pheromone signaling pathway is dispensable for self-fertility in the homothallic ascomycete Gibberella zeae. *Fungal Genet. Biol.* **45**, 1188–1196 (2008).

110. Bresso, E. *et al.* GPCRs from fusarium graminearum detection, modeling and virtual screening - the search for new routes to control head blight disease. *BMC Bioinformatics* **17**, 39–52 (2016).

111. Sridhar, P. S., Sharma, T. & Loewen, M. C. Selective Quantification of Chemotropic Responses of Fusarium graminearum. *Methods Mol. Biol.* **2659**, 61–71 (2023).

112. Boenisch, M. J. & Schäfer, W. Fusarium graminearum forms mycotoxin producing infection structures on wheat. *BMC Plant Biol.* **11**, 1–14 (2011).

113. O'Mara, S. P., Broz, K., Dong, Y. & Kistler, H. C. The Fusarium graminearum transporters Abc1 and Abc6 are important for xenobiotic resistance, trichothecene accumulation, and virulence to wheat. *bioRxiv* 2021.06.15.448535 (2021). doi:10.1101/2021.06.15.448535

114. Wang, S. C. *et al.* Expansion of the Major Facilitator Superfamily (MFS) to include novel

transporters as well as transmembrane-acting enzymes. *Biochim. Biophys. Acta - Biomembr.* **1862**, 183277 (2020).

115. Stolz, J., Caspari, T., Carr, A. M. & Sauer, N. Cell Division Defects of Schizosaccharomyces pombe liz1− Mutants Are Caused by Defects in Pantothenate Uptake. *Eukaryot. Cell* **3**, 406–412 (2004).

116. Ene, I. V. *et al.* Cell Wall Remodeling Enzymes Modulate Fungal Cell Wall Elasticity and Osmotic Stress Resistance. *MBio* **6**, (2015).

117. Dalto, M. & Daniels, J. Fungi. *Pract. Handb. Microbiol. Third Ed.* 937–962 (2017). doi:10.1101/GLYCOBIOLOGY.3E.023

118. Hurley, J. H. THE SUGAR KINASE/HEAT SHOCK PROTEIN 7O/ACTIN SUPERFAMILY: Implications of Conserved Structure for Mechanism. *Annu. Rev. Biophys. Biomol. Struct* **25**, 137–62 (1996).

119. Ding, Y., Gardiner, D. M., Xiao, D. & Kazan, K. Novel regulators of nitric oxide signaling triggered by host perception in a plant pathogen. *bioRxiv* 779173 (2019). doi:10.1101/779173

120. Goodman, A. L. *et al.* Direct interaction between sensor kinase proteins mediates acute and chronic disease phenotypes in a bacterial pathogen. *Genes Dev.* **23**, 249 (2009).

121. Davies, J. A. *et al.* The GacS sensor kinase controls phenotypic reversion of small colony variants isolated from biofilms of Pseudomonas aeruginosa PA14. *FEMS Microbiol. Ecol.* **59**, 32–46 (2007).

122. Tanaka, S. & Nojima, H. Nik1: a Nim1-like protein kinase of S. cerevisiae interacts with the Cdc28 complex and regulates cell cycle progression. *Genes to Cells* **1**, 905–921 (1996).

123. A, P.-C., D, S., J, A. & S, A.-B. Retinal biosynthesis in fungi: characterization of the carotenoid oxygenase CarX from Fusarium fujikuroi. *Eukaryot. Cell* **6**, 650–657 (2007).

124. Buhrow, L. M., Cram, D., Tulpan, D., Foroud, N. A. & Loewen, M. C. Exogenous abscisic acid and gibberellic acid elicit opposing effects on Fusarium graminearum infection in wheat. *Phytopathology* **106**, 986–996 (2016).

125. Buhrow, L. M. *et al.* Wheat transcriptome profiling reveals abscisic and gibberellic acid treatments regulate early-stage phytohormone defense signaling, cell wall fortification, and metabolic switches following Fusarium graminearum-challenge. *BMC Genomics* **22**, 1–21 (2021).

126. Falter, C. & Reumann, S. The essential role of fungal peroxisomes in plant infection. *Mol. Plant Pathol.* **00**, 1–14 (2022).

127. Wu, P. C., Chen, Y. K., Yago, J. I. & Chung, K. R. Peroxisomes Implicated in the Biosynthesis of Siderophores and Biotin, Cell Wall Integrity, Autophagy, and Response to Hydrogen Peroxide in the Citrus Pathogenic Fungus Alternaria alternata. *Front. Microbiol.* **12**, 1588 (2021).

128. Zhang, D. *et al.* Aim32 is a dual-localized 2Fe-2S mitochondrial protein that functions in redox quality control. *J. Biol. Chem.* **297**, 101135 (2021).

129. Black, B., Lee, C., Horianopoulos, L. C., Jung, W. H. & Kronstad, J. W. Respiring to infect: Emerging links between mitochondria, the electron transport chain, and fungal pathogenesis. *PLOS Pathog.* **17**, e1009661 (2021).

130. Verma, S., Shakya, V. P. S. & Idnurm, A. Exploring and exploiting the connection between mitochondria and the virulence of human pathogenic fungi. *Virulence* **9**, 426–446 (2018).

131. Liu, X., Han, Q., Xu, J., Wang, J. & Shi, J. Acetohydroxyacid synthase FgIlv2 and FgIlv6 are involved in BCAA biosynthesis, mycelial and conidial morphogenesis, and full virulence in Fusarium graminearum. *Sci. Rep.* **5**, (2015).

132. Liu, X. *et al.* Two FgLEU2 Genes with Different Roles in Leucine Biosynthesis and Infection-Related Morphogenesis in Fusarium graminearum. *PLoS One* **11**, (2016).

133. Sieber, C. M. K., Lee, W., Wong, P., Mü Nsterkö Tter, M. & Mewes, H.-W. The Fusarium graminearum Genome Reveals More Secondary Metabolite Gene Clusters and Hints of Horizontal Gene Transfer. *PLoS One* **9**, 110311 (2014).

134. Fredriksson, R. & Schiöth, H. B. The repertoire of G-protein-coupled receptors in fully sequenced genomes. *Mol. Pharmacol.* **67**, 1414–1425 (2005).

135. Natarajan, S. K., Muthukrishnan, E., Khalimonchuk, O., Mott, J. L. & Becker, D. F. Evidence for pipecolate oxidase in mediating protection against hydrogen peroxide stress. *J. Cell. Biochem.* **118**, 1678 (2017).

136. Haberland, A., Müller, J., Wallukat, G. & Wenzel, K. Antigen-free control wells in an ELISA set-up for the determination of autoantibodies against G protein-coupled receptors—a requisite for correct data evaluation. *Anal. Bioanal. Chem.* **410**, 5101–5105 (2018).

137. Rocha, A. L. M., Di Pietro, A., Ruiz-Roldán, C. & Roncero, M. I. G. Ctf1, a transcriptional activator of cutinase and lipase genes in Fusarium oxysporum is dispensable for virulence. *Mol. Plant Pathol.* **9**, 293 (2008).

138. Rerngsamran, P., Murphy, M. B., Doyle, S. A. & Ebbole, D. J. Fluffy, the major regulator of conidiation in Neurospora crassa, directly activates a developmentally regulated hydrophobin gene. *Mol. Microbiol.* **56**, 282–297 (2005).

139. Cohrs, K. C. & Schumacher, J. The two cryptochrome/photolyase family proteins fulfill distinct roles in DNA photorepair and regulation of conidiation in the gray mold fungus Botrytis cinerea. *Appl. Environ. Microbiol.* **83**, (2017).

140. Carmen Ruiz-Roldán, M. *et al.* Role of the White Collar 1 Photoreceptor in Carotenogenesis, UV Resistance, Hydrophobicity, and Virulence of Fusarium oxysporum. *Eukaryot. Cell* **7**, 1227–1230 (2008).

141. M Cuperlovic-Culf, M. L. N. R. A. S. Perspectives on the specific targeting of Fusarium graminearum for the development of alternative head blight treatment approaches. *Plant Pathol.* **66**, 1391–1403 (2017).

142. SH, M., BD, W., MJ, W. & ET, S. Causes and consequences of variability in peptide mating pheromones of ascomycete fungi. *Mol. Biol. Evol.* **28**, 1987–2003 (2011).

143. Turrà, D., El Ghalid, M., Rossi, F. & Di Pietro, A. Fungal pathogen uses sex pheromone receptor for chemotropic sensing of host plant signals. *Nature* **527**, 521–524 (2015).

144. Hinterdobler, W. *et al.* Integration of chemosensing and carbon catabolite repression impacts fungal enzyme regulation and plant associations. *bioRxiv* 2021.05.06.442915 (2021). doi:10.1101/2021.05.06.442915

145. Rampitsch, C., Leung, W., Blackwell, B. & Subramaniam, R. Volume 64 2011 P L A N T B R E E D I N G A N D S E E D S C I E N C E MAP KINASE MGV1: A POTENTIAL SHARED CONTROL POINT OF BUTENOLIDE AND DEOXYNIVALENOL BIOSYNTHESIS IN FUSARIUM GRAMINEARUM. doi:10.2478/v10129-011-0031-0

146. Van Dyck, L., Dembowski, M., Neupert, W. & Langer, T. Mcx1p, a ClpX homologue in mitochondria of Saccharomyces cerevisiae. *FEBS Lett.* **438**, 250–254 (1998).

147. Mondal, S. *et al.* Membrane Driven Spatial Organization of GPCRs. *Sci. Reports 2013 31*

3, 1–9 (2013).

148. Shi, C., Paige, M. F., Maley, J. & Loewen, M. C. In vitro characterization of ligand-induced oligomerization of the S. cerevisiae G-protein coupled receptor, Ste2p. *BBA - Gen. Subj.* **1790**, 1–7 (2008).

149. Thaler, J. S., Humphrey, P. T. & Whiteman, N. K. Evolution of jasmonate and salicylate signal crosstalk. *Trends Plant Sci.* **17**, 260–270 (2012).

150. Di, X., Gomila, J. & Takken, F. L. W. Involvement of salicylic acid, ethylene and jasmonic acid signalling pathways in the susceptibility of tomato to Fusarium oxysporum. *Mol. Plant Pathol.* **18**, 1024 (2017).

151. Buhrow, L. M. *et al.* Wheat transcriptome profiling reveals abscisic and gibberellic acid treatments regulate early-stage phytohormone defense signaling, cell wall fortification, and metabolic switches following Fusarium graminearum-challenge. *BMC Genomics 2021 221* **22**, 1–21 (2021).

152. Goodman, J. L. *et al.* Ornithine cyclodeaminase: structure, mechanism of action, and implications for the mu-crystallin family. *Biochemistry* **43**, 13883–13891 (2004).

153. Lamb, C. & Dixon, R. A. THE OXIDATIVE BURST IN PLANT DISEASE RESISTANCE. *Annu. Rev. Plant Physiol. Plant Mol. Biol.* **48**, 251–275 (1997).

154. Perez, P. & Rincón, S. A. Rho GTPases: regulation of cell polarity and growth in yeasts. *Biochem. J.* **426**, 243–253 (2010).

155. Al Abdallah, Q., Ge, W. & Fortwendel, J. R. A Simple and Universal System for Gene Manipulation in Aspergillus fumigatus: In Vitro -Assembled Cas9-Guide RNA Ribonucleoproteins Coupled with Microhomology Repair Templates . *mSphere* **2**, (2017).

156. Frandsen, R. J. N., Andersson, J. A., Kristensen, M. B. & Giese, H. Efficient four

fragment cloning for the construction of vectors for targeted gene replacement in filamentous fungi. *BMC Mol. Biol.* **9**, 70 (2008).

157. Koch, A. *et al.* The Antimicrobial Peptide Thanatin Reduces Fungal Infections in Arabidopsis. *J. Phytopathol.* **160**, 606–610 (2012).

158. Koch, A. *et al.* Host-induced gene silencing of cytochrome P450 lanosterol C14α-demethylase-encoding genes confers strong resistance to Fusarium species. *Proc. Natl. Acad. Sci. U. S. A.* **110**, 19324–19329 (2013).

159. Walkowiak, S. *et al.* Intraspecies Interaction of Fusarium graminearum Contributes to Reduced Toxin Production and Virulence. *Mol. Plant. Microbe. Interact.* **28**, 1256–1267 (2015).

160. Yun, Y. *et al.* Functional analysis of the Fusarium graminearum phosphatome. *New Phytol.* **207**, 119–134 (2015).

161. CA Schneider, W. R. K. E. NIH image to ImageJ: 25 years of image analysis. *Nat. Methods* **9**, 671–675 (2012).

162. King, R., Urban, M., Hammond-Kosack, M. C. U., Hassani-Pak, K. & Hammond-Kosack, K. E. The completed genome sequence of the pathogenic ascomycete fungus Fusarium graminearum. *BMC Genomics* **16**, 1–21 (2015).

163. Robinson, M. D., McCarthy, D. J. & Smyth, G. K. edgeR: a Bioconductor package for differential expression analysis of digital gene expression data. *Bioinformatics* **26**, 139–140 (2010).

164. Benjamini, Y. & Hochberg, Y. Controlling the False Discovery Rate: A Practical and Powerful Approach to Multiple Testing. *J. R. Stat. Soc. Ser. B* **57**, 289–300 (1995).

165. Basenko, E. Y. *et al.* FungiDB: An Integrated Bioinformatic Resource for Fungi and

Oomycetes. *J. fungi (Basel, Switzerland)* **4**, (2018).

166. Bu, D. *et al.* KOBAS-i: intelligent prioritization and exploratory visualization of biological functions for gene enrichment analysis. *Nucleic Acids Res.* **49**, W317–W325 (2021).

167. Calebiro, D. & Godbole, A. Internalization of G-protein-coupled receptors: Implication in receptor function, physiology and diseases. *Best Pract. Res. Clin. Endocrinol. Metab.* **32**, 83–91 (2018).

168. Sleno, R. & Hébert, T. E. The Dynamics of GPCR Oligomerization and Their Functional Consequences. *Int. Rev. Cell Mol. Biol.* **338**, 141–171 (2018).

169. Marshall, F. H., Jones, K. A., Kaupmann, K. & Bettler, B. GABAB receptors - the first 7TM heterodimers. *Trends Pharmacol. Sci.* **20**, 396–399 (1999).

170. Sevlever, F., Di Bella, J. P. & Ventura, A. C. Discriminating between negative cooperativity and ligand binding to independent sites using pre-equilibrium properties of binding curves. *PLoS Comput. Biol.* **16**, (2020).

171. Breit, A., Lagacé, M. & Bouvier, M. Hetero-oligomerization between beta2- and beta3-adrenergic receptors generates a beta-adrenergic signaling unit with distinct functional properties. *J. Biol. Chem.* **279**, 28756–28765 (2004).

172. Angers, S. *et al.* Detection of β2-adrenergic receptor dimerization in living cells using bioluminescence resonance energy transfer (BRET). *Proc. Natl. Acad. Sci. U. S. A.* **97**, 3684–3689 (2000).

173. Marshall, F. H., Jones, K. A., Kaupmann, K. & Bettler, B. GABAB receptors - the first 7TM heterodimers. *Trends Pharmacol. Sci.* **20**, 396–399 (1999).

174. AbdAlla, S., Lother, H. & Quitterer, U. AT1-receptor heterodimers show enhanced G-

protein activation and altered receptor sequestration. *Nature* **407**, 94–98 (2000).

175. Dijkman, P. M. *et al.* Dynamic tuneable G protein-coupled receptor monomer-dimer populations. *Nat. Commun. 2018 91* **9**, 1–14 (2018).

176. Benkirane, M., Jin, D. Y., Chun, R. F., Koup, R. A. & Jeang, K. T. Mechanism of transdominant inhibition of CCR5-mediated HIV-1 infection by ccr5delta32. *J. Biol. Chem.* **272**, 30603–30606 (1997).

177. Cvejic, S. & Devi, L. A. Dimerization of the δ Opioid Receptor: *J. Biol. Chem.* **272**, 26959–26964 (1997).

178. Romano, C., Yang, W. L. & O'Malley, K. L. Metabotropic glutamate receptor 5 is a disulfide-linked dimer. *J. Biol. Chem.* **271**, 28612–28616 (1996).

179. Bai, M., Trivedi, S. & Brown, E. M. Dimerization of the extracellular calcium-sensing receptor (CaR) on the cell surface of CaR-transfected HEK293 cells. *J. Biol. Chem.* **273**, 23605–23610 (1998).

180. Shi, C., Kaminskyj, S., Caldwell, S. & Loewen, M. C. A role for a complex between activated G protein-coupled receptors in yeast cellular mating. *Proc. Natl. Acad. Sci. U. S. A.* **104**, 5395–5400 (2007).

181. Mueller, B. K., Subramaniam, S. & Senes, A. A frequent, GxxxG-mediated, transmembrane association motif is optimized for the formation of interhelical Cα-H hydrogen bonds. *Proc. Natl. Acad. Sci. U. S. A.* **111**, E888 (2014).

182. Sharma, T. *et al.* Fusarium graminearum Ste3 G-Protein Coupled Receptor: A Mediator of Hyphal Chemotropism and Pathogenesis . *mSphere* **7**, (2022).

183. Thannickal, V. J. & Fanburg, B. L. Reactive oxygen species in cell signaling. *Am. J. Physiol. - Lung Cell. Mol. Physiol.* **279**, 1005–1028 (2000).

184. Schieber, M. & Chandel, N. S. ROS Function in Redox Signaling and Oxidative Stress. *Curr. Biol.* **24**, R453 (2014).

185. Lee, G. *et al.* Oxidative Dimerization of PHD2 is Responsible for its Inactivation and Contributes to Metabolic Reprogramming via HIF-1α Activation. *Sci. Reports 2016 61* **6**, 1–12 (2016).

186. Miki, H. & Funato, Y. Regulation of intracellular signalling through cysteine oxidation by reactive oxygen species. *J. Biochem.* **151**, 255–261 (2012).

187. Baba, S. P. & Bhatnagar, A. Role of thiols in oxidative stress. *Curr. Opin. Toxicol.* **7**, 133–139 (2018).

188. Gotoh, Y. & Cooper, J. A. Reactive Oxygen Species-and Dimerization-induced Activation of Apoptosis Signal-regulating Kinase 1 in Tumor Necrosis Factor-Signal Transduction*. (1998).

189. Hancock, J. *et al.* Doing the unexpected: proteins involved in hydrogen peroxide perception. *J. Exp. Bot.* **57**, 1711–1718 (2006).

190. Petry, A. & Görlach, A. Regulation of NADPH Oxidases by G Protein-Coupled Receptors. *Antioxid. Redox Signal.* **30**, 74–94 (2019).

191. Lee, S. L., Wang, W. W. & Fanburg, B. L. Superoxide as an intermediate signal for serotonin-induced mitogenesis. *Free Radic. Biol. Med.* **24**, 855–858 (1998).

192. Griendling, K. K., Minieri, C. A., Ollerenshaw, J. D. & Alexander, R. W. Angiotensin II stimulates NADH and NADPH oxidase activity in cultured vascular smooth muscle cells. *Circ. Res.* **74**, 1141–1148 (1994).

193. Schneider, W. D. H., Camassola, M. & Fontana, R. C. How ligninolytic enzymes can help in the degradation of biomass polysaccharides, cleavage, and catalytic mechanisms?

Polysacch. Degrad. Biocatal. 177–190 (2023). doi:10.1016/B978-0-323-99986-1.00007-7

194. Lüthje, S. & Martinez-Cortes, T. Membrane-Bound Class III Peroxidases: Unexpected Enzymes with Exciting Functions. *Int. J. Mol. Sci.* **19**, (2018).

195. Sridhar, P. & 20036922. How Fusarium graminearum GPCRs Contribute To Fungal Virulence On Wheat. (2023).

196. Pello, O. M. *et al.* Ligand stabilization of CXCR4/delta-opioid receptor heterodimers reveals a mechanism for immune response regulation. *Eur. J. Immunol.* **38**, 537–549 (2008).

197. Somvanshi, R. K. & Kumar, U. Pathophysiology of GPCR Homo- and Heterodimerization: Special Emphasis on Somatostatin Receptors. *Pharmaceuticals* **5**, 417 (2012).

198. E, L., DY, T. & M, W. Pheromone signalling and polarized morphogenesis in yeast. *Curr. Opin. Genet. Dev.* **7**, 59–66 (1997).

199. Vitale, S., Di Pietro, A. & Turrà, D. Autocrine pheromone signalling regulates community behaviour in the fungal pathogen Fusarium oxysporum. *Nat. Microbiol.* **4**, 1443–1449 (2019).

200. C, C. *et al.* Screening for Protein-Protein Interaction Inhibitors Using a Bioluminescence Resonance Energy Transfer (BRET)-Based Assay in Yeast. *SLAS Discov. Adv. life Sci. R D* **22**, 751–759 (2017).

201. Loewen, M. C. *et al.* Solution 19F nuclear Overhauser effects in structural studies of the cytoplasmic domain of mammalian rhodopsin. *Proc. Natl. Acad. Sci. U. S. A.* **98**, 4888–4892 (2001).

202. Gietz, R. D. & Schiestl, R. H. High-efficiency yeast transformation using the LiAc/SS

carrier DNA/PEG method. *Nat. Protoc. 2007 21* **2**, 31–34 (2007).

203. Shi, C., Kendall, S. C., Grote, E., Kaminskyj, S. & Loewen, M. C. N-terminal residues of the yeast pheromone receptor, Ste2p, mediate mating events independently of G1-arrest signaling. *J. Cell. Biochem.* **107**, 630–638 (2009).

204. Besson, B. *et al.* Optimization of BRET saturation assays for robust and sensitive cytosolic protein–protein interaction studies. *Sci. Reports 2022 121* **12**, 1–11 (2022).

205. Zhang, J. H., Chung, T. D. Y. & Oldenburg, K. R. A Simple Statistical Parameter for Use in Evaluation and Validation of High Throughput Screening Assays. *J. Biomol. Screen.* **4**, 67–73 (1999).

206. Hauser, M., Kauffman, S., Lee, B. K., Naider, F. & Becker, J. M. The first extracellular loop of the Saccharomyces cerevisiae G protein-coupled receptor Ste2p undergoes a conformational change upon ligand binding. *J. Biol. Chem.* **282**, 10387–10397 (2007).

207. Waltenspühl, Y., Ehrenmann, J., Klenk, C. & Plückthun, A. Engineering of Challenging G Protein-Coupled Receptors for Structure Determination and Biophysical Studies. *Molecules* **26**, (2021).

208. C, X., YP, H. & J, H. Magnificent seven: roles of G protein-coupled receptors in extracellular sensing in fungi. *FEMS Microbiol. Rev.* **32**, 1010–1032 (2008).

209. Rosenbaum, D. M., Rasmussen, S. G. F. & Kobilka, B. K. The structure and function of G-protein-coupled receptors. *Nature* **459**, 356 (2009).

210. Velazhahan, V., Ma, N., Vaidehi, N. & Tate, C. G. Activation mechanism of the class D fungal GPCR dimer Ste2. *Nat. 2022 6037902* **603**, 743–748 (2022).

211. Abiko, L. A., Rogowski, M., Gautier, A., Schertler, G. & Grzesiek, S. Efficient production of a functional G protein-coupled receptor in E. coli for structural studies. *J. Biomol. Nmr*

75, 25 (2021).

212. André, N. *et al.* Enhancing functional production of G protein-coupled receptors in Pichia pastoris to levels required for structural studies via a single expression screen. *Protein Sci.* **15**, 1115 (2006).

213. Massotte, D. G protein-coupled receptor overexpression with the baculovirus–insect cell system: a tool for structural and functional studies. *Biochim. Biophys. Acta - Biomembr.* **1610**, 77–89 (2003).

214. Shimamura, T. *et al.* Structure of the human histamine H1 receptor complex with doxepin. *Nature* **475**, 65–72 (2011).

215. Deutschmann, S. M. & Jäger, V. Optimization of the growth conditions of Sf21 insect cells for high-density perfusion culture in stirred-tank bioreactors. *Enzyme Microb. Technol.* **16**, 506–512 (1994).

216. Davis, T. R. *et al.* Comparative recombinant protein production of eight insect cell lines. *In Vitro Cell. Dev. Biol. Anim.* **29A**, 388–390 (1993).

217. Ono, C., Okamoto, T., Abe, T. & Matsuura, Y. Baculovirus as a Tool for Gene Delivery and Gene Therapy. *Viruses* **10**, (2018).

218. Hu, Y. C. Baculovirus as a highly efficient expression vector in insect and mammalian cells. *Acta Pharmacol. Sin. 2005 264* **26**, 405–416 (2005).

219. Shi, Y. *et al.* Abnormal SDS-PAGE migration of cytosolic proteins can identify domains and mechanisms that control surfactant binding. *Protein Sci.* **21**, 1197 (2012).

220. Rath, A., Glibowicka, M., Nadeau, V. G., Chen, G. & Deber, C. M. Detergent binding explains anomalous SDS-PAGE migration of membrane proteins. *Proc. Natl. Acad. Sci. U. S. A.* **106**, 1760–1765 (2009).

221. Esteban, P. F. & Molina-Holgado, E. Tips and tricks for cannabinoid receptor 1 detection, interaction and interpretation. *Neural Regen. Res.* **16**, 1535 (2021).

222. Perincherry, L., Lalak-Kánczugowska, J. & Stepién, L. Fusarium-Produced Mycotoxins in Plant-Pathogen Interactions. *Toxins (Basel).* **11**, (2019).

223. NA Brown, S. S. P. D. G. G. Fungal G-protein-coupled receptors: Mediators of pathogenesis and targets for disease control. *Nat. Microbiol.* **3**, 402–414 (2018).

224. Lafon, A., Han, K. H., Seo, J. A., Yu, J. H. & d'Enfert, C. G-protein and cAMP-mediated signaling in aspergilli: a genomic perspective. *Fungal Genet. Biol.* **43**, 490–502 (2006).

225. Dias, M. M. *et al.* Insect High Five™ cell line development using site-specific flipase recombination technology. *G3 Genes|Genomes|Genetics* **11**, (2021).

226. Krammer, F. *et al.* Trichoplusia ni cells (High Five™) are highly efficient for the production of influenza A virus-like particles: a comparison of two insect cell lines as production platforms for influenza vaccines. *Mol. Biotechnol.* **45**, 226 (2010).

227. Jakowiecki, J., Orzeł, U., Chawananon, S., Miszta, P. & Filipek, S. The Hydrophobic Ligands Entry and Exit from the GPCR Binding Site-SMD and SuMD Simulations. *Molecules* **25**, (2020).

228. Boone, C., Davis, N. G. & Sprague, G. F. Mutations that alter the third cytoplasmic loop of the a-factor receptor lead to a constitutive and hypersensitive phenotype. *Proc. Natl. Acad. Sci.* **90**, 9921–9925 (1993).

229. Wang, H. W. & Wang, J. W. How cryo-electron microscopy and X-ray crystallography complement each other. *Protein Sci.* **26**, 32–39 (2017).

230. Shoemaker, S. C. & Ando, N. X-rays in the Cryo-Electron Microscopy Era: Structural Biology's Dynamic Future. *Biochemistry* **57**, 277–285 (2018).

231. Vénien-Bryan, C., Li, Z., Vuillard, L. & Boutin, J. A. Cryo-electron microscopy and X-ray crystallography: Complementary approaches to structural biology and drug discovery. *Acta Crystallogr. Sect. Struct. Biol. Commun.* **73**, 174–183 (2017).

232. Jumper, J. *et al.* Highly accurate protein structure prediction with AlphaFold. *Nat. 2021 5967873* **596**, 583–589 (2021).

233. Bradford, M. A rapid and sensitive method for the quantitation of microgram quantities of protein utilizing the principle of protein-dye binding. *Anal. Biochem.* **72**, 248–254 (1976).

234. Hauser, F., Waadt, R. & Schroeder, J. I. Evolution of Abscisic Acid Synthesis and Signaling Mechanisms. *Curr. Biol.* **21**, R346 (2011).

235. Hartung, W. The evolution of abscisic acid (ABA) and ABA function in lower plants, fungi and lichen. doi:10.1071/FP10058

236. De Torres-Zabala, M. *et al.* Pseudomonas syringae pv. tomato hijacks the Arabidopsis abscisic acid signalling pathway to cause disease. *EMBO J.* **26**, 1434–1443 (2007).

237. De Torres Zabala, M., Bennett, M. H., Truman, W. H. & Grant, M. R. Antagonism between salicylic and abscisic acid reflects early host–pathogen conflict and moulds plant defence responses. *Plant J.* **59**, 375–386 (2009).

238. Oide, S. *et al.* A novel role of PR2 in abscisic acid (ABA) mediated, pathogen-induced callose deposition in Arabidopsis thaliana. *New Phytol.* **200**, 1187–1199 (2013).

239. Spence, C. A., Lakshmanan, V., Donofrio, N. & Bais, H. P. Crucial roles of abscisic acid biogenesis in virulence of rice blast fungus Magnaporthe oryzae. *Front. Plant Sci.* **6**, 170475 (2015).

240. Lievens, L., Pollier, J., Goossens, A., Beyaert, R. & Staal, J. Abscisic acid as pathogen effector and immune regulator. *Front. Plant Sci.* **8**, 587 (2017).

241. Okamoto, M., Hirai, N. & Koshimizu, K. Biosynthesis of abscisic acid from α-ionylideneethanol in Cercospora pini-densiflorae. *Phytochemistry* **27**, 3465–3469 (1988).

242. Oritani, T. & Kiyota, H. Biosynthesis and metabolism of abscisic acid and related compounds. *Nat. Prod. Rep.* **20**, 414–425 (2003).

243. Inomata, M., Hirai, N., Yoshida, R. & Ohigashi, H. The biosynthetic pathway to abscisic acid via ionylideneethane in the fungus Botrytis cinerea. *Phytochemistry* **65**, 2667–2678 (2004).

244. Takino, J. *et al.* Elucidation of biosynthetic pathway of a plant hormone abscisic acid in phytopathogenic fungi. *Biosci. Biotechnol. Biochem.* **83**, 1642–1649 (2019).

245. Siewers, V. *et al.* Functional analysis of the cytochrome P450 monooxygenase gene bcbot1 of Botrytis cinerea indicates that botrydial is a strain-specific virulence factor. *Mol. Plant. Microbe. Interact.* **18**, 602–612 (2005).

246. Siewers, V., Kokkelink, L., Smedsgaard, J. & Tudzynski, P. Identification of an Abscisic Acid Gene Cluster in the Grey Mold Botrytis cinerea. *Appl. Environ. Microbiol.* **72**, 4619 (2006).

247. Gong, T., Shu, D., Yang, J., Ding, Z. T. & Tan, H. Sequencing and Transcriptional Analysis of the Biosynthesis Gene Cluster of Abscisic Acid-Producing Botrytis cinerea. *Int. J. Mol. Sci.* **15**, 17396 (2014).

248. Siewers, V., Smedsgaard, J. & Tudzynski, P. The P450 Monooxygenase BcABA1 Is Essential for Abscisic Acid Biosynthesis in Botrytis cinerea. *Appl. Environ. Microbiol.* **70**, 3868 (2004).

249. Ortiz De Montellano, P. R. Hydrocarbon Hydroxylation by Cytochrome P450 Enzymes. *Chem. Rev.* **110**, 932 (2010).

250. Gillam, E. M. J. & Hunter, D. J. B. Chemical Defense and Exploitation. Biotransformation of Xenobiotics by Cytochrome P450 Enzymes. *Met. Ions Life Sci.* **3**, 477–560 (2007).

251. Wei, Z. *et al.* The BcLAE1 is involved in the regulation of ABA biosynthesis in Botrytis cinerea TB-31. *Front. Microbiol.* **13**, (2022).

252. Troncoso, C., Cárcamo, J., Hedden, P., Tudzynski, B. & Cecilia Rojas, M. Influence of electron transport proteins on the reactions catalyzed by Fusarium fujikuroi gibberellin monooxygenases. *Phytochemistry* **69**, 672–683 (2008).

253. Malonek, S. *et al.* Distribution of gibberellin biosynthetic genes and gibberellin production in the Gibberella fujikuroi species complex.

254. Lim, C. W., Baek, W., Jung, J., Kim, J. H. & Lee, S. C. Function of ABA in Stomatal Defense against Biotic and Drought Stresses. *Int. J. Mol. Sci. 2015, Vol. 16, Pages 15251-15270* **16**, 15251–15270 (2015).

255. Spence, C. A., Lakshmanan, V., Donofrio, N. & Bais, H. P. Crucial roles of abscisic acid biogenesis in virulence of rice blast fungus Magnaporthe oryzae. *Front. Plant Sci.* **6**, 1–13 (2015).

256. Pandey, S., Nelson, D. C. & Assmann, S. M. Two novel GPCR-type G proteins are abscisic acid receptors in Arabidopsis. *Cell* **136**, 136–148 (2009).

257. da Silva Ripardo-Filho, H. *et al.* From Genes to Molecules, Secondary Metabolism in Botrytis cinerea: New Insights into Anamorphic and Teleomorphic Stages. *Plants 2023, Vol. 12, Page 553* **12**, 553 (2023).

258. Izquierdo-Bueno, I. *et al.* Biosynthesis of abscisic acid in fungi: identification of a sesquiterpene cyclase as the key enzyme in Botrytis cinerea. *Environ. Microbiol.* **20**, 2469–2482 (2018).

259. Durairaj, P., Hur, J. S. & Yun, H. Versatile biocatalysis of fungal cytochrome P450 monooxygenases. *Microb. Cell Factories 2016 151* **15**, 1–16 (2016).

260. He, D. *et al.* Contribution of NADPH-cytochrome P450 Reductase to Azole Resistance in Fusarium oxysporum. *Front. Microbiol.* **12**, 709942 (2021).

261. Takeuchi, J. *et al.* Designed abscisic acid analogs as antagonists of PYL-PP2C receptor interactions. *Nat. Chem. Biol. 2014 106* **10**, 477–482 (2014).

262. Schmidt, K. *et al.* Accumulation of the hormone abscisic acid (ABA) at the infection site of the fungus Cercospora beticola supports the role of ABA as a repressor of plant defence in sugar beet. *Mol. Plant Pathol.* **9**, 661–673 (2008).

263. Hartung, W. & Hartung, W. The evolution of abscisic acid (ABA) and ABA function in lower plants, fungi and lichen. *Funct. Plant Biol.* **37**, 806–812 (2010).

264. Marchler-Bauer, A. *et al.* CDD/SPARCLE: functional classification of proteins via subfamily domain architectures. *Nucleic Acids Res.* **45**, D200–D203 (2017).

265. Bailey, T. L., Williams, N., Misleh, C. & Li, W. W. MEME: discovering and analyzing DNA and protein sequence motifs. *Nucleic Acids Res.* **34**, (2006).

266. Canadian Plant Disease Survey 2020 Volume 100: Disease Highlights 2019. *Can. J. Plant Pathol.* **42**, 1–175 (2020).

267. Köhl, J., De Haas, B. H., Kastelein, P., Burgers, S. L. G. E. & Waalwijk, C. Fusarium Head Blight, Mycotoxins and Strategies for Their Reduction. *Agron. 2020, Vol. 10, Page 509* **10**, 509 (2020).

268. Davies, D. R., Bindschedler, L. V., Strickland, T. S. & Bolwell, G. P. Production of reactive oxygen species in Arabidopsis thaliana cell suspension cultures in response to an elicitor from Fusarium oxysporum: implications for basal resistance. *J. Exp. Bot.* **57**,

1817–1827 (2006).

269. Schopfer, P., Plachy, C. & Frahry, G. Release of Reactive Oxygen Intermediates (Superoxide Radicals, Hydrogen Peroxide, and Hydroxyl Radicals) and Peroxidase in Germinating Radish Seeds Controlled by Light, Gibberellin, and Abscisic Acid. *Plant Physiol.* **125**, 1591 (2001).

270. Peng, Y., Van Wersch, R. & Zhang, Y. Convergent and divergent signaling in PAMP-triggered immunity and effector-triggered immunity. *Mol. Plant-Microbe Interact.* **31**, 403–409 (2018).

271. Zhang, J. & Zhou, J. M. Plant immunity triggered by microbial molecular signatures. *Mol. Plant* **3**, 783–793 (2010).

272. Irieda, H. *et al.* Conserved fungal effector suppresses PAMP-triggered immunity by targeting plant immune kinases. *Proc. Natl. Acad. Sci. U. S. A.* **116**, 496–505 (2019).

273. Meena, M., Prasad, V., Zehra, A., Gupta, V. K. & Upadhyay, R. S. Mannitol metabolism during pathogenic fungal–host interactions under stressed conditions. *Front. Microbiol.* **6**, (2015).

274. Jones, S. K. & Bennett, R. J. Fungal mating pheromones: Choreographing the dating game. (2011). doi:10.1016/j.fgb.2011.04.001

275. Perry, A. M., Hernday, A. D. & Nobile, C. J. Unraveling How Candida albicans Forms Sexual Biofilms. *J. Fungi* **6**, (2020).

276. Okagaki, L. H. *et al.* Cryptococcal Titan Cell Formation Is Regulated by G-Protein Signaling in Response to Multiple Stimuli. *Eukaryot. Cell* **10**, 1306 (2011).

277. Ni, M., Feretzaki, M., Sun, S., Wang, X. & Heitman, J. Sex in Fungi. *Annu. Rev. Genet.* **45**, 405 (2011).

278. Li, T., Kim, D. & Lee, J. NADPH Oxidase Gene, FgNoxD, Plays a Critical Role in Development and Virulence in Fusarium graminearum. *Front. Microbiol.* **13**, (2022).

279. Pritsch, C. Systemic expression of defense response genes in wheat spikes as a response to Fusarium graminearum infection. *Physiol. Mol. Plant Pathol.* **58**, 1–12 (2001).

280. Jain, N. Large-scale stage-specific regulation of gene expression during host-pathogen interactions in CSP44 bread wheat carrying APR gene Lr48. *Funct. Plant Biol.* **47**, 203–225 (2020).

281. Kong, X. *et al.* FgPex3, a Peroxisome Biogenesis Factor, Is Involved in Regulating Vegetative Growth, Conidiation, Sexual Development, and Virulence in Fusarium graminearum. *Front. Microbiol.* **10**, 2088 (2019).

282. Zhang, L. *et al.* Peroxin FgPEX22-Like Is Involved in FgPEX4 Tethering and Fusarium graminearum Pathogenicity. *Front. Microbiol.* **12**, (2021).

283. Mandal, M. *et al.* Reactive Oxygen Species (ROS) and Reactive Nitrogen Species (RNS) in plants– maintenance of structural individuality and functional blend. *Adv. Redox Res.* **5**, 100039 (2022).

284. Lismont, C., Revenco, I. & Fransen, M. Peroxisomal Hydrogen Peroxide Metabolism and Signaling in Health and Disease. *Int. J. Mol. Sci.* **20**, (2019).

285. López-Berges, M. S., Rispail, N., Prados-Rosales, R. C. & di Pietro, A. A Nitrogen Response Pathway Regulates Virulence Functions in Fusarium oxysporum via the Protein Kinase TOR and the bZIP Protein MeaB. *Plant Cell* **22**, 2459 (2010).

286. Faron-Górecka, A. *et al.* Understanding GPCR dimerization. *Methods Cell Biol.* **149**, 155–178 (2019).

287. Gurevich, V. V. & Gurevich, E. V. How and why do GPCRs dimerize? *Trends*

Pharmacol. Sci. **29**, 234 (2008).

288. Su, L. J. *et al.* Reactive Oxygen Species-Induced Lipid Peroxidation in Apoptosis, Autophagy, and Ferroptosis. *Oxid. Med. Cell. Longev.* **2019**, (2019).

289. Eze, M. O. Membrane fluidity, reactive oxygen species, and cell-mediated immunity: Implications in nutrition and disease. *Med. Hypotheses* **37**, 220–224 (1992).

290. Mellado, M. *et al.* Chemokine receptor homo- or heterodimerization activates distinct signaling pathways. *EMBO J.* **20**, 2497–2507 (2001).

291. Mao, C. *et al.* Cryo-EM structures of inactive and active GABAB receptor. *Cell Res.* **30**, 564–573 (2020).

292. Yang, M. Y., Kim, S. K. & Goddard, W. A. G protein coupling and activation of the metabotropic GABAB heterodimer. *Nat. Commun. 2022 131* **13**, 1–9 (2022).

293. Borroto-Escuela, D. O. *et al.* Mapping the interface of a GPCR Dimer: A structural model of the A2A Adenosine and D2 dopamine receptor heteromer. *Front. Pharmacol.* **9**, 362180 (2018).

294. Singh, B. K. *et al.* Climate change impacts on plant pathogens, food security and paths forward. *Nat. Rev. Microbiol. 2023* 1–17 (2023). doi:10.1038/s41579-023-00900-7

295. Chakraborty, S. & Newton, A. C. Climate change, plant diseases and food security: an overview. *Plant Pathol.* **60**, 2–14 (2011).

296. Bresso, E. *et al.* GPCRs from fusarium graminearum detection, modeling and virtual screening - the search for new routes to control head blight disease. *BMC Bioinformatics* **17**, (2016).

297. Martelle, J. L. & Nader, M. A. A Review of the Discovery, Pharmacological Characterization, and Behavioral Effects of the Dopamine D2-Like Receptor Antagonist

Eticlopride. *CNS Neurosci. Ther.* **14**, 248 (2008).

298. Velazhahan, V., McCann, B. L., Bignell, E. & Tate, C. G. Developing novel antifungals: lessons from G protein-coupled receptors. *Trends Pharmacol. Sci.* **44**, 162–174 (2023).

299. Roemer, T. & Krysan, D. J. Antifungal Drug Development: Challenges, Unmet Clinical Needs, and New Approaches. *Cold Spring Harb. Perspect. Med.* **4**, (2014).

300. Modrzewska, M., Bryła, M., Kanabus, J. & Pierzgalski, A. Trichoderma as a biostimulator and biocontrol agent against Fusarium in the production of cereal crops: Opportunities and possibilities. *Plant Pathol.* **71**, 1471–1485 (2022).

301. ASPERELLO® T34 Biocontrol® (Canada) | Biobest. Available at: https://www.biobestgroup.com/en/biobest/products/biological-disease-control-15998/biofungicides-15999/asperello-t34-biocontrol-%28canada%29-302597/. (Accessed: 7th July 2023)

302. Robinson, K. A. ; *et al.* Multiple Clonostachys rosea UDP-Glycosyltransferases Contribute to the Production of 15-Acetyl-Deoxynivalenol-3-O-Glycoside When Confronted with Fusarium graminearum. *J. Fungi 2023, Vol. 9, Page 723* **9**, 723 (2023).

303. Maidan, M. M. *et al.* The G Protein-coupled Receptor Gpr1 and the Gα Protein Gpa2 Act through the cAMP-Protein Kinase A Pathway to Induce Morphogenesis in Candida albicans. *Mol. Biol. Cell* **16**, 1971 (2005).

304. Filho, A. P. da C. *et al.* Aspergillus fumigatus G-Protein Coupled Receptors GprM and GprJ Are Important for the Regulation of the Cell Wall Integrity Pathway, Secondary Metabolite Production, and Virulence. *MBio* **11**, 1–25 (2020).

305. Yang, Q. *et al.* Broad-spectrum chemicals block ROS detoxification to prevent plant fungal invasion. *Curr. Biol.* **32**, 3886-3897.e6 (2022).

306. Gil-ad, N. L., Bar-Nun, N., Noy, T. & Mayer, A. M. Enzymes of Botrytis cinerea capable of breaking down hydrogen peroxide. *FEMS Microbiol. Lett.* **190**, 121–126 (2000).

307. Tavassolifar, M. J., Vodjgani, M., Salehi, Z. & Izad, M. The Influence of Reactive Oxygen Species in the Immune System and Pathogenesis of Multiple Sclerosis. *Autoimmune Dis.* **2020**, (2020).

Appendix A

Supplemental Information for Chapter 2

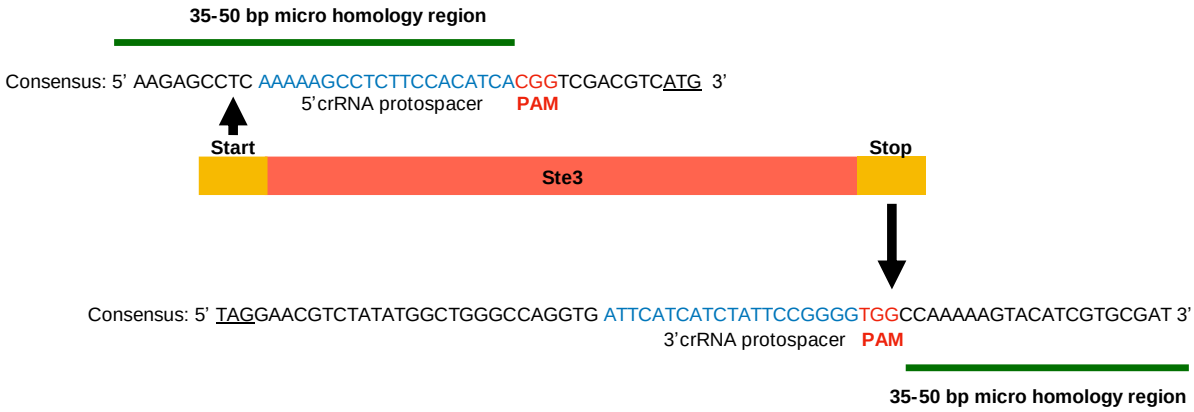

Supplemental Figure A1: Design of the protospacer regions for CRISPR-generated *Fgste3Δ* knockout. Sequences of the *STE3* upstream and downstream regions from the start and stop codons are shown. The PAM motifs are marked in red and the start and stop codons are underlined in black. The sequences used for the microhomology regions are shown underlined in green and the light blue color indicates the crRNA for both 5' and 3' regions.

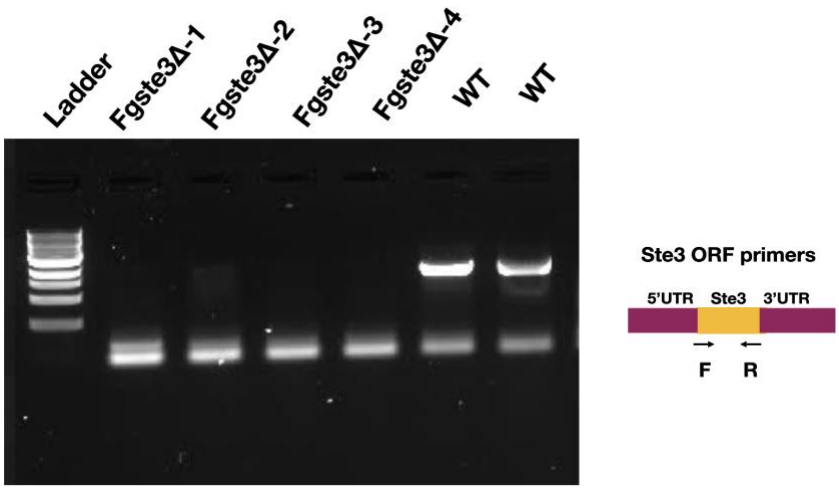

Supplementary Figure A2. Confirmation of *STE3* deletion by PCR. The hygromycin-resistant transformants (*Fgste3Δ-1*, *Fgste3Δ-2, Fgste3Δ-3, Fgste3Δ-4*) were screened through PCR with *STE3* ORF primers P3 and P4 (Table 1). The expected DNA fragment size is ≈1400 bp.

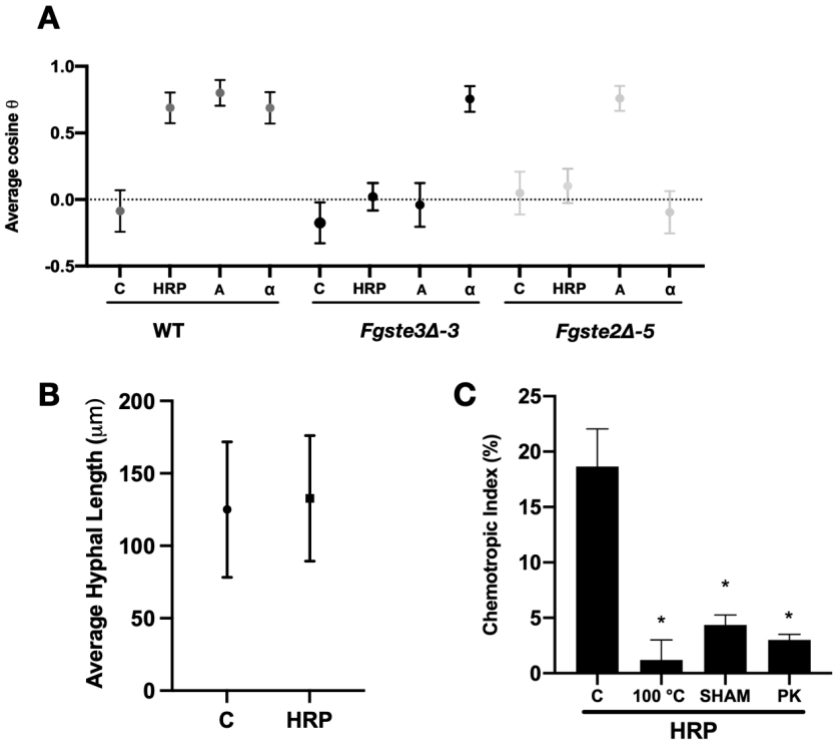

Supplementary Figure A3. Characterization of *Fgste3Δ-3* hyphal length and sensitivity to HRP activity. A) Hyphal tip projection angle assay: Average cosine of hyphal tip projection angles were measured for the *F. graminearum* WT, Δ*Fgste3-3* and Δ*Fgste2-5* strains towards a gradient of solvent control (C), horseradish peroxidase (HRP), Pheromone a (A) and Pheromone α (α). Data is presented as the mean from three experiments (n = 100 hyphae / interaction / replicate). Bars indicate upper and lower 95 % significance limits for cosine means according to a *t*-test. A cosine of 1 means perfect orientation while 0 means random orientation. Chemotropism was considered significant when the lower confidence limit was > 0. **B**) Control experiment for average length of hyphae of WT *F. graminearum* towards a gradient of solvent control (C) or horseradish peroxidase (HRP). Data is representative of three experiments. n = 100 hyphae. **C)** The peroxidase chemoattractant sample was treated with its inhibitor, salicylhydroxamic acid (SHAM) at 60 mM concentration for 5 minutes, or underwent heat

denaturation at 95 °C for 10 minutes or was proteolysed by Proteinase K (1mg/ml) for 30 minutes at room temperature.

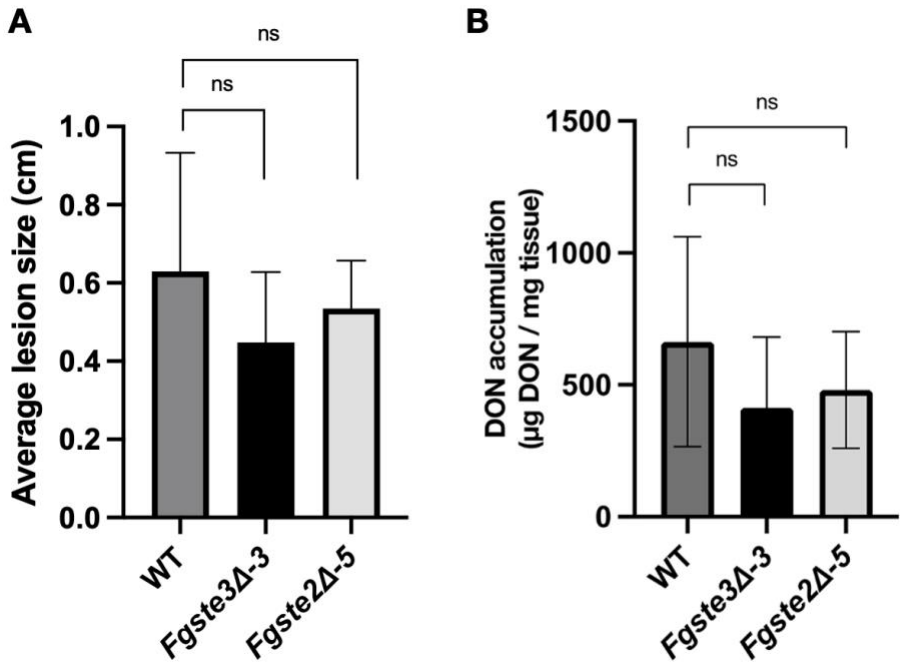

Supplementary Figure A4. Wheat head infection assays and DON quantification. A) Flowering wheat heads were point inoculated with conidia of wild type and mutant strains *Fgste3*Δ*-3* and *Fgste2*Δ*-5.* Infected plants were transferred to a contained misting facility and monitored for the development of disease symptoms such as spikelet discoloration. Data was collected when heads in the control treatment group exhibited approximately >90% infection**. B)** DON quantification of wild type and *Fgste3Δ-3* and *Fgste2Δ-5* mutants grown in liquid culture with tricothecene-inducing media.

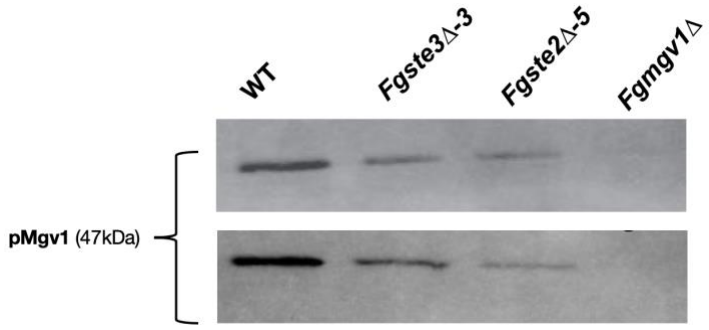

Supplementary Figure A5: Probing of Mgv1 phosphorylation: Biological replicates of quantitative Western blot to probe CWI pathway activation by tracking phosphorylation of Mgv1 isolated from wild type and mutant strains *Fgste3Δ-3* and *Fgste2Δ-5 and Fgmgv1Δ.* The conidia were grown for 48 h in regular PDB culture and treated with commercially available HRP for 1 h before total protein extraction. In contrast, the band with water control showed no variation in the WT and mutants as shown in Fig 5A.

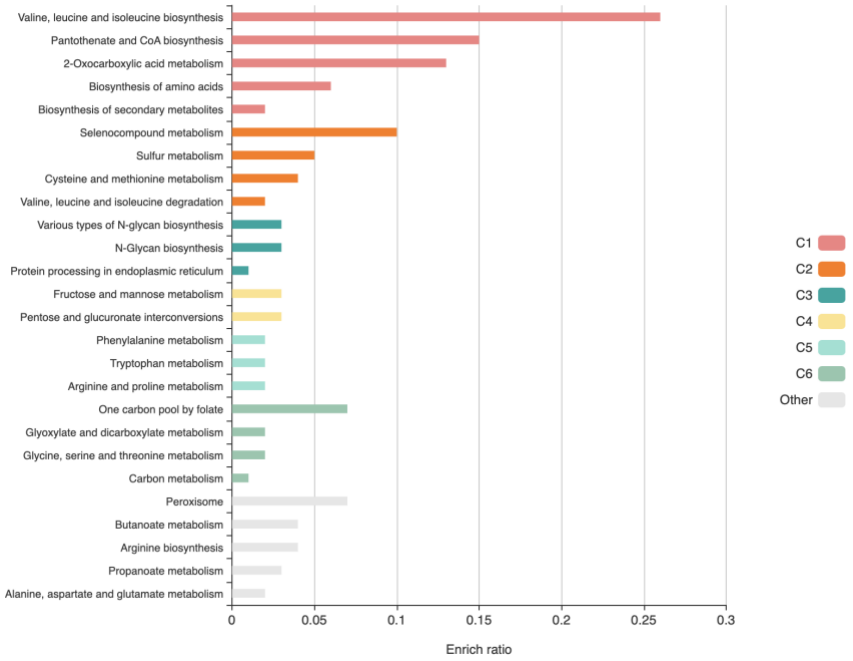

Supplementary Figure A6. Gene enrichment analysis for wild type + HRP vs wild type uninduced (up-regulated genes only) using KOBAS. The differentially expressed genes were grouped into different categories based on pathway enrichment tool. Each row represents an enriched function, and the length of the bar represents the enrichment ratio, which is calculated as input gene number/background gene number. In the KOBAS algorithm, clusters are divided according to the values calculated for the enriched terms. The colors of the bars represent different clusters and show the top 6 with the highest enrichment ratios and p-values. (KOBAS, http://kobas.cbi.pku.edu.cn).

Appendix B

Supplemental Information for Chapter 3

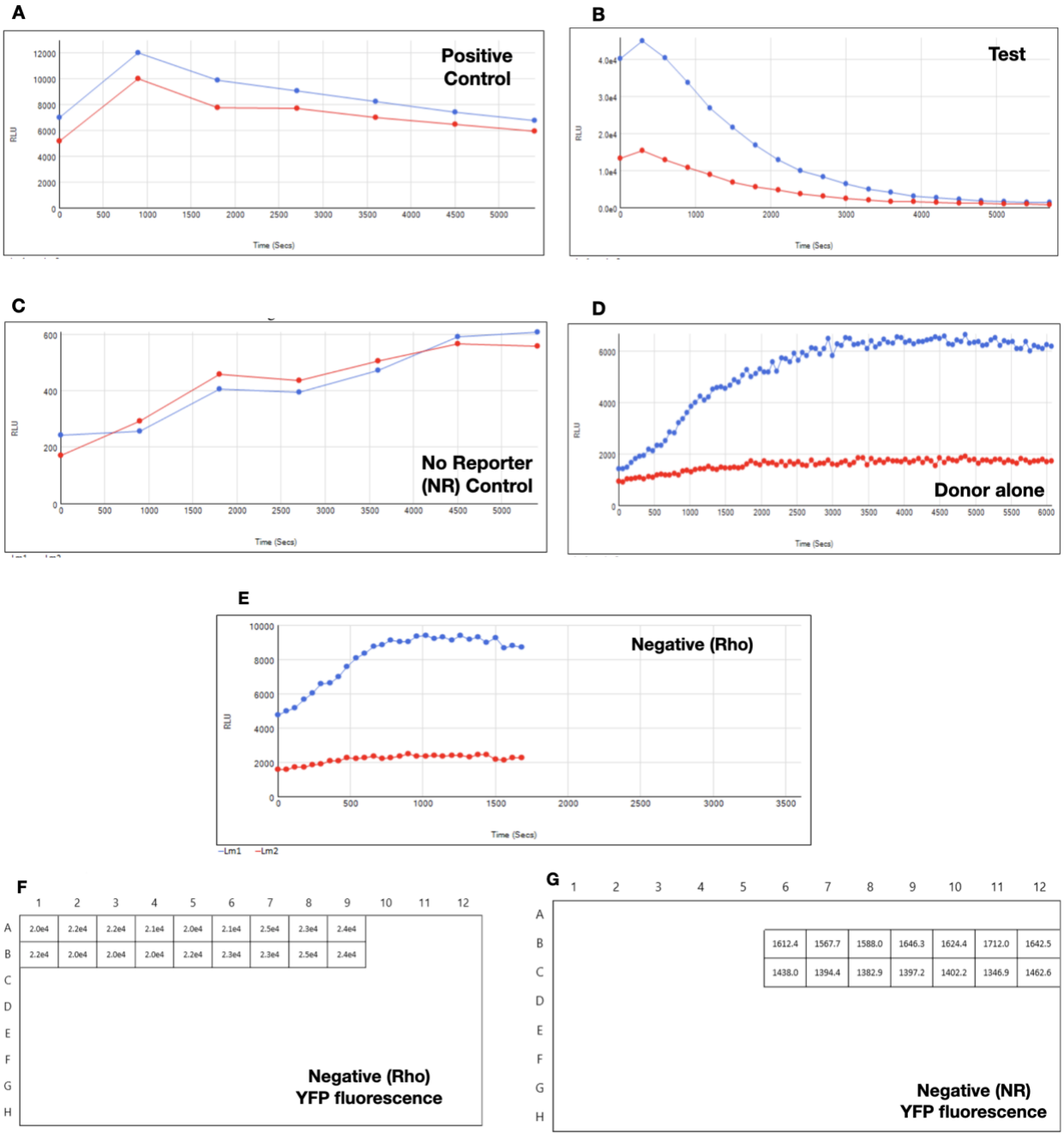

Supplementary Figure B1: Raw data for each strain used in the BRET study. The line in blue represents the Relative Luminescence Units (RLU) for NLuc and red represents the RLU for YFP. BRET ratio was calculated for each of the above strains (A-E). F and G denote the fluorescence values obtained to quantify YFP expression in Negative control (Rho) and No reporter (NR) negative control.

Ste3-Turbo ID

In this study, we also generated Ste3- Turbo ID proximity biotinylation strain with a goal to investigate the interactome of the Ste3 GPCR on peroxidase stimulation, specifically to mine the activating downstream G-Proteins that lead to activation of CWI-MAPK pathway. The knock-in was confirmed through PCR and whole genome sequencing. The construct was confirmed to be expressing well in *Fusarium graminearum*.

We developed Proximity biotinylation based enhanced Turbo ID system in *Fusarium graminearum* that offers a powerful approach to identify the downstream activating G proteins, signaling pathways, and adaptor proteins associated with GPCR activation. Here a novel Ste3-TurobID expressing fusarium strain is created with the aim of uncovering novel components of GPCR signaling networks downstream of the protein in future studies.

Proximity biotinylation enables the labeling and capture of proteins in close proximity to a target protein of interest. This approach relies on the expression of a fusion protein consisting of the target protein and a promiscuous biotin ligase enzyme. Upon addition of biotin, the biotin ligase enzyme catalyzes the covalent attachment of biotin to proximal proteins, allowing for their subsequent enrichment and identification. Turbo ID is an improved version of the BioID system

with increased biotinylation efficiency in shorter time and reduced background labeling mass spectrometry analysis, providing insights into the specific G protein subtypes involved.

Table B1. The crRNAs and primers designed for Ste3-TurboID knock-in

5'crRNA	AAAAAGCCTCTTCCACATCA
3'crRNA	ATTCATCATCTATTCCGGGG
5' Primer	CTCACTCAAGAGCCTCAAAAAGCCTCTTCCACATC**ATGGCCGATTCAATTCACTTGTTCGG**
3' Primer	ATCAAATAGGGTATCGCACGATGTACTTTTTGG**CCATCACTCCTTGGCCCTAGGCCTGGTGGA**

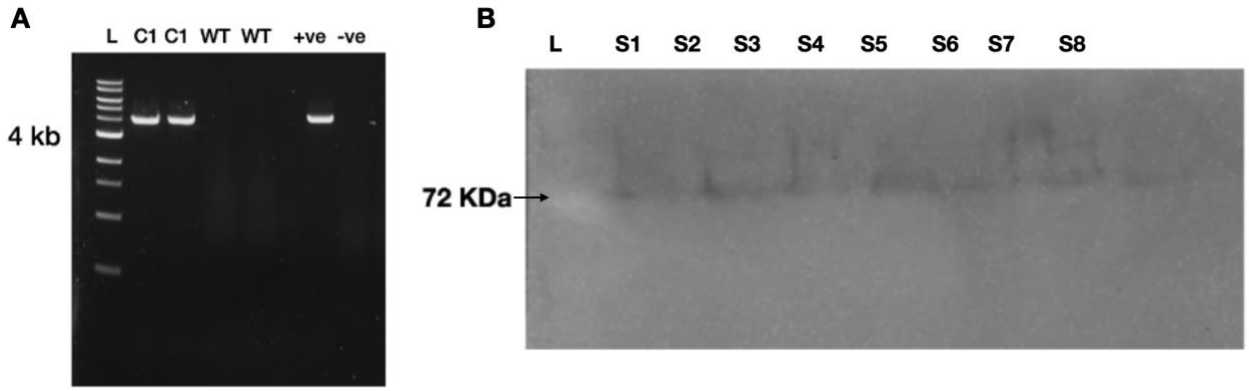

Supplementary Figure B2 A. Confirmation of knock-in through PCR using primer pair P1 and P2 (**Table B1**). C1 represents transformed colony with Ste3-TurboID fusion protein and WT represents wildtype in which the corresponding band is missing, serving as the negative control. Positive construct (+ve) is the plasmid control and -ve represents no template control. **B**. Expression verification of Ste3-TurboID fusion construct was carried out using anti-FLAG antibody. A band detected at around 80kDa represents the fusion protein.

Material and Methods:

Preparation of protoplasts and *F. graminearum* CRISPR transformation:

Carried out as before. Kindly refer to section 2.5.1 and 2.5.2 in Chapter 2.

Fungal genomic DNA isolation and whole-genome sequencing

Fungal conidia stocks of the transformants at −80°C were thawed on ice and grown in potato dextrose broth (PDB) media. Mycelia were collected from 2-day-old *F. graminearum* liquid cultures by filtration and ground into a fine powder in liquid nitrogen. Genomic DNA (gDNA) was then isolated from the ground tissue using an E.Z.N.A. Fungal DNA Mini Kit (Omega Biotek, D3390-01) and eluted in sterile water. The deletion of the target STE3 sequence and knock-in of the repair template was confirmed by PCR, using primer set P1 and P2 for the gene segment knocked in. Whole-genome sequencing performed on a NovaSeq 6000 PE100 (5M reads) platform, following Illumina shotgun library preparation. The FASTQ files were uploaded, and the data were analyzed using the Qiagen CLC-Genomics platform (v. 21.0.5), using the default settings.

Results

Knock-in verification of Ste3-TurboID construct

The Ste3 TurboID construct was generated and verified through PCR using primers pair P1 and P2 (**Table B1**) with a band detected at 4Kb corresponding to the Ste3-TurboID fusion construct knocked in using CRISPR-HDR. Whole genome Illumina sequencing was performed on Novaseq6000 platform to verify the knock-in with no off-target effects.

Expression verification of Ste3-TurboID construct: The Ste3-TurboID fusion protein was followed by a FLAG tag. Western blot was performed for expression verification following immunoblotting with FLAG tag. A band was observed at expected size for Ste3-TurboID fusion protein of 71kDa representing the fusion protein being expressed. Optimizations involving biotinylation time and concentration are being performed with our collaborators at AAFC, Ottawa for further experimentation.

Expression verification of Ste3-Turbo ID construct

Western blot was carried out for expression verification of the knocked-in Ste3-TurboID construct carrying a FLAG tag. Approximately 10^5 *F. graminearum* conidia were grown in PDB for 24 h at 28°C in the dark. Biotin (100 μM) or an equivalent water control was then added to the growing culture and shaken for 1 h. The cells were lysed as previously described (82). The solubilization of membrane fraction was performed with 0.1% SDS, 1% triton X and 0.1% sodium deoxycholic acid. Protein (20 μg) was loaded and resolved on a 12% SDS polyacrylamide gel and transferred to a polyvinylidene difluoride membrane (PVDF, Bio-Rad) via wet electroblotting at 100 V for 2 h. The membranes were blocked for 1 h in 5% (wt/vol) nonfat, dried, skim milk in TBST buffer (50 mM Tris [pH 7.5], 150 mM NaCl, 0.05% [vol/vol] Tween 20) at 4°C. The membranes were subsequently incubated in mouse anti-FLAG (1:1,000 dilution, Sigma Cat# A8592-.2MG) primary antibody. For visualization, enhanced chemiluminescent substrate (Thermo Scientific, 32209) was added to the membranes, and the emitted light was captured using a GelDoc Imager and the Image Lab software package (Bio-Rad).